CHRONIC EXPOSURE TO AN INSULIN-CONTAINING LIPOGENIC STIMULUS RESULTS IN ECTOPIC CYTOPLASMIC LIPID ACCUMULATION AND ALTERED PRO-INFLAMMATORY FUNCTION IN MAST CELLS

A DISSERTATION SUBMITTED TO THE GRADUATE DIVISION OF THE UNIVERSITY OF HAWAIʻI AT MĀNOA IN PARTIAL FULFILLMENT OF THE REQUIREMENTS FOR THE DEGREE OF

DOCTOR OF PHILOSOPHY

IN

BIOMEDICAL SCIENCES

(PHYSIOLOGY)

MAY 2013

By

William E. Greineisen

Dissertation Committee:

Steven W. Ward, Chairperson

Helen Turner

Peter Hoffmann

Scott Lozanoff

Claire Wright

Keywords: Mast cells, obesity, diabetes, metabolic syndrome, lipid bodies, steatosis

UMI Number: 3572474

All rights reserved

INFORMATION TO ALL USERS
The quality of this reproduction is dependent upon the quality of the copy submitted.

In the unlikely event that the author did not send a complete manuscript
and there are missing pages, these will be noted. Also, if material had to be removed,
a note will indicate the deletion.

UMI 3572474

Published by ProQuest LLC (2013). Copyright in the Dissertation held by the Author.

Microform Edition © ProQuest LLC.
All rights reserved. This work is protected against
unauthorized copying under Title 17, United States Code

ProQuest LLC.
789 East Eisenhower Parkway
P.O. Box 1346
Ann Arbor, MI 48106 - 1346

Acknowledgements

It's impossible to concisely express the contribution various individuals in my life have made throughout this journey, however, what can be said is that if you've made a difference, you've constantly heard it from my lips along the way and I couldn't be more fortunate to have crossed your paths in this life. Those more directly associated with the content of this dissertation are illuminated below for their tireless investment in my success.

Dr. Helen Turner: I fall miserably short in saying that you are the single most extraordinary person that I've ever interfaced with in this world. The greatest dilemma is that my appreciation cannot be articulated into narrative suitable for this document for all you've invested and mean to me. There will never be a time that you are not welcome in my life. Thank you a million times for your relentless trust, faith, love and passion for what we do.

My laboratory: Lori Shimoda-my only lab mate when we built the lab at Chaminade and the single largest contributor to what is presented in the subsequent pages. You've been absolutely amazing and have done such a great job integrating me both in the lab and into your family. We are all so fortunate to have your love and I will never take that for granted. Carl Sung-you really took our lab to the next level and always made me feel important by going out of your way to share your wisdom with me. You're a great father and an impressive friend. Thank you for all you continue to do. To my fellow lab mates and post-docs, the adjacent groups of investigators and their staff, the countless volunteers and student help over the years, and the various faculty, all of which have provided some level of support, optimism or empathy, thank you for your generosity and kindness.

I'd like to express my gratitude to my committee members for their constant support and guidance through the process of completing this body of work and the kind humanizing words each of you have expressed to me during our one-on-one interactions. A special thank you to Dr. Alexander Stokes who has always been an ally to our lab and always available when we needed anything.

My mother, father and brother-thank you for getting me to the starting line. I love you all.

Abstract

This thesis presents evidence that mast cells (MC) chronically exposed to insulin respond by developing steatotic levels of cytosolic lipid bodies, suggesting that immunocytes, like hepatocytes and myocytes, are sites of lipid sequestration in response to dysregulated insulin levels. This ectopic lipid accumulation influences mast cell functionality, biasing mast cell phenotype towards the production of bioactive lipid mediators (LTC4) and away from the release of histamine and other secretory granule components. In the current study we present an analysis of the whole cell and lipid body lipidome in control, and insulin-exposed mast cells. Our data show a significant upregulation in lipid-associated pro-inflammatory precursor molecules in response to chronic insulin exposure. We also show that the lipid body population in these cells are heterogeneous to a previously unsuspected degree. Moreover, due to the intimate relationship between the endoplasmic reticulum (ER) and lipid body production, we tested the hypothesis that the ER may be altered in response to chronic insulin exposure. Indeed, our data show that (in a manner analogous to observations in hepatocytes from obese models) the ER is reprogrammed towards a lipogenic phenotype, is morphologically distended, is compromised as a calcium store and exhibits certain indicators of a unfolded protein response (UPR)/ER stress response in response to chronic insulin. Taken together, these data show that chronic insulin exposure in a model mast cell system drives lipidomic remodeling in a manner that alters lipid body formation and mast cell pro-inflammatory function.

Table of Contents

ACKNOWLEDGEMENTS ..... **II**

ABSTRACT ..... **III**

LIST OF FIGURES ..... **VIII**

LIST OF ABBREVIATIONS ..... **XI**

CHAPTER ONE **1**

GENERAL INTRODUCTION **1**

1. 1. OBESITY AND METABOLIC SYNDROME 1

1.1.1. Health burdens associated with metabolic diseases *1*

1.1.2. Definitions of obesity and the metabolic syndrome *2*

1.1.3. Insulin balance and progression to type II diabetes *3*

1.1.4. Basic biochemistry of lipogenesis/lipolysis and their relationship to metabolic syndrome progression *4*

1.2. IMMUNOLOGICAL AND INFLAMMATORY EFFECTS OF METABOLIC PERTURBATION 6

1.2.1. Systemic inflammation associated with obesity and metabolic syndrome *6*

1.2.2. Adipose inflammation *7*

1.2.3. Altered immunocyte function in obesity and metabolic syndrome *8*

1.3. ECTOPIC LIPID DEPOSITION AT THE ORGAN, TISSUE AND CELLULAR LEVEL 10

1.4. THE LIPID BODY 13

1.4.1. Lipid body structure and composition *13*

1.4.2. Lipid body biogenesis from the endoplasmic reticulum *14*

1.4.3. Lipid body formation and ER stress *15*

1.4.4. The cycle of lipogenesis/lipolysis at the level of the lipid body *15*

1.5. LIPID BODIES IN MAST CELLS AND BASOPHILS 16

1.6. QUESTIONS 18

1.7. CENTRAL HYPOTHESIS OF THIS WORK 19

CHAPTER TWO **20**

MATERIALS AND METHODS **20**

2.1. CELL CULTURE 20

2.2. CHEMICALS, REAGENTS AND DYES 20

2.3. CELL STIMULATIONS 20

2.4. ANTIBODIES 21
2.5. CELL LYSIS AND WESTERN BLOT 21
2.6. HISTOLOGY STAINING FOR LIPID CONTENT 22
2.7. CALCIUM ASSAY (BULK METHOD) 22
2.8. CALCIUM ASSAY (SINGLE CELL METHOD) 23
2.9. LEUKOTRIENE C4 ASSAY 23
2.10. BETA-HEXOSEAMINIDASE ASSAY 23
2.11. FLOW CYTOMETRY 23
2.12. TRIGLYCERIDE ASSAY 24
2.13. QUANTITATIVE REAL TIME PCR ANALYSIS 24
2.14. MICRO ARRAY ANALYSIS 24
2.15. LIPIDOMIC ANALYSIS 25
2.16. ER/MICROSOMAL AND LIPID BODY PREPARATION BY ULTRACENTRIFUGATION 26
2.17. LIPID BODY ISOLATION 26
2.18. LIPID BODY MICRO-ASPIRATION 27
2.19. DIFFERENTIAL GEL ELECTROPHORESIS (DIGE) 27
2.20. TRANSMISSION ELECTRON MICROSCOPY (EM) 28
2.21. BCA ASSAY FOR PROTEIN DETERMINATION 28
2.22. STATISTICAL ANALYSIS 29

CHAPTER THREE 30

CHARACTERIZATION OF LIPID BODIES INDUCED BY INSULIN/HIGH NUTRIENT CONDITIONS IN MODEL MAST CELLS 30

3.1. INTRODUCTION 30
3.1.1 Lipogenic effects of insulin 30
3.1.2. Mast cells and insulin: review of previous studies 33
3.1.3. Mast cell and adipocyte lipid droplets: commonalities and contrasts 34
3.1.4. Experimental Approach: Exploring insulin-directed lipogenesis in mast cells 35
3.2. RESULTS 36
3.2.1. Chronic insulin induces lipogenesis in mast cells 36
3.2.2. Subcellular heterogeneity of lipid bodies in mast cells 43
3.2.3. Lipid body heterogeneity between the adipocyte and mast cell systems: commonalities and contrasts 51
3.3. DISCUSSION 60

CHAPTER FOUR **65**

FUNCTIONAL IMPACT OF STEATOSIS ON MAST CELL PRO-INFLAMMATORY FUNCTION **65**

4.1. INTRODUCTION 65

4.1.1 Ectopic lipid deposition and cellular function *65*

4.1.2. Ectopic lipid deposition, the ER and ER stress *66*

4.1.3. Potential impacts of steatosis on pro-inflammatory functions of the mast cell *67*

4.1.4. Experimental Approach: Exploring the phenotype of steatotic mast cells *68*

4.2. RESULTS 69

4.2.1. Altered mast cell granularity phenotype in response to chronic insulin exposure *69*

4.2.2. Degranulation is suppressed in mast cells chronically-exposed to insulin *69*

4.2.3. Altered enzyme expression in the eicosanoid synthesis pathways and altered eicosanoid production in insulin-exposed mast cells *69*

4.2.4. Cytokine gene expression in insulin-exposed mast cells *70*

4.2.5. Characteristics of the $SSC^{lo}FSC^{hi}$ insulin-induced population in model mast cells *75*

4.2.6. Suppression of FcεRI-induced calcium fluxes in insulin-exposed mast cells *81*

4.2.7. Calcium signal dynamics in insulin-treated mast cells *82*

4.2.8. Endoplasmic reticulum remodeling, reprogramming and stress in insulin-treated mast cells *90*

4.3. DISCUSSION 100

CHAPTER FIVE **103**

IMPACT OF STEATOSIS ON THE MAST CELL LIPIDOME **103**

5.1. INTRODUCTION 103

5.1.1. Fat and cellular lipid classes *103*

5.1.2. Lipidomes – cellular lipid fingerprints *104*

5.1.3. Prior studies of lipidomes in steatosis and immunocytes *105*

5.1.4. Experimental Approach: Lipidomics in steatotic mast cells *106*

5.2. RESULTS 106

5.2.1. Whole cell lipidome of steatotic and control mast cells *106*

5.2.2. Lipidome of lipid bodies purified from normal and steatotic mast cells using ultracentrifugation *117*

5.2.3. Development and testing of a microaspiration technique to highly purify lipid bodies *121*

5.3. DISCUSSION 126

CHAPTER SIX 130

DISCUSSION AND FUTURE PERSPECTIVES 130

BIBLIOGRAPHY 134

List of Figures

Title	Page
Figure 1.1. Schematic representation of the basis for metabolic syndrome.	2
Figure 1.2. Insulin and glucose dynamics during the progression of the metabolic syndrome.	5
Figure 1.3. Normal and ectopic lipid deposition resulting from a positive energy balance.	12
Figure 1.4. Compositional model for the adipocyte lipid body.	13
Figure 1.5. Models for lipid body biogenesis.	14
Figure 1.6. Lipogenesis and lipolysis at the level of the individual lipid droplet.	16
Figure 3.1. Membrane-proximal signaling by the insulin receptor.	31
Figure 3.2. The role of insulin in lipogenesis and lipolysis in the adipocyte.	32
Figure 3.3. Insulin-FDI induced accumulation of homogeneous Oil Red O-positive lipid bodies in 3T3-L1 adipocytes.	33
Figure 3.4. Insulin-containing lipogenic stimuli induce lipid bodies in mast cells.	39
Figure 3.5. Flow cytometric quantification of lipid body accumulation in adipocytes and mast cells.	42
Figure 3.6. Chronic insulin exposure induces a heterogeneous lipid body population in mast cells.	44
Figure 3.7. Chronic insulin exposure induces a heterogeneous lipid body population in mast cells.	46
Figure 3.8. Diversity in lipid body ultrastructural appearance revealed by EM.	48
Figure 3.9. 3-D rendered confocal z stacks of individual and clustered lipid bodies in steatotic mast cells.	50
Figure 3.10. Lipid body biogenesis is mechanistically different in mast cells and adipocytes.	55
Figure 3.11. Different chemical environments can be resolved by fluorescence emission shifts in the lipophilic dye Nile Red.	57

Figure 3.12. Nile Red emission spectra in 3T3L-1 adipocytes.	58
Figure 3.13. Nile Red emission spectra in RBL3H3 mast cells.	59
Figure 4.1. Insulin-containing lipogenic stimuli induce phenotypic change in mast cell granule content.	72
Figure 4.2. Characterization of insulin-FDI-induced sub-populations in mast cells.	77
Figure 4.3. Suppression of calcium signaling and ER phenotypic alterations in lipid body-enriched mast cells.	85
Figure 4.4. Suppression of calcium signaling and downstream targets in lipid body-enriched mast cells.	86
Figure 4.5. Calcium dynamics in cytosol and lipid bodies within insulin-exposed mast cells.	87
Figure 4.6. Calcium dynamics in cytosolic stores and lipid bodies within antigen stimulated, insulin-exposed, mast cells.	89
Figure 4.7. Chronic insulin exposure induces ER stress and altered metabolism in RBL2H3 mast cells.	93
Figure 4.8. Proteomic analysis and Golgi trafficking in insulin-FDI treated mast cells.	95
Figure 4.9. Characterization of the ER lipidomic landscape in insulin-FDI treated mast cells.	99
Figure 5.1. Lipidomic characterization (fold change) of insulin-FDI treated mast cells.	109
Figure 5.2. Lipidomic characterization (percent change) of insulin-FDI treated mast cells.	111
Figure 5.3. Insulin containing lipogenic stimulus alters fatty acid class presentation in mast cells.	113
Figure 5.4. Insulin containing lipogenic stimulus alters precursor molecules associated with the arachidonic acid biosynthetic pathway in mast cells.	114

Figure 5.5. Insulin containing lipogenic stimulus alters absolute concentrations of precursor molecules associated with the arachidonic acid biosynthetic pathway in mast cells.	115
Figure 5.6. Insulin containing lipogenic stimulus alters absolute concentrations of precursor molecules associated with the arachidonic acid biosynthetic pathway in mast cells.	116
Figure 5.7. Lipidomic characterization (percent abundance) of insulin-FDI treated lipid bodies in mast cells.	119
Figure 5.8. Novel lipidomic characterization of microaspirated lipid bodies from insulin-FDI treated adipocytes.	123
Figure 5.9. Development of a novel microaspiration technique for isolating cytoplasmic lipid bodies.	125

List Of Abbreviations

ABHD	alpha beta hydrolase domain
ADFP	adipose differentiation-related protein
AKT	protein kinase B
AMPK	adenosine monophosphate activated protein kinase
ATF	activating transcription factor 3
ATL	adipose tissue lipase
BMMC	bone marrow derived mast cells
BMI	body mass index
BSA	bovine serum albumin
cAMP	cyclic adenosine monophosphate
CD	cluster of differentiation
CE	cholesterol ether
CL	cardiolipin
COX	cyclo-oxygenase
CRAC	calcium release activate channel
DAG	diacylglycerol,
DAPI	4′,6-diamidino-2-phenylindole
DIGE	differential gel electrophoresis
DIO	diet-induced obesity
DMEM	Dulbecco's modification of Eagle's medium
DMSO	dimethyl sulfoxide

ECL	enhanced chemi-luminescence
EDTA	ethylenediaminetetraacetic acid
EGTA	ethylene glycol tetraacetic acid
EIA	enzyme immunoassay
ELD	ectopic lipid deposition
EM	electron microscopy
ER	endoplasmic reticulum
FACS	fluorescence activated cell sorting
FAME	fatty acid methyl ester standard set
FBS	fetal bovine serum
FC	free cholesterol
FcεRI	high affinity receptor for the Fc portion of immunoglobulin E
FFA	free fatty acids
FSG	fish skin gelatin
GLUT	glucose transporter
HBSS	Hank's buffered salt solution
HEPES	n-2-hydroxyethylpiperazine-n'-2-ethanesulphonic acid
HRP	horse-radish peroxidase
HSL	hormone sensitive lipase
IBMX	isobutylmethylxanthine
IFN	interferon
Ig	immunoglobulin
IL	interleukin

iNOS	inducible nitric oxide synthase
IRS	insulin receptor substrate
Ins (1,4,5) P3	inositol (1,4,5) trisphosphate
ITPR, Ins (1,4,5) P3R	inositol (1,4,5) trisphosphate receptor
JNK	c-jun N terminal kinase
kDA	kilodaltons
KLH-DNP	keyhole limpet hemocyanin conjugated dinitrophenol
MAPK	mitogen activated protein kinase
MPI	mean peak fluorescence intensity
mRNA	messenger RNA
MUFA	mono-unsaturated fatty acids
NKT	natural killer T cell
nm	nanometers
nM, μM, mM	nanomolar, micromolar, millimolar
OD	optical density
ORO	oil red O
PAGE	polyacrylamide gel electrophoresis
PBS	phosphate-buffered saline
PC, PE, PS	Phosphatidylcholine, phosphatidylethanolamine, phosphatidylserine
PCR	polymerase chain reaction
PERK	protein kinase-like endoplasmic reticulum kinase
PFA	paraformaldehyde
PI3K	phosphatidyl inositol 3’ hydroxyl kinase

PMA	phorbol 12, 13 myristate acetate
PMCA	plasma membrane calcium ATPase
PMSF	phenylmethylsulfonylchloride
PPAR	peroxisome proliferator activated receptor
PUFA	poly-unsaturated fatty acids
PVDF	polyvinylidene difluoride
RBL2H3	rat basophilic leukaemia subclone 2H3
RFU	relative fluorescence units
RPMI	Roswell Park Memorial Institute medium
RT	room temperature
SDS	sodium dodecyl sulfate
SERCA	sarcoplasmic endoplasmic reticulum calcium ATPase
SFA	saturated fatty acid
TFA	total fatty acid
Th	T helper lymphocyte
TIP	tail interacting protein
Treg	regulatory T cell
TNF	tumor necrosis factor
UPR	unfolded protein response
μm	micrometer

Chapter One

General Introduction

1. 1. Obesity and metabolic syndrome

1.1.1. Health burdens associated with metabolic diseases

There is a widespread understanding in the health care community that major medical challenges in the 21st century stem from obesity (1-5). Obesity and its attendant list of pathologies centrally arise from access to nutrient overload coupled to a sedentary lifestyle (1-3). As of 2010 in the United States, over 35% of the adult population, or 78 million Americans, are categorized as obese. Disturbingly, this epidemic is now affecting youth populations, with 17%, or 12.5 million American children and adolescents considered to be obese. These challenges are shared worldwide between both high-income countries and in developing countries. Globally, 1/6th of the population is considered to be overweight with more than 300 million individuals defined as obese. Although the most recent data show that these trends have begun to stabilize, obesity rates have been constantly increasing for the last half-century.

In addition to being a major health concern, obesity has also become a significant contributor to rising health care costs in our country, responsible for 27% of the rise in inflation-adjusted health spending between 1987 and 2001 (6). In 1998, annual health care costs associated with being overweight and obese were estimated to be as high as $78.5 billion. In only 4 years, annual costs associated with obesity nearly doubled to over $147 billion in 2008. The costs pertaining to the treatment of obesity and the associated pathologies including obesity-attributable prescription drug costs have led to an increased burden on Medicare, Medicaid and private payers (6).

1.1.2. Definitions of obesity and the metabolic syndrome

In contrast to most of our history, modern humans are far more likely to die from the consequences of being overweight than underweight (7). Obesity is a condition in which the accumulation of excess body fat leads to an individual's health being negatively affected. The aggregation of large deposits of adipose tissue throughout the body contributes to elevated blood pressure (hypertension), increased plasma triglyceride levels (dyslipidaemia) and increased plasma glucose levels (hyperglycemia). Metabolic syndrome (8-10) refers to various combinations of visceral obesity (waist circumference >102 cm for men > 88 cm for women), insulin resistance (fasting glucose level of >5.6 mmol per liter untreated), high plasma triglycerides (>1.69 mmol/liter untreated), hypertension (blood pressure >130 mmHg) and low HDL-cholesterol levels (<1.03 mmol/l for men, <1.29 mmol/l for women). These contribute, in turn, to metabolic diseases such as diabetes mellitus (Type II), atherosclerosis, osteoarthritis, obstructive sleep apnea, respiratory disorders, and

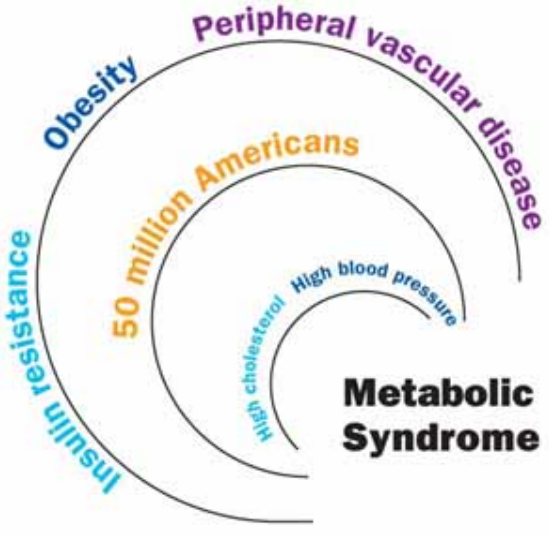

Figure 1.1 Schematic representation of the basis for metabolic syndrome. The progressive accumulation of co-morbidities causes severe pathology. *From Nature web resource on metabolic syndrome www.nature.com/focus/metabsyn/index.html.*

cardiovascular disease. Metabolic syndrome adversely affects the prognoses of various types of cancer (8-10).

Simply stated, managing one's weight is accomplished by balancing calories. In order to maintain a particular weight, the caloric amount taken in must match the calories utilized by the body. For example, if one consumes 2000 calories in a given day, in order to maintain weight for that day, one must also utilize 2000 calories in energy expenditure that same day.

When more calories are consumed than are utilized by the body for energy production, the body tends to store this extra energy in the form of fat tissue. The additive effect of excess calorie consumption would be weight gain. In contrast, the additive effect of utilizing more calories than consumed would be weight loss. If, day after day, a person consumes more energy then they are expending, a surplus of energy (fat) is deposited on and around that individual's body. Once a critical point in the amount of fat depot is reached, the person is considered obese. This critical point is typically measured in the form of an individual's Body Mass Index or BMI (3).

The two variables needed to calculate an individual's BMI are their weight and height. Although this calculation does not take into account variables such as bone density, gender or muscle mass, for most people, this calculation yields a convincingly strong correlation to an individual's body fat content. The BMI values range from approximately 15-30, with 15 being underweight and 30 being regarded as clinically obese. Weights regarded as normal range from 18.5-24.9. Although a clear advantage to being obese has not been proposed, human obesity does not always result in health deterioration, which suggests that fat tolerability differs among individuals raising questions of genetic and epigenetic variability. There is growing support for a 'fit versus fat' hypothesis (11), where certain individuals are metabolically healthily despite excess weight, prompting questions as to why they are protected from the pathology of metabolic syndrome.

1.1.3. Insulin balance and progression to type II diabetes

Feeding and storing energy is a basic requirement for survival and an inability to do these will inevitably result in death. In humans, energy storage is accomplished through the progressive cycle of breaking down ingested food into absorbable macronutrients followed by the accession of those nutrients by the vascular system, subsequent delivery of those nutrients to cellular targets and sequestration of those nutrients at the cellular level. Absorption at the cellular level is driven by insulin (12, 13), where binding to the insulin receptor leads to an ability of the cell to absorb glucose across the plasma membrane from the extracellular milieu. Feeding promotes the release of insulin from the pancreas and frequent bouts of feeding result in the chronic activation of pancreatic β-cells and the subsequent release of insulin. Metabolic homeostasis is dependent on a healthy balance

between feeding and fasting cycles and chronic deviations to either side of the spectrum may result in pathology. For example, during the progression into an obese state, a surplus of nutrients overwhelm the metabolic system and over activation of the feeding cycle leads to hyperinsulinaemia (8). Although many factors have been contriubuted to insulin resistance, it has been suggested that over-activation of this pathway for too long results in insulin resistance, which is an inability of insulin to properly ligate insulin receptors. Importantly, during the progression of metabolic syndrome, the development of insulin resistance (8, 14) is transiently associated with a compensatory over-production of insulin, prior to exhaustion of the pancreas and a long-term insulin deficiency (type II diabetes). Chronic bouts of insulin resistance eventually lead to hyperglycemia and the acquisition of type II diabetes. A positive feed-forward loop is engaged at a particular point in this progression when intracellular inflammatory signaling pathways are activated, which alter insulin signaling pathways (see Chapter 4), further exacerbating the problem.

1.1.4. Basic biochemistry of lipogenesis/lipolysis and their relationship to metabolic syndrome progression

Insulin drives lipogenesis (12, 13, 15), which is the process of converting simple sugars (glucose and their metabolic intermediates, such as acetyl-CoA) into lipids. These lipids are stored in subcellular organelles known as lipid bodies, which provide safe and efficient storage of these substrates against times of future metabolic demand (15-21). These lipid bodies can be further expanded by their absorption of cytosolic free fatty acids that have passively diffused through fatty acid transporter proteins (FATP) located on the surface of the plasma membrane. Excessive levels of blood sugars and lipids coupled with the hyper-secretion of insulin lead to hypertrophy of these stores. Excess volumes of fatty acids and the subsequent accumulation of lipid droplets have been classified as steatosis and linked to obesity, insulin resistance, type II diabetes and atherosclerosis (8). The accumulation of cytoplasmic lipid droplets at the cellular level contributes to steatosis and depots can be observed in the obese liver, heart, pancreas and skeletal muscle and adipose depositions (9, 22-24).

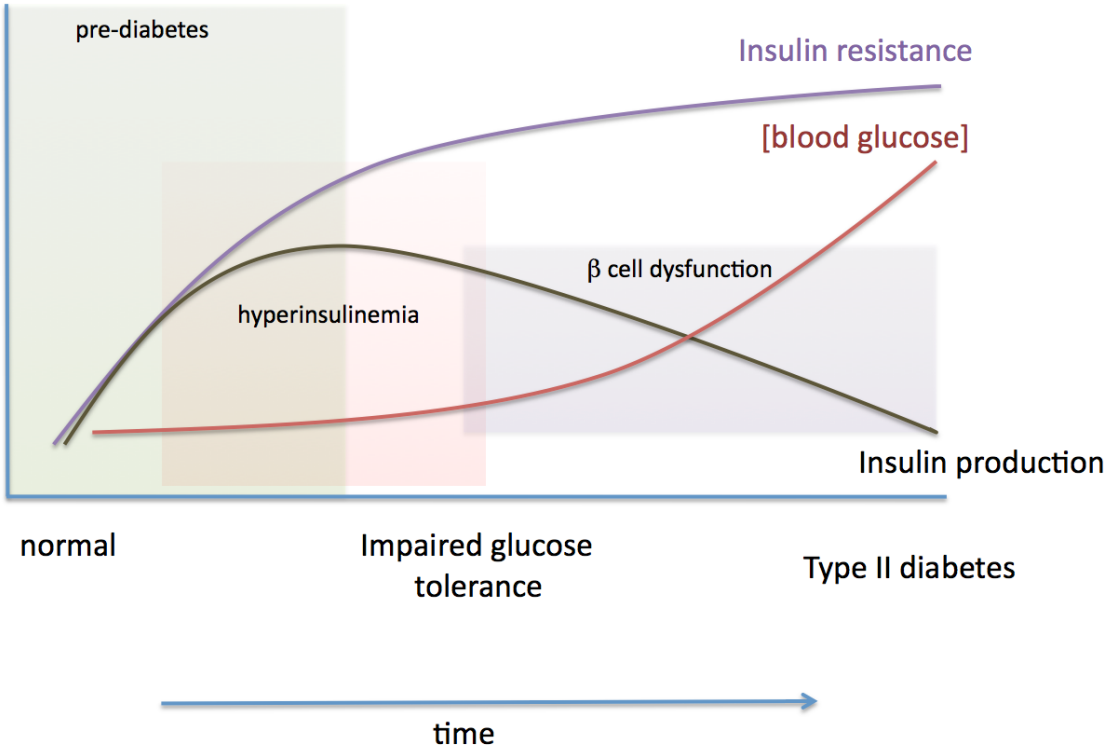

Figure 1.2. Insulin and glucose dynamics during the progression of the metabolic syndrome. As insulin resistance develops, transient compensatory insulin over-production is followed by pancreatic beta cell stress, dysfunction, exhaustion, and eventual loss of insulin producing capabilities. Adapted from Henry, J. *Am J Med*. (1998) 105: 20S-6S.

Lipolysis is the inverse process of lipogenesis (13, 15, 25). Lipolysis comprises the hydrolysis and utilization of the lipids stored in lipid bodies, and is primarily driven by glucagon, epinephrine and norepineprine. The cytokine tumor necrosis factor alpha (TNF-α) is also a major driver of lipolysis in some tissue contexts. This process is activated in times of metabolic demand where the need for energy is imminent. In situations of obesity, where adipocytes in adipose depots have reached their maximum lipid storage capacity, lipolytic cycles are activated in an attempt to ameliorate further conservation of these lipids. For example, the obese abdominal adipose produces high levels of TNF-α in an attempt to regain homeostasis, which is a highly pro-inflammatory event in the development of obesity-associated pathology. However, activated lipolytic cycles in conjunction with the dyslipidaemia most commonly found in obese subjects aid in the maturation of pre-adipocytes, exacerbating the already existing problem. This feed-forward cycle sustains high-

levels of blood fat (dyslipidaemia) and has therefore been implicated in the manifestation of atherosclerotic plaques, insulin resistance and the development of type II diabetes and the metabolic syndrome (8). Although these lipid body depositions are continually replenished through the cyclic process of lipolysis and lipogenesis, the continual surplus of nutrients, particurly dietary fats and carbohydrates, maintains a high-energy balance and progressively exacerbates ectopic lipid deposition (ELD).

1.2. Immunological and inflammatory effects of metabolic perturbation

Obesity is not simply a disease characterized by the deposition of inert fat. It is an inflammatory syndrome (10, 26, 27). When faced with the demands of storing excessive amounts of energy, insulin resistance develops and β-cells of the pancreas overcompensate by hyper-secreting insulin in an effort to clear the blood of sugars that may be toxic in excess (28). Insulin resistance precedes hyperglycemia and type II diabetes. In this chronic hyper-insulinaemic state, insulin, blood sugars and blood lipids are all elevated, exposing cells to a novel milieu of elevated metabolites (29). This state will have marked consequences for many cells and tissues, including those that are components of the immune system. While the effects of this novel milieu on immunological function are largely unstudied, there is clear evidence that individuals at all stages of the development of the metabolic syndrome exhibit baseline alterations in their inflammatory status. The fact that excessive nutrient uptake leads to a state of chronic inflammation creates a clear need to establish whether this 'paraflammation' is causally involved in the development of the symptoms of metabolic syndrome, and thus whether intervening in the inflammation may intervene in the disease.

1.2.1. Systemic inflammation associated with obesity and metabolic syndrome

Metabolic inflammation (10, 26, 30), also termed 'paraflammation', differs from what we classically define as inflammation, which is clinically characterized by the cardinal signs of rubor, calor, dolor and tumor (redness, heat, pain and swelling). For example, in contrast to innate inflammatory responses mounted by pathogenic insults or tissue damage, inflammatory responses in obesity derive from metabolic signals engaged through excessive nutrient uptake. There is also the aspect of chronicity. Normal pathogen- or tissue-induced inflammation is acute and resolved through the ablation of the threat and tissue homeostasis is therefore restored. However, in cases of metabolically-derived inflammation, where the

inflammatory signals are derived from excessive nutrients, inflammatory bouts are long-lived and are in fact made worse by positive feedback mechanisms leading to further dysfunction (10, 26, 30). Paraflammation is characterized by a local inflammatory response observed in metabolic tissue such as adipose tissue and the liver and by systemic increases in plasma IL-6, CRP and other inflammatory cytokines. Lastly, unlike the insulin resistance described in other inflammatory disease states (Hepatitis C, HIV and rheumatoid arthritis), observations of insulin resistance in the context of metabolic dysregulation originate from obese adipose tissue, which secrete inflammatory cytokines capable of inhibiting insulin signalling (31).

Obese patients exhibit increases in systemic inflammatory markers such as interleukin-6 (IL-6) and TNF-α (10, 26, 27, 30, 32). It has been shown that increased accumulation of visceral adipose tissue can lead to increased levels of plasma TNF-α, which in turn alters levels of various other immunological substances such as adiponectin, resistin, plasminogen activator inhibitor-1 (PAI-1) and inflammatory cytokines. It has been suggested that the insulin resistance seen in these patients is triggered by interaction between TNF-α and the TNF-α receptor. A positive feedback loop has been proposed to exist between increases in visceral adipose and increases in TNF-α leading to production of additional adipose and eventual insulin resistance. The recent descriptions of immunological disruption in obesity (and to a lesser extent other metabolic disorders such as anorexia), raises intriguing questions as to the potentially causal relationship between these two phenomena.

1.2.2. Adipose inflammation

The immunology of adipocyte inflammation is complex (10, 26, 27, 30, 32). It begins with the import of excess nutrients from the bloodstream, which are converted and stored as fat and stimulate the production of the hormone leptin. Excess leptin, spurred by a high calorie diet, causes CD4 T cells to produce a second signaling molecule, interferon gamma (IFNγ), which causes adipocytes to express (major histocompatibilty complex class II) MHC II. This dialogue between adipocytes and T cells appears to initiate the inflammatory response to high fat diet. The Hsueh laboratory demonstrated that overfed mice lacking MHCII experienced less inflammation (33). IFNγ from T cells exacerbates the adipocytes' pro-inflammatory behavior and causes another type of immune cell, M2 macrophages, to be converted to their pro-inflammatory (M1) form (34-36).

1.2.3. Altered immunocyte function in obesity and metabolic syndrome

T lymphocytes, macrophages and NKT cells reside in the adipose tissue, are recruited in elevated numbers to obese adipose, and have been suggested to causally contribute to paraflammation. In diet-induced obesity (DIO) models, causal links between the functionality of these cells and the pathologic outcomes of obesity have been established. T lymphocyte populations (T_{reg} and $CD4^+Foxp3^+$ cells) reside in normal adipose and act to restrict inflammation (37, 38). High fat diets promote T-helper (TH) 1 (pro-inflammatory) T lymphocyte biasing, and deficiency of TH1-derived IFNγ lessens the inflammatory phenotype and ameliorates metabolic parameters in obese animals (36, 39). In general, $CD8^+$ cytotoxic T cells accumulate, while a pool of $CD4^+Foxp3^+$, broadly anti-inflammatory, cells is depleted in fat versus lean animals (39). The role of macrophages as contributors to adipose tissue necrosis and inflammation has been widely studied, and these cells are sources of TNF-α and iNOS. In lean fat tissue, macrophages are predominantly the alternatively activated or M2 type (34, 39). In contrast M1 macrophages expressing high levels of TNF-α and IFNγ predominate in obese fat. Macrophages, in their phagocytic role, form 'necrotic crowns' around patches of stressed and dying adipocytes in extremely obese individuals, reflecting the toxic inflammatory environment that results when adipose angiogenesis cannot keep pace with tissue expansion, and together with cellular stress resulting from steatosis within the adipocytes pushes them into a necrotic program. Mice lacking NKT cells present decreased inflammation of the adipose and less glucose intolerance than control animals in models of DIO (26, 40).

The cell type at the center of the work in this thesis is the mast cell. The role of ***mast cells,*** a pro-inflammatory leukocyte (41-44), in obesity and metabolic syndrome is an emerging theme in recent studies. Mast cells are critical to the initiation and maintenance of inflammatory responses, releasing pro-inflammatory mediators including histamine, serotonin, matrix-active proteases, eicosanoids and prostanoids, cytokines and chemokines. Dysregulated inflammation is a feature of the metabolic syndrome and other metabolic disorders and mast cells may contribute causally to metabolic pathology. For example, mast cell deficient mice, or animals exposed to mast cell stabilizing drugs, have markedly different outcomes in obesity and type II diabetic models. In a seminal recent study, the Shi laboratory

showed that mice deficient in mast cells exhibit profoundly decreased weight gain, decreased atherosclerosis, decreased paraflammation, improved glucose metabolism and energy expenditure, in response to a high fat diet (45). Moreover, these benefits could be recapitulated by systemic exposure to a mast cell-stabilizing drug more commonly used to treat allergic inflammation (45). The potential mechanisms by which mast cells could influence adipose development are numerous. Mast cells secrete pro-angiogenic factors that may play a role in the neovascularization of expanding adipose depots, and are sources of growth factors that could drive adipocyte and interstitial fibroblast hyperplasia (46-48). They are sources of IL-4, which in lean adipose maintains the M2 bias of resident macrophages, and of TNFα and IL-6 (42), which may play roles in paraflammation.

These data suggest that mast cell-derived signals impact metabolic processes. Conversely, there is *in vivo* evidence that metabolic and endocrine signals alter the outcome of mast cell-derived inflammation. Rats with streptozotocin- or alloxan-induced type I diabetes exhibit severely compromised anaphylactic responses to antigenic ligation of the high affinity receptor for IgE (FcεRI) antigen or secretagogue, as well as diminished airway sensitivity (49-52). Indeed, reconstitution of mast cells responses reverses the refractoriness to allergen challenge that is seen in alloxan-induced diabetic rats (53). There is also epidemiological evidence that type I diabetics, who are insulin deficient, are protected from Th2/mast cell driven inflammatory disorders such as eczema, allergic asthma and other atopic spectrum disorders. These data suggest, intriguingly, that insulin deficiency directly affects mast cell responsiveness.

Mast cells have been long understood as pluri-responsive integrators of pro-inflammatory signals derived from diverse sources (innate and adaptive immune stimuli, physicochemical inputs and neurotransmitters). They are also understood as pluri-potent, with the ability to affect their tissue environment through the release of an extremely broad array of inflammatory mediators. It now seems clear that mast cells may be coupled to the metabolic status of tissues in which they reside. Our understanding of mast cell responses to metabolic and endocrine inputs is poor, but the study of these pathways will lead to new insights into the physiological and pathophysiological mechanisms by which inflammatory processes are controlled.

1.3. Ectopic lipid deposition at the organ, tissue and cellular level

Ectopic lipid deposition (ELD) is a central hallmark of excess lipid storage in response to a nutrient-dense environment (20, 21, 25). Lipid deposition (adipose expansion) is not always pathological. Indeed, humans are well adapted to the healthy storage of increased subcutaneous fat (Figure 1.3), which is an obvious evolutionary advantage. However, under conditions of continuous nutrient density (the obesogenic environment), to which we have not adapted evolutionarily, there is a spill-over effect (Figure 1.3) where lipid deposition starts to occur outside of the adipose, which itself becomes inflamed and unhealthy. This ELD is associated with the dyslipidemia that is a hallmark of metabolic syndrome.

The action of insulin is best studied in adipocytes, myocytes and hepatocytes, where insulin initiates and promotes the lipogenesis of neutral triglycerides, which are then stored within cytoplasmic lipid bodies. ELD occurs in the liver, heart, skeletal muscle and pancreas alongside the adipocyte hyperplasia and adipocyte steatosis that comprise the expansion of central fat depots during obesity. Moreover, an immunocyte, the macrophage, becomes steatotic (the 'foam cell' phenotype) when resident in the high fat environment of an atherosclerotic plaque (54).

At the cellular level, ELD manifests as the accumulation of lipid droplets in the cytosol, in strikingly high numbers (16, 17, 19, 20). It seems likely that occlusion of the cytosol with large numbers of lipid structures would impact the cell in numerous ways, from cytoskeletal rearrangement/disruption, to repositioning of organelles and potentially altered behaviour of signaling molecules and second messengers. Surprisingly, this is a little studied area in the steatosis literature. There is some evidence that calcium dynamics are altered in steatotic cells. For example, cardiomyocyte data suggests that calcium signals are dampened by the presence of LD in the cytosol, possibly due to the LD themselves acting as calcium sinks (55). In this case, then the addition of a large number of calcium sinks to the cytosol would dramatically alter activation outcomes for steatotic cells. In steatotic hepatocytes, intermediate filament expression is altered (56) and in foam cells, there is strong evidence for altered outcomes of innate receptor activation relative to non-steatotic macrophages. Thus while cells that exhibit this steatosis do have altered functional phenotypes, the mechanistic

links between cytosolic LD/LB accumulation and defective cellular signaling and functional responses have not been widely explored.

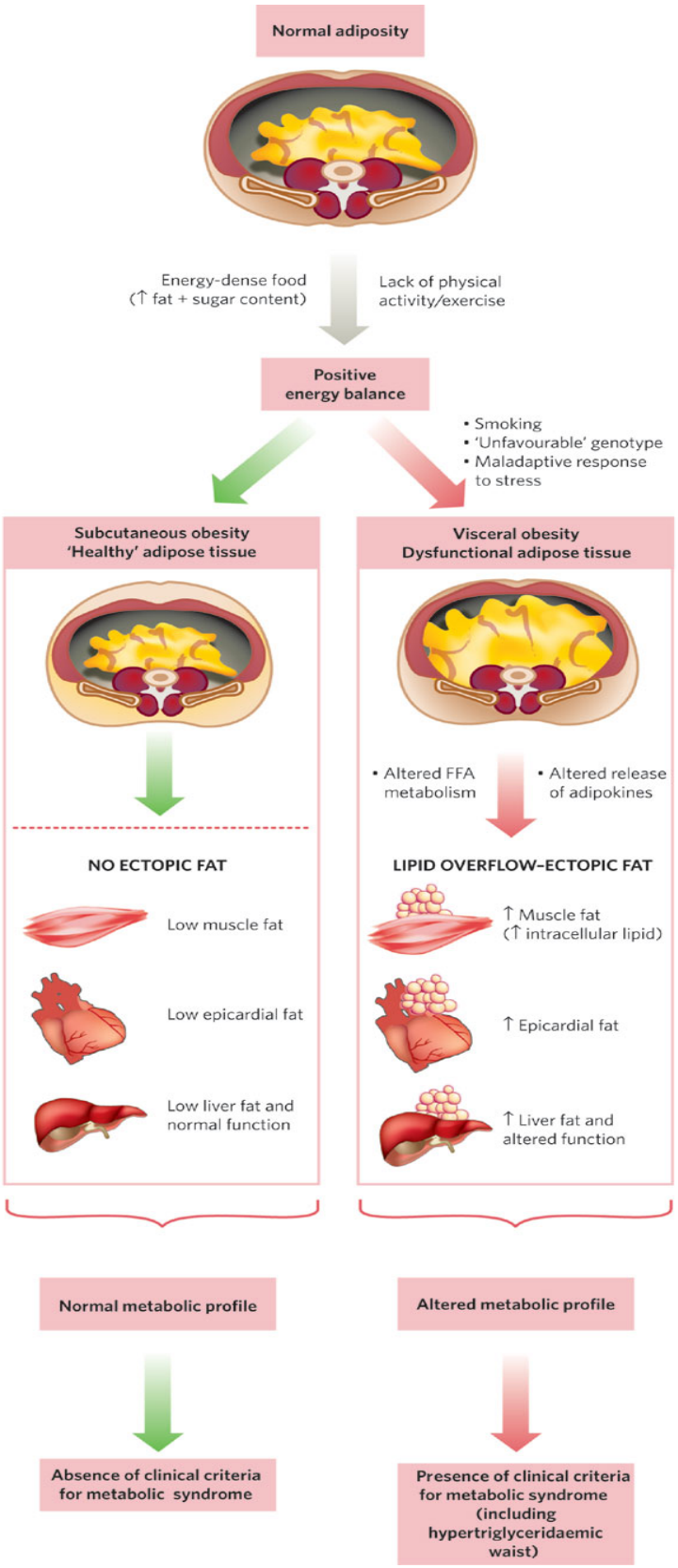

Figure 1.3. Normal and Ectopic lipid deposition resulting from a positive energy balance. Excess nutrient intake over expenditure results in positive energy balance. Deposition of subcutaneous ("healthy") adipose tissue proceeds and a normal metabolic profile is maintained. However, in response to chronic excess caloric intake, or when combined with other co-morbidity factors/predispositions, visceral deposition of dysfunctional, inflamed, adipose occurs. High circulating levels of free fatty acids overwhelm the storage capacity of the classical adipose depots, and new depots in ectopic locations (muscle, liver and the pericardium) are established. From Despres and Lemieux. Nature (2006) 444: 881-87.

1.4. The lipid body

1.4.1. Lipid body structure and composition

Lipid bodies, also known as lipid droplets, fat bodies, liposomes or adiposomes, can be found in most eukaryotic cells (16-20, 57-59). Lipid bodies are most appreciated for their role as intracellular lipid storage units and have been most characterized in the adipocyte system due to the ability of this cell system to generate large lipid droplet reserves. The lipid body itself is composed of a unilamellar phospholipid shell embedded with various regulatory proteins, such as the PAT family of proteins (described in more detail in Chapter 3) responsible for storing and mobilizing the core contents (60-63). This unilamellar layer partitions a neutral lipid core that is rich in triacylglycerols and cholesterol esters (19). During obesity, adipocyte lipid bodies are often highly enriched and other cells including macrophages, enterocytes, adrenocortical cells, pancreatic β-cells, skeletal and heart myocytes and hepatocytes may also develop large volumes of lipid droplets (20, 21, 25). Lipid bodies have historically been understudied and assumed to be fairly inert structures with little importance beyond providing an energy source for the cell, however, recent descriptions of protein variation between these organelles and the emerging importance of lipids in health and disease, have prompted further investigation (16, 18, 21, 64-66).

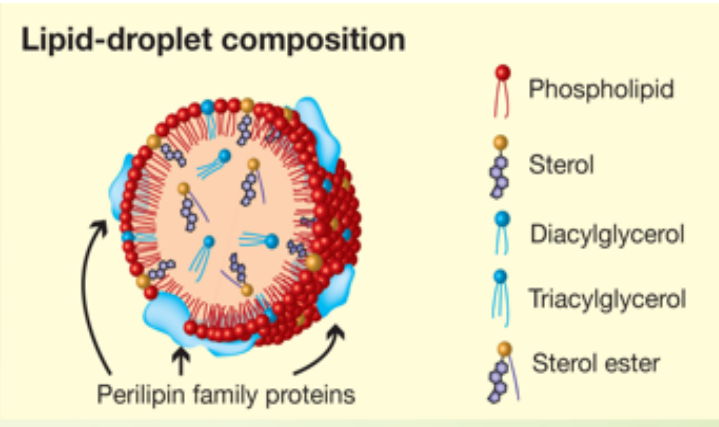

Figure 1.4. Compositional model for the adipocyte lipid body. A unilamellar phospholipid layer contains embedded PAT family proteins and proteins involved in biogenesis of the LB, lipogenesis and lipolysis. Various lipid species are stored in the hydrophobic lipid core. From Farese and Walther. J. Cell Sci. (2009) 122: 749-752.

1.4.2. Lipid body biogenesis from the endoplasmic reticulum

Eukaryotic lipid bodies have been suggested to stem from the ER based on ultrastructural observations of their close association with ER lamellae, in addition to the partial ER membrane sheets that are often observed on or around lipid bodies. It is also understood that the enzymes responsible for catalyzing the synthesis of neutral lipids (found in the lipid body core) reside within the lumen of the ER. Several theories exist as to the exact formation of lipid bodies from the ER, all of which involve some degree of contribution of the inner and outer leaflets of the ER membrane lensing or budding to accommodate the newly synthesized neutral lipids (20, 59, 60, 62, 67). Severance of the lipid body from the ER produces a nascent lipid body (the primordial lipid body population) that upon fission and fusion events with other lipid bodies, form larger and more mature lipid bodies.

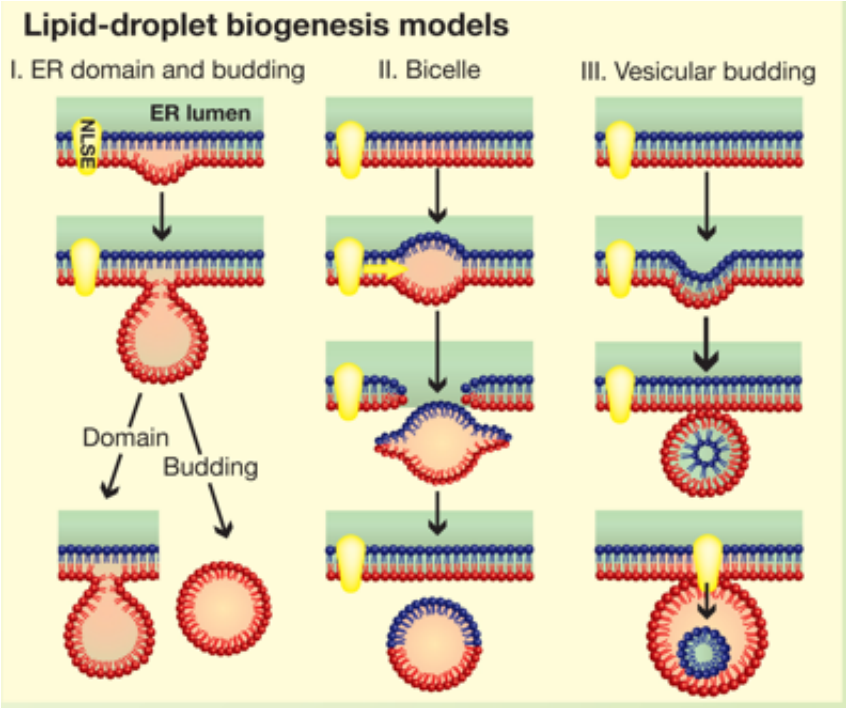

Figure 1.5. Models for lipid body biogenesis. In models I and II Neutral Lipid Synthesis Enzymes (NLSE) reside in the ER and produce lipid that forms a lens between the ER lamellae that buds in a unilateral or bilateral manner to form the lipid body. An alternate model III proposes that there is vesicular budding from a highly curved ER membrane, followed by NLSE-mediated filling of the nascent LB. From Farese and Walther. J. Cell Sci. (2009) 122: 749-752.

1.4.3. Lipid body formation and ER stress

Chronic bouts of metabolic stress induced through excessive nutrient intake have been shown induce ER stress in a number of different cell types and tissues. ER stress leads to the activation of endoplasmic reticulum associated degradation (ERAD), which involves the cessation of protein translation and an activation of a transcriptional program aimed to facilitate proper protein chaperoning and folding (68, 69). This stress response has particularly been observed in a variety of situations involving excessive lipid body deposition. For example, progressive atherosclerotic plaque formation due to the retention of apolipoprotein-B rich lipoproteins has been shown to induce ER stress (70). ER stress has also been observed in the obese liver and adipose tissue as demonstrated through the use of high fat diet fed *in vivo* mouse models. These data indicate a correlation between lipid body deposition and cellular stress responses and suggest that lipid body deposition may influence functional changes in a variety of cell types (71).

1.4.4. The cycle of lipogenesis/lipolysis at the level of the lipid body

In the adipocyte system, lipid body regulation is a highly orchestrated process involving a variety of protein mediators that participate in trafficking stored lipids (Figure 1.6). Specific proteins known to be involved in these processes are the PAT family of proteins, which is an abbreviation for perilipin, adipose differentiation-related protein (ADRP or adipophilin), and tail-interacting protein of 47 kDa (TIP47) (20, 60, 62, 63, 67, 72-74). Expression of the PAT family proteins are markers of adipocyte differentiation and these proteins, especially perilipin, act as gate-keepers on the surface of lipid bodies in regulating their contents (21), and the access of cellular metabolic pathways to those contents. For example, adrenalin-activated phosphorylation of perilipin leads to the disruption of the perilipin shell and allows access of hormone sensitive lipase (HSL), which is also phosphorylated in response to adrenalin, access to the neutral lipid core. HSL leads to the lipolytic release of stored lipids from within the lipid body and hyperactive lipolytic cascades have been implicated in more severe dyslipidaemia, insulin resistance and exacerbated atherosclerotic plaque formation.

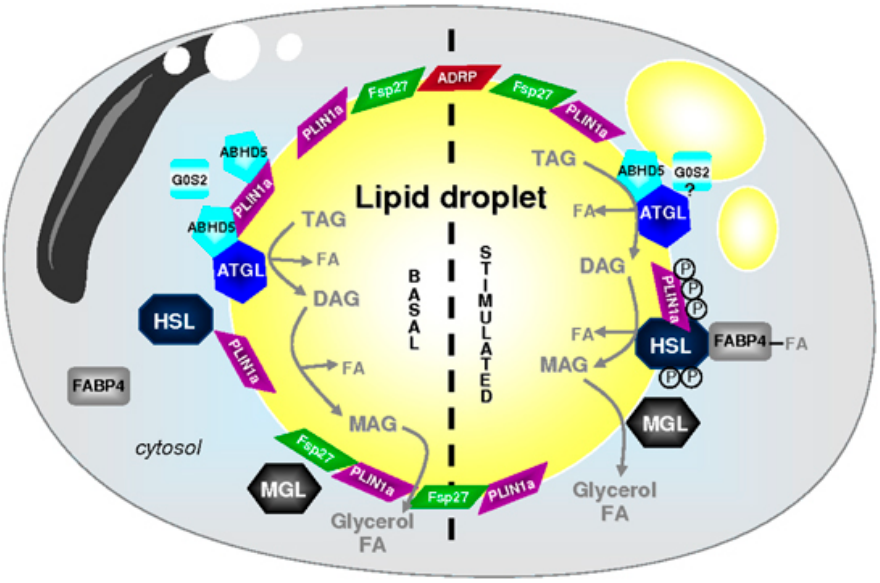

Figure 1.6. Lipogenesis and lipolysis at the level of the individual lipid droplet. PAT family proteins are involved in LB biogenesis, filling and metabolism. Stimulated conversion of FA and triglycerides occur in response to stimulation of either lipogenic or lipolytic pathways. Reproduced from Girousse and Langan, (2012) *Int. J. Obesity* 36: 581-594.

1.5. Lipid bodies in mast cells and basophils

The role of mast cells, a pro-inflammatory leukocyte, in obesity and metabolic syndrome is an emerging theme in recent studies (45, 48). Mast cells are critical to the initiation and maintenance of inflammatory responses, releasing pro-inflammatory mediators including histamine, serotonin, matrix-active proteases, eicosanoids and prostanoids, cytokines and chemokines. Dysregulated inflammation is a feature of the metabolic syndrome and other metabolic disorders and mast cells may contribute causally to metabolic pathology (45). For example, mast cell deficient mice, or animals exposed to mast cell stabilizing drugs, have markedly different outcomes in obesity and type II diabetic models (45). In an important recent study, the Shi laboratory showed that mice deficient in mast cells exhibit profoundly decreased weight gain, decreased atherosclerosis, decreased paraflammation, improved glucose metabolism and energy expenditure, in response to a high fat diet (45). Moreover, these benefits could be recapitulated by systemic exposure to a mast cell-stabilizing drug more commonly used to treat allergic inflammation (45). The potential mechanisms by which mast cells could influence adipose development are numerous. Mast cells secret pro-angiogenic factors that may play a role in the neovascularization of expanding adipose

depots, and are sources of growth factors that could drive adipocyte and interstitial fibroblast hyperplasia (42, 43, 48, 75). They are sources of IL-4, which in lean adipose maintains the M2 bias of resident macrophages, and of TNFα and IL-6, which may play roles in paraflammation (42). These data may suggest that mast cell-derived signals impact metabolic processes. In addition, there is *in vivo* evidence that metabolic and endocrine signals alter the outcome of mast cell-derived inflammation. Rats with chemically or surgically-induced type I diabetes exhibit attenuated anaphylaxis. These can be restored by reconstitution of mast cells. Thus insulin deficiency directly affects mast cell responses and their pro-inflammatory capacity by an unknown mechanism (49, 50, 53, 76, 77).

Mast cells contain two specialized pro-inflammatory organelles. Secretory granules are modified lysosomes that bear histamine, serotonin, and matrix active proteases within a proteoglycan matrix (42, 46, 75, 78-82). Far less studied are the cytoplasmic lipid bodies that are found in mast cells, neutrophils, macrophages and eosinophils (83-87). These lipid bodies may play a role in the immunocyte that is distinct from the contribution to neutral triglyceride storage and cellular metabolism made by the analogous organelle in adipocytes, although a comparative analysis of the lipid and protein complement of mast cell and adipocyte lipid bodies has not been undertaken.

Immunocyte lipid bodies (LB) are enigmatic structures, with their formation, content and dynamics largely unstudied. LB in granulocytes such as neutrophils and eosinophils increase in number during infection, and are mobilized (dynamically depleted of their contents) during cellular activation (85, 88-90). In mast cells, and other leukocytes, lipid bodies have been suggested as reservoirs of the eicosanoid precursors for bioactive signaling lipids such as leukotrienes, and sites for eicosanoid synthesis (54, 84, 91-93). Furthermore, it has been suggested that leukocyte associated lipid bodies are specialized, inducible intracellular domains that function as signaling platforms. Lipid bodies in this context have been linked to regulating lipid metabolism and lipid trafficking, controlling both the synthesis and secretion of particular inflammatory mediators and responding to infections. It is for these reasons that these lipid bodies appear as attractive potential therapeutic targets for both innate and acquired immunopathologies.

The volume, regulation, composition and therefore function of lipid bodies have been shown to vary considerably between cell types. For example, macrophage associated lipid bodies

have repeatedly been shown to store lipid bodies rich in cholesterol esters, a hallmark of atherosclerotic lesions (54). However, as alluded to above, the Dvorak and Weller laboratory have demonstrated through the use of electron micro-radiographic methods that the lipid bodies associated with eosinophils, neutrophils and mast cells incorporate the majority of the arachidonate lipids provided by the extracellular milieu, in addition to the enzymes responsible for their conversion to a variety of lipid-derived inflammatory mediators (84, 90, 94). Still not understood however, are the basal composition or any compositional changes induced in mast cell lipid bodies in response to acute or chronic stimulation.

Studies investigating lipid bodies in mast cells have largely been ultrastructural and qualitative. Several radiolabeling/radioincorporation studies performed using EM suggest that mast cell lipid bodies are reservoirs of arachidonic acid and synthetic enzymes for eicosanoid pro-inflammatory mediators, and that the contents of lipid bodies are discharged into exosomal structures upon antigen receptor stimulation (85, 95). Thus the potential for a mast cell to generate mediators such as leukotriene C4 (LTC4) may be related to the size of the pool of precursors represented by these lipid bodies. Recently, Kovanen *et al* have shown that human mast cells generate lipid bodies as they mature and that these lipid bodies are sources of triglycerides, analogous to adipocyte lipid bodies, when grown in the presence of serum free media (83). The group also concluded that although lipid bodies are present in mast cells from various human tissues, the exact factors that influence these organelles in the various tissue microenvironments is still largely unknown. With the exception of these few studies, very little is known regarding lipid bodies in the context of mast cells or the mechanisms responsible for their biosynthesis, regulation and contents.

1.6. Questions

The central questions that have driven the work presented in this thesis are:

(1) Do mast cells respond to insulin in a manner that changes their pro-inflammatory function?

(2) Could mast cells be involved causally in the generation of metabolic inflammation?

(3) Is the mast cell lipid body a central arbiter of the cells response to, and contribution to, metabolic and endocrine inputs?

1.7. Central hypothesis of this work

We hypothesize that the abundance and chemical composition of mast cell lipid bodies is regulated by insulin.

Chapter Two

Materials and Methods

2.1. Cell culture

RBL2H3 (96) were grown at 37 °C, 5% CO_2, in 95% humidity in Dulbecco's Modification of Eagle's Medium (Mediatech Inc., Herndon, VA) with 10% heat-inactivated Fetal Bovine Serum (Mediatech), 2mM Glutamine and 1mM Sodium pyruvate. C57.1 murine mast cells were grown in RPMI, 10% FBS, 2mM l-Gln, 2mM NEAA, 1mM Sodium pyruvate, 50μM 2-mercaptoethanol, and 5ng/ml IL-3 at 37 °C, 5% CO_2, in 95% humidity. 3T3-L1 were grown at 37 °C, 5% CO_2, in 95% humidity in Dulbecco's Modification of Eagle Medium (Mediatech Inc., Herndon, VA) with 10% heat-inactivated Bovine Calf Serum (Hyclone), 2mM Glutamine and 1mM Sodium pyruvate.

2.2. Chemicals, Reagents and Dyes

General chemicals were from VWR (West Chester, PA) and Sigma Aldrich (St. Louis, MO). PMA and Ionomycin were from Calbiochem (Gibbstown, NJ). IgE anti-DNP, Filipin and berberine sulfate were from Sigma and KLH-DNP was from Calbiochem. Nile Red, Oil Red O and hematoxylin were from EMD Chemicals (Gibbstown, NJ) and ScyTek Laboratories (Logan, UT) respectively. 6-Propionyl-2-Dimethylaminonaphthalene (Prodan), 1,6-Diphenyl-1,3,5-Hexatriene (DPH), 6-Dodecanoyl-2-Dimethylaminonaphthalene (Laurdan), LipidTOX, Concanavalin A, 4′,6-Diamidino-2-Phenylindole (DAPI), Fluo4, and HRP conjugated secondary antibodies were from Invitrogen (Temecula, CA) and Amersham (Piscataway, NJ).

2.3. Cell Stimulations

FcεRI stimulation used 0.1μg/ml IgE anti-DNP for 16 hours at 37^{o}C, followed by three washes and the addition of 250ng/ml KLH-DNP for the indicated times. PMA and ionomycin

were used at 500nM and 500nM respectively. Insulin-FDI (IFDI) comprised insulin, FBS, Dexamethasone and IBMX at 0.01mg/ml, 10% (w/v), 0.25μM and 2.5μM, respectively. Induction of lipogenesis/adipogenesis was performed in both 3T3-L1 adipocytes and RBL2H3 mast cells through the treatment of the lipogenic cocktail (mentioned above) for 6 days, beginning 24 hours after seeding. Unless otherwise indicated, cells were then harvested for analysis on day 7.

2.4. Antibodies

Antibodies were from the following suppliers: anti-COX1, anti-COX2, anti-Perilipin A and B, anti-PPARγ, anti-HSL, anti-ATL, anti-GLUT4, Abcam (Cambridge, MA); anti-5-LO, anti-GLUT5, Santa Cruz (Santa Cruz, CA), anti-TIP47, Novus (Littleton, CO); anti-ADFP, Biovision (Mountain View, CA); anti-LTC4 Synthase, Santa Cruz (Santa Cruz, CA); anti-ABHD5, anti-phospho JNK1/2, anti-ATF6, anti-GLUT4, anti-CD36, anti-NFATC1, anti-ITPR1, anti-ITPR2, anti-ITPR3, anti-SERCA 2a/2b, anti-PMCA1, Abcam (Cambridge, MA); anti-phospho PERK-thr380, anti-IRE1α, anti-phospho AMPKβ1-ser108, anti-phospho Acetyl-CoA Carboxylase-ser79, anti-phospho AMPKα-thr172, anti-AMPKα, anti-AMPKβ1/2, anti-Acetyl-CoA Carboxylase, anti-IRS1, anti-IRS2 and anti-Grb2, Cell Signalling (Danvers, MA); anti-CRACM1, ProSci (Poway, CA).

2.5. Cell Lysis and Western blot

Cells were pelleted (2000*g*, 2 min) and washed once in ice cold PBS. Western blots were performed using $5x10^6$ cells/lane unless otherwise indicated. Cells were lysed (ice/30 minutes) in 350μl of lysis buffer (50mM Hepes pH 7.4, 250mM NaCl, 20mM NaF, 10mM iodoacetamide, 0.5% (w/v) Triton X100, 1mM PMSF (phenylmethylsulfonylfluoride), 500 mg/ml aprotinin, 1.0 mg/ml leupeptin and 2.0 mg/ml chymostatin). Lysates were clarified (17,000*g*, 20 min). For preparation of total protein, lysates were acetone precipitated (1.4 volumes acetone for 1h at -20^oC, followed by centrifugation at 10,000*g* for 5 min). Protein samples were resolved by 10% SDS-PAGE under reducing conditions in a modified Laemmli buffer. Resolved proteins were electro-transferred to PVDF membrane in 192mM glycine, 25mM Tris (pH 8.8). For Western blotting, membranes were blocked using 5% non-fat milk in PBS for 1 hour at room temperature. Primary antibodies were dissolved in

PBS/0.05% Tween-20/0.05% NaN_3 and incubated with membranes for 16 hours at 4°C. Developing antibodies comprised anti-rabbit or anti-mouse IgGs conjugated to horseradish peroxidase (Amersham). These were diluted to 0.1μg/ml in PBS/0.05% Tween-20 and incubated with membranes for 45 minutes at room temperature. A standard washing protocol (four washes of 5 min in 50ml PBS/0.1% Tween-20 at room temperature) was employed between primary and secondary antibodies and following secondary antibody. Signal was visualized using enhanced chemiluminescence (Amersham) and exposure to Kodak BioMax film. Films were scanned at >600 dpi and quantification was performed using Image J (NIH).

2.6. Histology staining for lipid content

Cells were plated on coverslips and fixed with 0.4% (w/v) paraformaldehyde (1h, RT), washed twice with dH_2O and stained with 200 μl Hematoxylin-Gill #2 (5 min RT). Coverslips were washed twice with tap water before staining with Oil Red (0.35% in 6:4 EtOH:water, 15 min RT followed by two dH_2O washes). Berberine sulfate was used at 0.025%, pH4.0, 30 minutes at RT (97, 98). Coverslips were mounted in Crystal-Mount (Electron Microscopy Sciences, Hatfield, PA) for imaging. Bright field and fluorescence imaging were performed on a Nikon Ti Eclipse fluorescence microscopy system, and analysed in NIS Elements (Nikon).

2.7. Calcium assay (bulk method)

RBL2H3 were washed incubated with 1μM Fluo-4 for 30 minutes at 37°C in a standard modified Ringer's solution of the following composition (in mM): NaCl 145, KCl 2.8, CsCl 10, $CaCl_2$ 10, $MgCl_2$ 2, glucose 10, Hepes·NaOH 10, pH 7.4, 330 mOsm. Cells were transferred to 96-well plates at 50 000 cells/well and stimulated as indicated. Calcium signals were acquired using a Flexstation 3 (Molecular Devices, Sunnydale, USA). Data was analyzed using SoftMax® Pro 5 (Molecular Devices). Where indicated, nominally calcium-free external conditions were achieved by the preparation of 0mM added $CaCl_2$ Ringer solution containing 1mM EGTA.

2.8. Calcium assay (single cell method)

RBL2H3 were plated on glass coverslip dishes and incubated with 1μM Fluo-4 for 30 minutes at 37°C in a standard modified Ringer's solution as above. Cells were stimulated as indicated on a 37° C heated stage. Calcium signals were acquired using a Nikon Ti Eclipse confocal microscopy system, using EZ C1 software for acquisition and NIS Elements software (Nikon) for analysis. Where indicated, nominally calcium-free external conditions were achieved by the preparation of 0mM added $CaCl_2$ Ringer solution containing 1mM EGTA.

2.9. Leukotriene C4 Assay

RBL2H3 were treated as indicated and stimulated via the FcεRI or using PMA/ionomycin. After a 1 hour incubation, supernatants were assayed for the concentration of LTC4 using a specific EIA kit (Cayman Chemicals, Ann Arbor, MI) and in reference to a standard curve. Color development proceeded for 45 minutes and absorbance was read at 405 nm.

2.10. Beta-hexoseaminidase assay

RBL2H3 were plated in cluster plates at $5x10^4$ cells/well. Monolayers were washed and incubated in 200 μl Tyrode's buffer before stimulating as described. After 45 minutes at 37°C, 25 μl supernatant was removed, clarified by microcentrifugation, and transferred to a 96 well plate containing 100 μl per well 1 mM *p*-N-acetyl glucosamine (Sigma) in 0.05 M citrate buffer pH 4.5. After 1 hour at 37°C reactions were quenched by the addition of 100 μl per well 0.2 M glycine, pH 9.0. Beta-hexosaminidase levels were read as OD at 405 nm. Results are shown as the mean $\pm$ standard deviation.

2.11. Flow cytometry

Cells were fixed in 0.4% paraformaldehyde (45 min, RT) and resuspended at $1x10^6$ cells/ml in FACS buffer (HBSS, 0.5% BSA, 0.05% NaN_3). For lipid body analysis, cells were stained with Nile Red (0.1 μg/ml, 30 min RT). For berberine sulfate (BS) staining, cells were incubated with 0.025% BS, pH 4.0 (20 min RT) (98). For immunocytochemistry analysis, cells were harvested as above and resuspended in FACS buffer. Appropriate flow cytometry controls were performed to block non-specific binding of primary and secondary antibodies

to surface Fcγ receptors on mast cells. Unpermeabilized cells were blocked for 1 hour with BSA followed by rabbit anti-mouse mixed IgGs. Permeabilization was with 0.1% TX100 for 4 minutes, followed by washing. Primary antibodies were incubated for 30 minutes at RT at a concentration of 0.1-1 μg/ml. After three washes, cells were incubated with 0.05 μg/ml of the indicated Alexa-coupled secondary antibody (Invitrogen). Fluorescence was assessed on a FACSAria Flow Cytometer (BD Bioscience, Franklin Lakes, NJ) at the John A. Burns School of Medicine Flow Cytometry Facility. Flow cytometry data were analyzed in FlowJo version 9.02.

2.12. Triglyceride Assay

A Triglyceride Quantification Kit (99) from BioVision was used as follows: Cells were harvested, washed in PBS and homogenized in 5% Triton X-100. The homogenate was twice heated slowly to 100^{o}C then slowly cooled to RT. After centrifugation the supernatant was incubated with lipase for 20 minutes at RT, followed by incubation with triglyceride reaction mix for 1 hour at RT. The O.D. was read at 570 nm.

2.13. Quantitative Real Time PCR Analysis

RNA was extracted from 6 day unstimulated and IFDI stimulated RBL2H3 cells using a Qiagen protocol. cDNA was synthesized from 600 ng of total RNA using the High-Capacity cDNA Transcriptase Kit (Applied Biosystems, Foster City, USA). TaqMan Gene Expression Assays were used (Applied Biosystems) for IL-6 (Assay ID Rn01410330_m1) and beta-actin (Assay ID Rn00667869_m1). The amplifications were carried out in 10μl containing 1xTaqman Fast Universal Master Mix, 1xTaqman Gene Expression Assay and purified target cDNA. The cycling parameters were 30 seconds at 94^{O}C; 40 cycles at 94^{O}C for 3 seconds; 60^{O}C for 30 seconds using the StepOnePlus (Applied Biosystems). Amplifications were performed in triplicate. Signals were normalized to expression of beta-actin. Analysis used the method of Pfaffl *et al* (100).

2.14. Micro array analysis

RNA was extracted from 6 day unstimulated and IFDI stimulated RBL2H3 cells as described above. Agilent RNA Spike-In, One Color Mix (Agilent, Santa Clara, USA) was prepared as

instructed by the manufacturer. 100ng RNA was converted into cRNA and labeled with cyanine-3 with Low Input Quick Amp Labelling Kit (Agilent Technologies, Santa Clara, USA) on the Thermocycler (MJ Research Thermocycler Tetrad Model PTC-225). The samples were purified using RNeasy mini columns (Qiagen, Hilden, Germany) and the quality and quantity of the cRNA was assessed using Nanodrop (ND-2000C). Using the one-color protocol, equal amounts of Cy3-labeled cRNA (1500ng) from stimulated and non-treated cells were hybridized in duplicates to Agilent Whole Rat Genome Microarray 4x44K (G4131F) for 17 hrs at 65 °C. The microarray comprised of 45,000 probes, representing over 41,000 transcripts. The hybridized microarrays were then washed using the manufacturers recommended conditions and scanned using an Agilent G2565CA scanner. Data were extracted from the scanned image using Agilent Technologies Feature Extraction software version (10.5.1.1). All data columns present in the extracted data files are described in detail in the Agilent Feature Extraction Software Reference Guide v 10.7. All data was processed using Agilent Genespring Gene Expression Software v 11.5. Intensities were scaled to the median of all samples and no baseline normalization was performed. Using the software, fold changes with associated p-values were calculated. For statistical analyses, an unpaired t-test was performed, using Benjamini-Hochberg for multiple testing amongst the duplicates. Fold-changes above 2 were regarded as upregulated. Down-regulation was defined as a change to less than 50% of the control spot intensity.

2.15. Lipidomic analysis

The lipids were extracted in the presence of authentic internal standards by the method of Folch et al. using chloroform:methanol (2:1 v/v). For the separation of neutral lipid classes (FFA, TAG, DAG, FC, CE), a solvent system consisting of petroleum ether/diethyl ether/acetic acid (80:20:1, by vol) was employed. Individual phospholipid classes within each extract were separated by liquid chromatography (Agilent Technologies model 1100 Series). Each lipid class was trans esterified in 1% sulfuric acid in methanol in a sealed vial under a nitrogen atmosphere at 100°C for 45 min. The resulting fatty acid methyl esters were extracted from the mixture with hexane containing 0.05% butylated hydroxytoluene and prepared for gas chromatography by sealing the hexane extracts under nitrogen. Fatty acid methyl esters were separated and quantified by capillary gas chromatography (Agilent

Technologies model 6890) equipped with a 30 m DB 88 capillary column (Agilent Technologies) and a flame ionization detector. Whole cell and microaspirated lipid body lipidomic analysis was performed in collaboration with Metabolon Inc, while isolated ER fraction lipidomic analysis was performed in collaboration with Dr. Shari Forbes (University of Ottowa Institute of Technology). ER lipids were isolated using a modified Folch method and analyzed utilizing the Supelco FAME-23 lipid standards (Sigma). The datasets presented in the form of heatmaps were generated using Tree View, a software program developed by Michael Eisein, which provides a computational and interactive graphical environment for analyzing, visualizing and browsing data from DNA microarray experiments, or other large 'omic' datasets.

2.16. ER/microsomal and lipid body preparation by ultracentrifugation

A protocol was adapted from Endoplasmic Reticulum Isolation kit from Sigma. Cells were trypsinized, harvested and counted. Cells were then washed twice in PBS and centrifuged at 600*g* for 5 minutes in a 15ml centrifuge tube. The cell pellet volume was estimated and resuspended in 3 volumes of hypotonic buffer (1 ml 10X stock, 100 µL protein inhibition cocktail, 8.9 ml dH_2O) and incubated on ice for 20 minutes. Cells were centrifuged at 600*g* for 5 minutes at 4ºC. Cells were resuspended in 2 volumes of Isotonic buffer (4 ml 5X stock, 200 µL protein inhibition cocktail, 15.8 ml dH_2O) and broken open using a syringe and 19 gauge needle (~20 strokes). Cells were centrifuged at 1000*g* for 10 minutes at 4ºC. The thin floating lipid layer was aspirated and the supernatant was transferred to a microfuge tube. Supernatant was centrifuged at 12,000*g* for 12 minutes at 4ºC. The thin floating lipid layer was aspirated again and the supernatant was transferred to an ultra-centrifuge tube with the volume topped off with isotonic buffer, which was centrifuged 100,000*g* for 60 minutes at 4ºC. Supernatant was aspirated and the ER pellet was stored at -80ºC prior to lipidomic analysis.

2.17. Lipid body isolation

Mast cells exposed to the insulin-FDI treatment for 6 days were harvested, washed twice in PBS and resuspended in 1.15 ml disruption buffer (25 mM Tris-HCl, 100 mM KCl, 1 mM EDTA, 5 mM EGTA, adjusted to a pH of 7.4) and then homogenized using a Dounce manual

homogenizer. The cavitate was collected drop-wise and mixed with an equal volume (1.15ml) of disruption buffer containing 1.08 mol/L sucrose, which was then centrifuged at 1500*g* for 10 minutes in order to pellet the nuclei. The supernatant was then transferred to a 4.6ml ultracentrifugation tube and sequentially overlaid with 767μL each of 0.27mol/L sucrose buffer, 0.135mol/L sucrose buffer and a TOP solution (25mM Tris, 1mM EDTA, 1mM EGTA, adjusted to a pH of 7.4). The solution was then centrifuged at 150,500*g* (60,000rpm) for 60M at 4°C. 8 fractions of 575μL were collected from top to bottom as follows: the buoyant lipid bodies (layers #1 and 2) = 1.15ml, the mid-zone (layers #3 and 4) between lipid bodies and cytosol = 1.15ml, the cytosol (layers #5-8) = 2.30ml, the microsomal pellet (layer #9) and the nuclei (layer #10). The fractions were then resuspended in 1.5ml of TOP solution by sonication. The protein content in each fraction was measured by a micro BCA assay using bovine serum albumin as a standard.

2.18. Lipid body micro-aspiration

3T3-L1 pre-adipocytes and RBL2H3 cells were grown in the presence of insulin-FDI for 6 days on Matek dishes equipped with glass coverslips. Cells were visualized using a Nikon Eclipse C1 plus confocal microscope system using a 100X objective and digital zoom capabilities when necessary. Lipid bodies were extracted from individual cells using our developed intracellular lipid body microaspiration apparatus consisting of a TransferMan NK2 micromanipulator (Eppendorf), a CellTram Vario (Eppendorf) and an ICSI TransferTip micropipette (Eppendorf). Individual lipid bodies were extracted in small numbers (~10-100) to prevent lipid peroxidation and manually deposited into Target I-D vials with a polyspring insert (National Scientific) containing ~150 μl of hexane. Lipid isolation was validated by microscopically observing TransferTip micropipettes post-lipid body collection both before and after solvent treatment. Collection tubes and inserts were supplied by Dr. Bob Borris at the University of Hawaii Pharmacy School (Hilo, Hawaii).

2.19. Differential Gel Electrophoresis (DIGE)

DIGE analysis was performed at the W.M. Keck Foundation Biotechnology Resource Laboratory at Yale University. Protocols at Yale were performed as outlined in *Methods in Molecular Biology, Vol. 328: New and Emerging Proteomic Techniques.* Peptides were

separated on a Waters nanoACQUITY (75 μm x 250 mm eluted at 300 nl/min.) with MS analysis on a LTQ Orbitrap mass spectrometer. Database (swissprot) searching was performed using Mascot distiller and the Mascot search algorithm. A confidence level was set to 95% within the MASCOT search engine for protein hits based on randomness.

2.20. Transmission Electron Microscopy (EM)

Mast cells exposed to the insulin-FDI treatment for 6 days were trypsinized, harvested, washed twice in PBS. The cell pellet was resuspended in 4% formaldehyde and 1% glutaraldehyde by mixing an equal volume of fixative and cell suspension. Cells were transferred to a centrifuge tube and spun for 10 minutes at 850*g*. Fixatives were carefully removed and cells were resuspended in fresh fixative overnight. Fixatives were replaced with 8% (0.2M) sucrose in 0.1 M PBS 3x15 minutes or overnight at 4°C. Cells were post-fixed with 1% OsO_4 in 0.1 M PBS for 1 hour. OsO_4 were removed and cells were rinsed in 0.1 M PB 3x10 minutes. Dehydration were performed as follows: 0% ethanol (15 min), 70% Ethanol (15 min), 95% Ethanol (15 min), 100% Ethanol (2 x 15min), 100% Propylene oxide (2 x 15min), 1:1 EMBed 812 and Propylene Oxide (1-2 hour) and 2:1 EMBed 812:Propylene Oxide (overnight in dessicator with top off). Embedding was performed with Embed in Beam capsules and baked at 60 ºC for 48 hours. Sectioning was performed using Semithin (thick sections, 0.5-1 μm) and toluidine blue staining. EM blocks were trimmed further if needed to acquire ultrathin sectioning, which were collected on grids. Staining grids were treated with uranyl acetate for 15 minutes, rinsed with distilled water and then stained with lead citrate for 3-5 minutes then rinsed with distilled water. EM images were produced on a fee-for-service basis by either IHC World, LLC (Woodstock, MD) or the Biological EM Facility at the Pacific Biosciences Research Center of the University of Hawaii at Manoa.

2.21. BCA assay for protein determination

Protein determination using a modified bichinchonic acid protocol (BCA) was performed using the BioRad (Temecula, CA) *Dc* protein determination kit according to the manufacturer's instructions. BSA was used as a standard.

2.22. Statistical analysis

Results are shown as the mean $\pm$ standard deviation. Statistical significance was determined based on a two-way analysis of variance (Student's t-test). Experiments were performed in triplicate unless otherwise indicated in text. Adjacent to data points in the respective graphs, significant differences were recorded as follows: single asterisk, $p < 0.05$; double asterisk, $p < 0.01$; triple asterisk, $p < 0.001$; no symbol, $p > 0.05$. Experiments are all *n* of at least 3.

Chapter Three

Characterization of lipid bodies induced by insulin/high nutrient conditions in model mast cells

3.1. Introduction

Insulin is a primary physiological indicator of metabolic status and nutrient availability (12). There is striking *in vivo* and epidemiological data suggesting that mast cells are responsive to insulin, and the pathologies that result from dysregulated insulin production are characterized by poorly understood, systemic, inflammatory responses. The central premise of the work presented in Chapter 3 is that mast cells sense and respond to insulin both physiologically and pathophysiologically. We tested the hypothesis that insulin is a lipogenic stimulus in mast cells, and that insulin exposure modulates the complement of mast cell lipids.

3.1.1 Lipogenic effects of insulin

(a) The insulin receptor and signaling pathway

The insulin receptor (IR) is a receptor tyrosine kinase (RTK) transmembrane receptor activated in response to insulin or insulin-like growth factor (IGF) (12, 13). Ligation of insulin or IGF to the extracellular alpha chains of the IR lead to dimerization and an autophosphorylation of the tyrosine residues located on the cytoplasmic portion of the beta chains. Cellular activation of the IR via phosphoinositide-3-kinase (PI3K) and protein kinase B (PKB/AKT) lead to the translocation of glucose transporter type 4 (GLUT4) to the cell membrane making possible the entry of glucose into the cell as shown schematically in Figure 3.1. The insulin receptor plays a vital role in metabolic homeostasis and clearance of glucose from the blood, and dysfunction of this receptor or an inability to activate this pathway has been implicated in clinical pathologies such as type II diabetes and cancer.

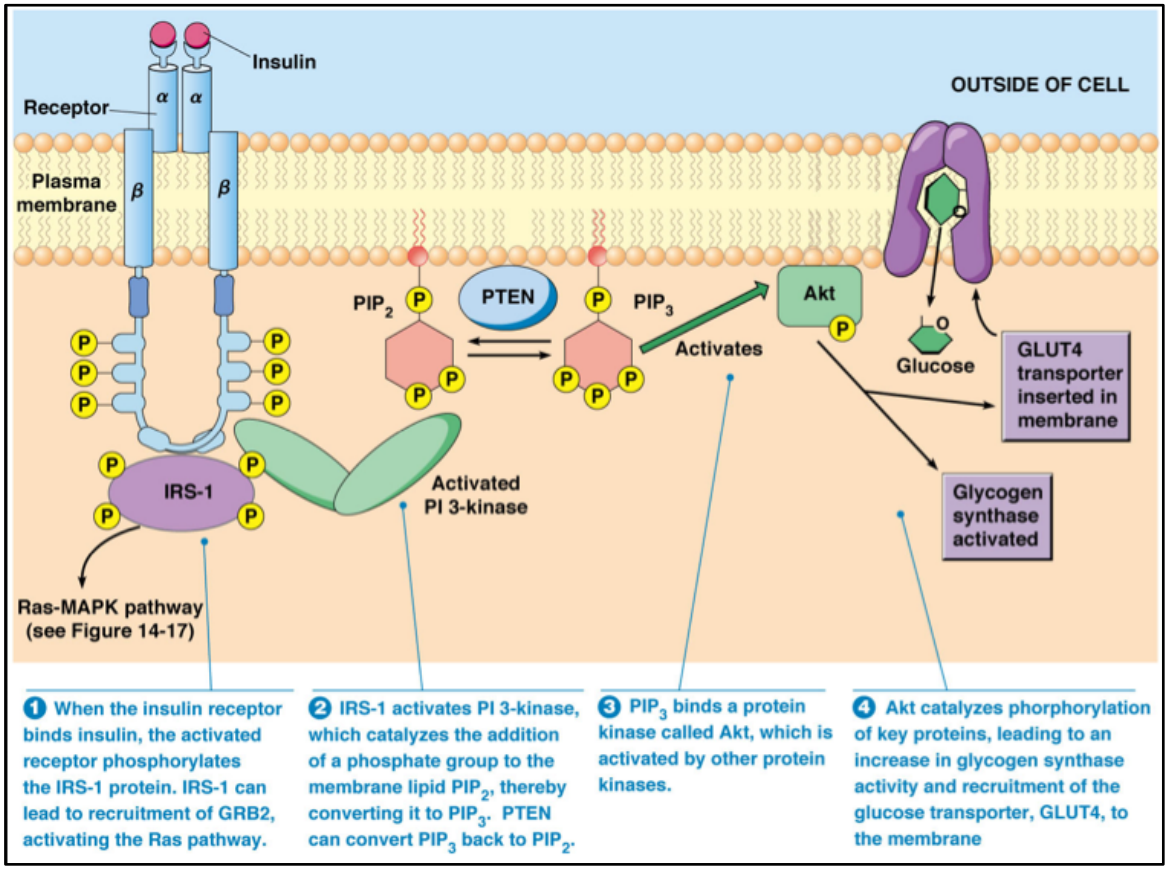

Figure 3.1. Membrane-proximal signaling by the Insulin Receptor. Insulin, produced by beta cells of the pancreas, binds insulin receptors (IR) expressed on a large number of target tissues, including cells of the immune system. A PI3K kinase-dependent pathway links the IR to Glut 4, with a critical component being the phosphorylation status of the IRS-1 insulin receptor substrate molecule. This image is reproduced from Pearson Education, Inc (2012).

(b) Lipogenesis and Experimental Use of Insulin and Complex Lipogenic Stimuli

As described above, insulin drives lipogenesis (12, 13, 25, 101), which is the process of converting simple sugars (glucose and their metabolic intermediates, such as acetyl-CoA) into lipids. These lipids are then stored in the form of lipid bodies as a way to compartmentalize and efficiently store energy in time of nutrient abundance, in advance of future metabolic demand. Excessive levels of blood sugars and lipids coupled with hyper-secretion of insulin lead to hypertrophy of these stores. The lipogenic effect of insulin has been best studied in the context of the adipocyte where the deposition of large cytoplasmic lipid bodies occur in response to insulin and nutrient dense conditions. We used the adipocyte (and hepatocyte) literature as a guide to identify experimental conditions that used insulin to drive lipogenesis (102-105). We noted a number of key practices in multiple *in vitro* studies performed to examine lipogenesis: (1) use of insulin alone or in combination with a pro-lipogenic/anti-lipolytic agent, (2) concentrations of insulin mimicking high local levels achieved in plasma during hyperinsulinaemia or feeding (local concentrations of up to

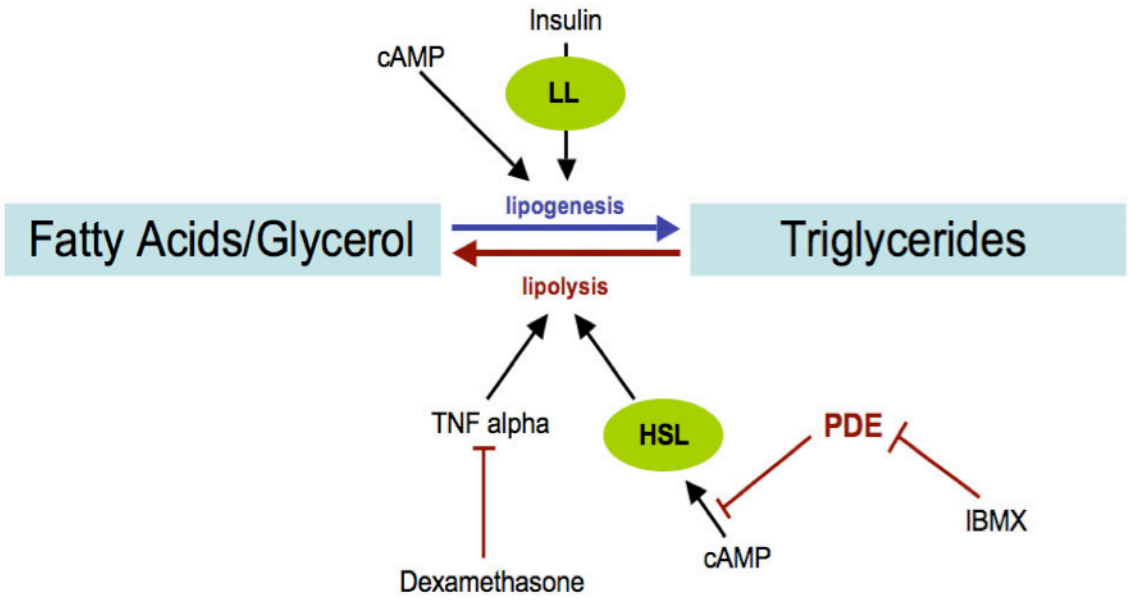

Figure 3.2. The role of insulin in lipogenesis and lipolysis in the adipocyte. Insulin promotes the activation of lipoprotein lipase (LL) and the subsequent accumulation of triglycerides in adipocytes by stimulating the process shown by the blue arrow. Similar inhibitory effects occur in the lipolytic pathway shown by the red arrow, which utilizes the accumulation of triglyceride to produce fatty acids and glycerol.

80 μg/ml), and (3) chronic application of insulin over a period of multiple days. Provided with the above information, we embraced early on a mimetic of insulinaemia/nutrient density established in the adipocyte literature as a pro-lipogenic/anti-lipolytic agent that we refer to as insulin-FDI or IFDI that we administered over the course of 6 days. The insulin-FDI cocktail is a combination of insulin, which is the primary driver of lipogenesis, (F) FBS, (D) Dexamethasone, which opposes the natural autocrine production of TNF-α (a lipolytic cytokine) and (I) Isobutylmethylxanthine (IBMX), a stabilizer of cAMP levels, which assists in potentiating the activity of the insulin receptor (103-105). The use of insulin-FDI, in our experiments and those from the literature, maximizes pro-lipogenic pathways, simultaneously minimizes anti-lipolytic pathways, but does not engender any qualitatively different responses than insulin alone.

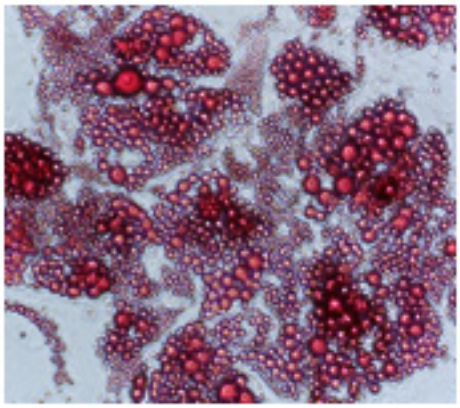

Figure 3.3. Insulin-FDI induced accumulation of homogeneous Oil Red O-positive lipid bodies in 3T3-L1 adipocytes. Image reproduced from ZenBio.com.

3.1.2. Mast cells and insulin: review of previous studies

The *in vivo* and epidemiological evidence for a connection between insulin, metabolic status and mast cell-driven inflammatory responses are reviewed in Chapter 1. Here, we review the few published studies where mast cells have been directly exposed to insulin *in vitro*, and various dimensions of their pro-inflammatory responses subsequently assayed. Various endocrine hormones have been investigated for their ability to regulate mast cell histamine release and cytokine production. The ability of insulin to act as an acute primary stimulator of mast cell activation does not seem to be generally supported by published studies.

A number of studies have previously suggested that mast cells are largely refractory to insulin over acute time courses (minutes to hours), although chronic insulin (supplied for 1-2

weeks) does affect bone marrow-derived mast cell (BMMC) proliferation (106). Functional assays in this immature mast cell type (BMMC) do not recapitulate all aspects of the functionality of a mature, tissue-conditioned, mast cell and did not reveal altered secretion over a 1-2 h time course of insulin exposure (106). A recent revisiting of this idea suggested that insulin, added in acute pre-stimulation or concurrently with antigen, activates tyrosine kinase pathways in mouse BMMC and somewhat potentiates early FcεRI-associated kinase signaling pathways (107). While each of these studies agree that, in principle, mast cells express the insulin receptor and must have some responses that are engendered by insulin, they present only underwhelming effects of acute insulin exposure and assay of functional capacity are limited to, again, acute effects of insulin on histamine release. Although lipogenesis is the primary physiological action of insulin, and mast cells contain lipid bodies that are analogous structure to the lipid droplets that insulin causes to form in adipocytes, it is surprising that none of the above studies considered lipid body formation when exposing the mast cells to insulin. There are currently no published studies exploring the lipogenic effects of insulin in the mast cell system even though the effect of insulin in this cell type mast cell may have dramatic functional ramifications. Our present study addresses the idea that insulin fluctuations over chronic, time courses may modulate mast cell phenotype, and that through acting as a driver of lipid body accumulation in mast cells, insulin could be a determinant of the intensity and duration of subsequent mast cell responses to challenge.

3.1.3. Mast cell and adipocyte lipid droplets: commonalities and contrasts

In the well-studied adipocyte system, lipid body formation is a highly orchestrated process involving a variety of protein mediators that participate in trafficking lipid derived substrates, lipid body synthesis and the concomitant inhibition of lipolysis (15, 17, 18, 21, 60, 62, 67). The general structure and the various lipid body associated proteins in adipocytes were shown in Figure 1.4. Far less studied are the cytoplasmic lipid bodies found in mast cells but neutrophils, macrophages and eosinophils. In these cells lipid bodies (LB) are enigmatic structures, with their formation, content and dynamics largely unstudied. LB in granulocytes increase in number during infection, and are mobilized during cellular activation (57, 88-90, 108, 109). In mast cells, and other leukocytes, lipid bodies have been suggested as reservoirs of the eicosanoid precursors for bioactive signaling lipids such as leukotrienes, and sites for eicosanoid synthesis. Thus the potential for a mast cell to generate mediators such as

leukotriene C4 (LTC4) may be related to the size of the pool of precursors represented by these lipid bodies. These lipid bodies may play a role in the immunocyte that is distinct from the contribution to neutral triglyceride storage and cellular metabolism made by the comparable organelle in adipocytes. While it is clear that metabolic status can drive the steatotic accumulation of LB in adipocytes and hepatocytes, it is unclear whether the counterpart structures in immunocytes are also elevated under conditions of nutrient abundance. This is an important question, since their steatotic proliferation could lead to an increase in the pool of precursors for pro-inflammatory lipid mediators, in turn altering the intensity of subsequent mast cell-driven inflammatory responses. No comparative analysis of the content, formation, or sensitivity to nutrient environment between LB in adipocytes and immunocytes has been undertaken and we do not currently have a detailed understanding of the cell biology, biochemistry or biophysics of mast cell lipid bodies.

While heterogeneity between adipocyte and immunocyte LB is deserving of analysis between the cell types, there is a further question of the possible heterogeneity of lipid storage structures within the same cell. While LD in adipocytes and hepatocytes are usually represented as homogeneous, Oil Red-accumulating structures, there are clearly different types of LD with reference to their lipoprotein types (HDL, LDL, etc.) (16, 103-105). Moreover, EM ultrastructural work on the mast cell LB performed by the Dvorak laboratory hinted at subpopulations of LB that could be distinguished on the basis of their electron density/opacity, the presence or absence of an electron-dense delimiting single membrane layer and the accumulation of ^{14}C-labeled arachidonic acid molecules and immunogold labels to 5-lipoxygenase and ribosomes (85, 92, 110, 111). These data raise the interesting possibility that all LB are not created equally, and there is an opportunity to revisit this idea using contemporary fluorescence techniques.

3.1.4. Experimental Approach: Exploring insulin-directed lipogenesis in mast cells

In this Chapter we asked whether insulin directs the biogenesis of lipid bodies in mast cells, and we analysed the heterogeneity of lipid bodies both within the mast cell population and comparatively between mast cells and a classical adipocyte model of lipogenesis.

3.2. Results

3.2.1. Chronic insulin induces lipogenesis in mast cells

The response of mast cells to chronic insulin exposure is currently unknown and we asked what effects this exposure may have, if any, in the mast cell system. In the current study, we are testing the hypothesis that insulin could have chronic effects on mast cell pro-inflammatory responses. By analogy with adipocytes, we hypothesized that chronic insulin exposure induces lipogenesis, and may contribute to the induction of lipid body synthesis.

Over an acute timecourse, we can reproduce published experiments showing only moderate insulin activation of kinase pathways, such as AKT phosphorylation and ERK1/2 activation, and the refractoriness of histamine release to acute insulin (data not shown) (106, 107) in mast cells. Figure 3.4A shows that RBL2H3 mast cells express the insulin receptor. We find that insulin is sufficient to drive the accumulation of mast cell lipid bodies, which stain positively with neutral lipid dyes (Oil Red O, Nile Red), however in the adipocyte literature, optimal lipogenesis is routinely achieved *in vitro* through addition of insulin, in combination with an inhibitor of autocrine TNFα production and stabilization of cAMP levels. Here, insulin is driving the lipogenic process while the addition of dexamethasone acts to oppose constitutive lipolysis. Dexamethasone, a corticosteroid, opposes endogenous TNF-α production, a lipolytic cytokine produced by both adipocytes and mast cells, and inhibits expression of the Hormone Sensitive Lipase (HSL). Thus the prediction arising from the adipocyte literature is that the effects of insulin and dexamethasone would be independently able to induce lipogenesis, and act in an additive manner with one promoting lipogenesis and the other opposing lipolysis. In mast cells, we note a similar additive effect, where insulin is sufficient to drive lipid body accumulation, but its effect is enhanced by the anti-lipolytic dexamethasone. Figure 3.4B-D show that exposure to this combinatorial stimulus (insulin-FDI) dramatically enhances the lipid content of RBL2H3, 3T3-L1 and primary C57.1 BMMC. Figure 3.4F presents quantification of both the mean number of lipid bodies observable as discrete structures averaged from 100 cells (left panel) and the area of apparent ORO-positive staining averaged across 10 cells (right panel), showing that insulin-FDI and insulin alone can both act as primary drivers of lipogenesis, and that the effects of the lipogenic insulin and anti-lipolytic dexamethasone are, as expected, additive. In contrast with

the adipocyte, we find that the cAMP-elevating reagent IBMX is not a major factor in the effect of the insulin-FDI lipogenic stimulus. Figure 3.4F shows that in isolation IBMX does not induce marked lipogenesis, and it does not have an additive or synergistic effect when combined with insulin. We later developed a quantitative assay based in flow cytometry to measure the accumulation of lipid bodies in both 3T3-L1 and RBL2H3 (Figure 3.5). Taken together, these data reflect similar dissections of the composite insulin-FDI stimulus published in adipocytes; i.e. insulin is necessary and sufficient to cause lipid body accumulation in the presence of a lipid rich medium.

Lipid bodies in macrophages, eosinophils and neutrophils are dynamically regulated in response to challenge. Moreover, Dvorak *et al* have shown by electron microscopy that lipid bodies in basophils disperse their contents into degranulation channels (85). Both FcεRI and PMA/ionomycin stimulation cause depletion of the insulin-FDI-induced lipid bodies in mast cells (Figure 3.4G). Taken together, these data indicate that lipid body accumulation in mast cells can be induced by insulin and an insulin-containing lipogenic stimulus that initiates similar pathways in adipocytes. The large number of insulin-FDI-induced lipid bodies in mast cells are mobilized by antigen receptor stimulation.

Lipid body accumulation in insulin-FDI treated mast cells is significant and we sought to further understand the extent to which these lipid bodies occupy the cytosol, in addition to the structure of the induced lipid bodies in steatotic mast cells. We employed the use of electron microscopy (EM) to obtain high-resolution images detailing the ultrastructure of lipid bodies in insulin-FDI treated mast cells. Figure 3.4E show the appearance of a population of insulin-FDI induced structures at low (upper left panel) and high (lower left panel) magnification, which bear some ultrastructural resemblance to previously described lipid bodies in the literature. These induced translucent structures appear as semi-circular and elliptical shaped and are approximately 0.1-1.0 μm in diameter. These lipid bodies, which are encapsulated by a thin layer of membrane and are consistently located proximally to the ER, appear to be pervasive and occupy a large volume of the cytosol. Unexpectedly, these lipid bodies do not present the homogenous morphology previously described in the literature raising the question of lipid body heterogeneity in these cells. These data complement our existing fluorescence and confocal microscopic data and provide further resolution into the ectopic accumulation of lipid bodies in mast cells driven by the effects of chronic insulin

exposure. In addition, these data raise several questions regarding lipid body heterogeneity and create the need to further investigate these findings.

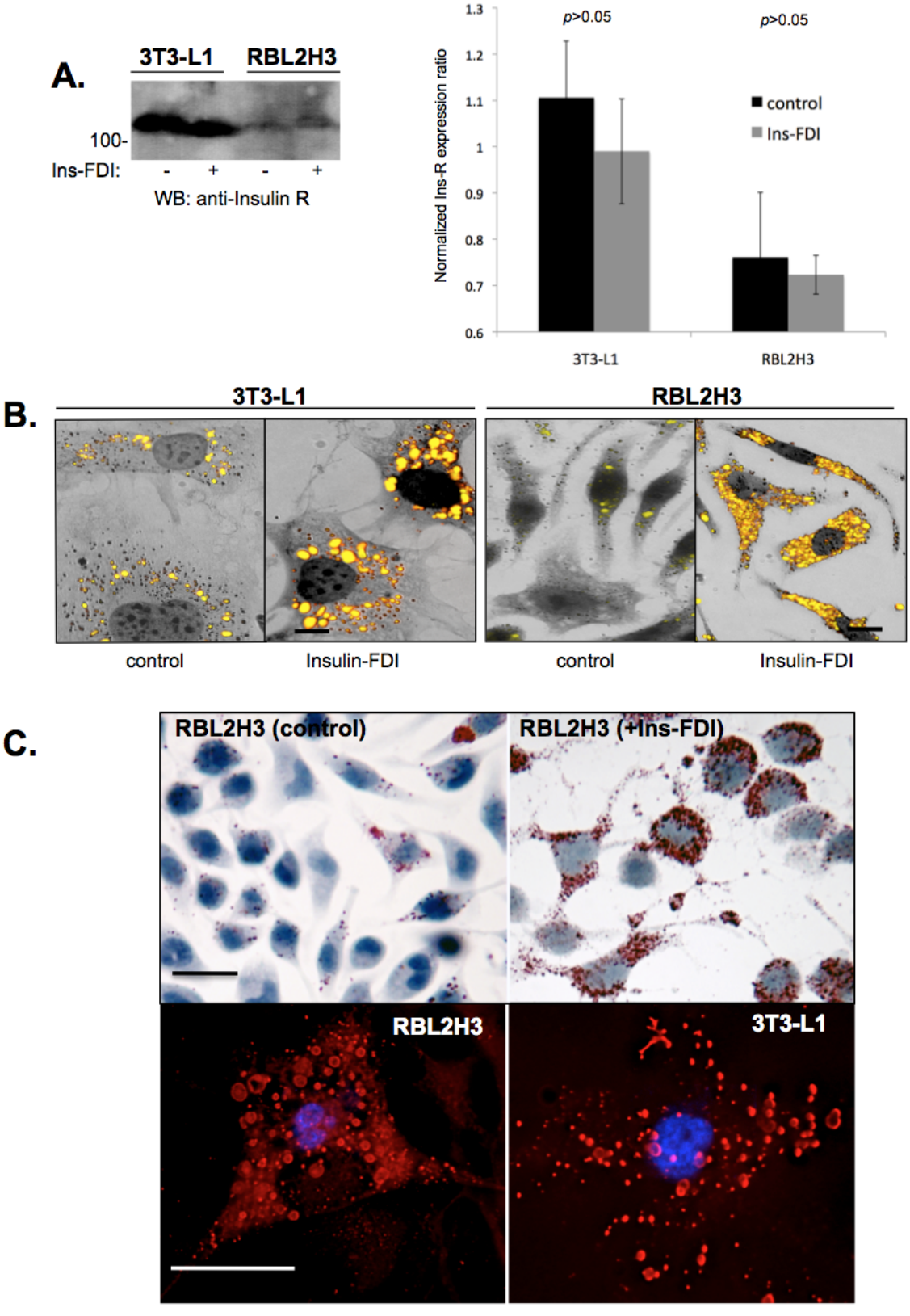
A.
3T3-L1
RBL2H3
100-
Ins-FDI: - + - +
WB: anti-Insulin R
p>0.05
p>0.05
Normalized Ins-R expression ratio
1.3
1.2
1.1
1
0.9
0.8
0.7
0.6
control
Ins-FDI
3T3-L1
RBL2H3
B.
3T3-L1
RBL2H3
control
Insulin-FDI
control
Insulin-FDI
C.
RBL2H3 (control)
RBL2H3 (+Ins-FDI)
RBL2H3
3T3-L1

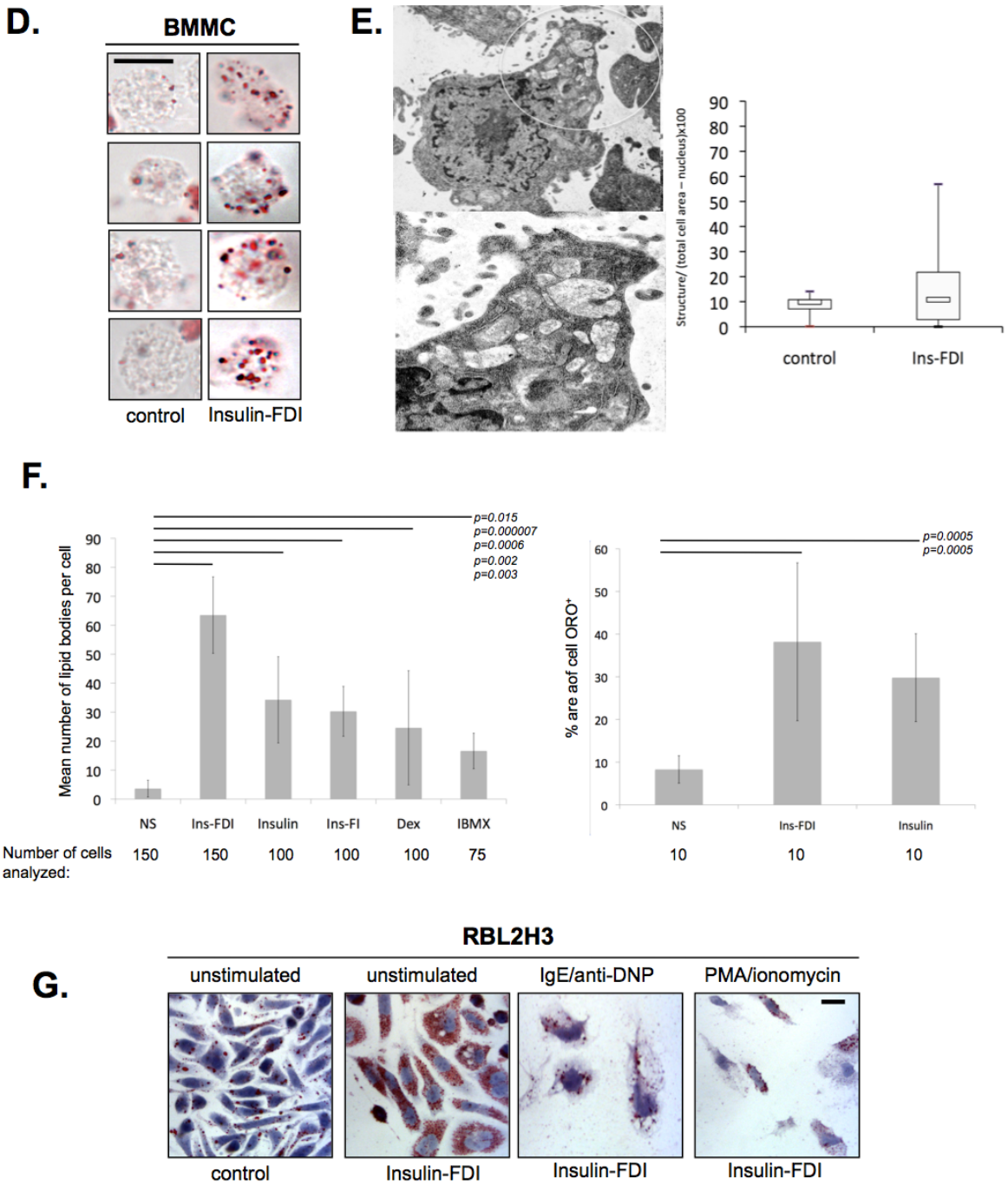
D.
BMMC
control
Insulin-FDI
E.
Structure/ (total cell area – nucleus)x100
control
Ins-FDI
F.
Mean number of lipid bodies per cell
p=0.015
p=0.000007
p=0.0006
p=0.002
p=0.003
NS
Ins-FDI
Insulin
Ins-FI
Dex
IBMX
Number of cells analyzed:
150
150
100
100
100
75
% are aof cell ORO+
p=0.0005
p=0.0005
NS
Ins-FDI
Insulin
10
10
10
G.
RBL2H3
unstimulated
unstimulated
IgE/anti-DNP
PMA/ionomycin
control
Insulin-FDI
Insulin-FDI
Insulin-FDI

Figure 3.4. Insulin-containing lipogenic stimuli induce lipid bodies in mast cells. **A. Insulin receptor expression in mast cells.** 3T3-L1 and RBL2H3 cells (5 x10^6 cells per lane) were lysed as described in Methods. Total protein was acetone precipitated and resolved using 10% SDS-PAGE. After electrotransfer, resolved proteins were probed for the presence of the Ins-R *(left panel)* using 0.01μg/ml rabbit anti-InsR and an HRP-conjugated secondary. MW are shown in kDa. Expected MW of the InsR is 121kDa. Quantification presented in *right panel*. **B, C, D. Multi-component lipogenic treatment induced marked lipid body accumulation in mast cells**. RBL2H3 and 3T3-L1 cells were plated on glass coverslips (B, C) while C57.1 BMMC (D) were grown in suspension, in the presence or absence of a stimulus comprising 10% FBS, 0.01 mg/ml insulin, 0.25μM dexamethasone and 2.5μM isobutylmethylxanthine (insulin-FDI) for 6 days at 37^{o}C. After PFA fixation, cells were stained with Oil Red O and hematoxylin then visualized using bright field alone (upper panels of C and all of D), bright field and FITC emission overlaid on phase images (B) or by rendering a 3D confocal z-stack (lower panels of C). **E. Visualization of ectopic lipid body formation in mast cells**. SEM of 6d Insulin-treated mast cells at 5,000x (upper left panel) and 20,000x zoom (lower left panel). Examples of insulin-induced cytosolic structures shown in bottom left panel. Quantitation (NIH Image J) from EM of % cytosol that are apparent *de novo*-formed lipid bodies in control and 6d insulin-treated mast cells (right panel). **F. Quantification of lipid body abundance.** Cells were stimulated as described above, and mounted coverslips were stained with ORO. *Left panel*. Number of lipid bodies per cell averaged from the indicated number of cells. Lipid bodies were counted in a sample-blinded fashion as observably discrete structures using 100x objective. *Right panel*. Averaged area of ORO staining per cell assessed by IMAGE J analysis. **G. Intracellular lipid bodies are mobilized in response to both to antigenic and pharmacological stimulation in mast cells.** RBL2H3 cells were incubated with insulin-FDI for 6 days at 37^{o}C and then stimulated via either the FcεRI (IgE 1 μg/ml for 16h followed by 250ng/ml KLH-DNP for 60 min) or PMA/ionomycin (1μM each for 60 min). Post-stimulation, cells were immediately fixed in PFA, stained with Oil Red O and hematoxylin. ***Analysis***. *n>3; *p < 0.05; ** p < 0.01; *** p < 0.001; no symbol, p > 0.05*.

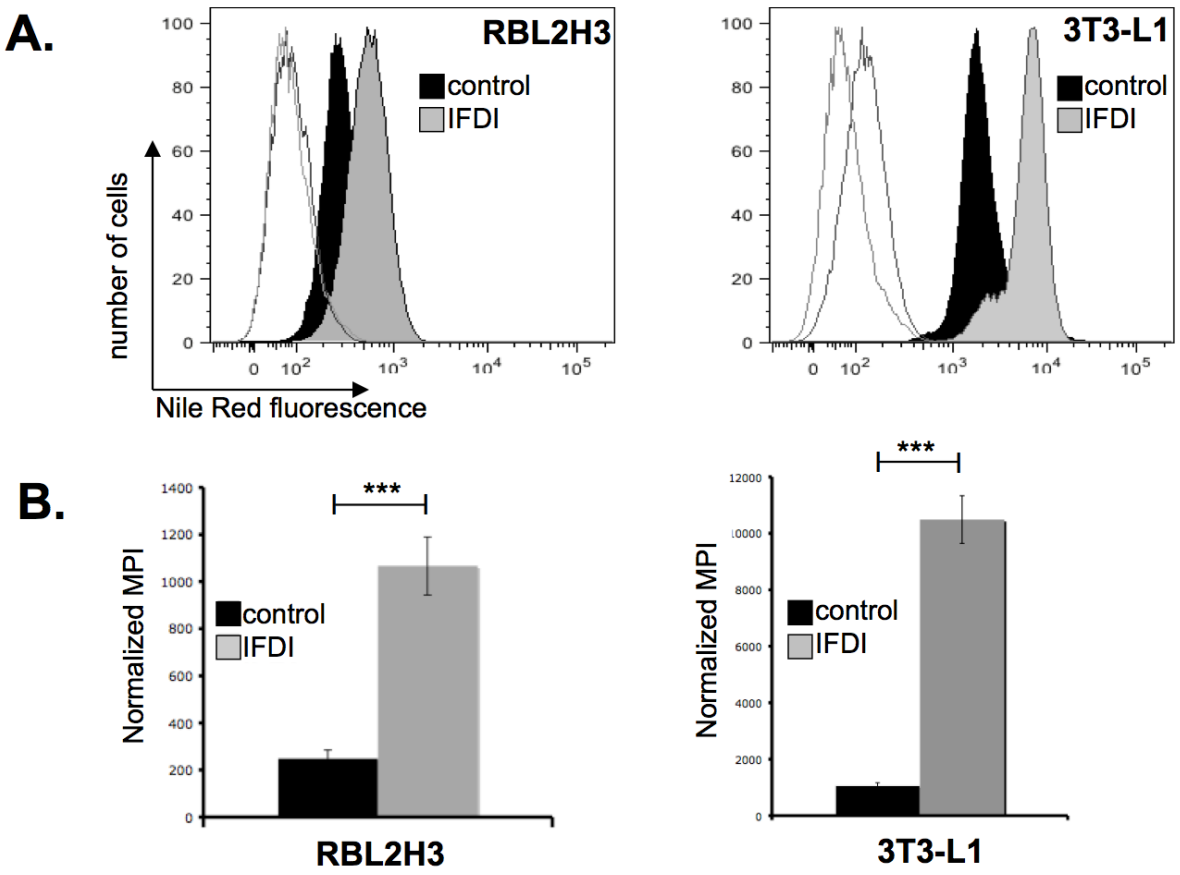

Figure 3.5. Flow cytometric quantification of lipid body accumulation in adipocytes and mast cells. A. RBL2H3 (*left panel*) and 3T3-L1 (*right panel*) were incubated with insulin-FDI for 6 days at 37°C. After PFA fixation, cells were stained with Nile Red (1h RT). Flow cytometry was used to establish quantitative values of intracellular lipid body accumulation by evaluating mean peak fluorescence intensities (MPI) of the Nile Red emission in the Texas Red channel. Light and dark grey unfilled traces represent autofluorescence of control and insulin-FDI-treated cells, respectively. **B. Quantification of fluorescence gain.** Normalized increase in MPI in response to insulin-FDI treatment of RBL2H3 *(left panel)* and 3T3-L1 (*right panel*) (data averaged from 3 experiments)

3.2.2. Subcellular heterogeneity of lipid bodies in mast cells

In adipocytes and hepatocytes, lipid bodies and their contents are viewed as homogenous structures with little variability between these organelles. This idea is based on the pervasive use of Oil Red O to visualize the LB structures. However, some of our early observations challenged this view of a highly homogeneous population. While screening lipophilic dyes as reagents for live cell imaging of LB, we noted that reagents such as LipidTOX and Filipin (a cholesterol binding compound), both established dyes for LB/LD staining, did not appear to completely colocalize as expected with ORO. Furthermore, not all lipophilic dyes were represented from cell-to-cell within the same population. These observations presented the possibility that LBs may be heterogeneous, with different chemical compositions (lipid content) that would lead them to accumulate dyes of different lipophilicities differently.

We performed an extensive analysis of MC LB using various lipophilic stains, some of which are environment-sensitive probes of their lipid content. Figure 3.6 highlights the non-overlapping nature of the insulin-FDI induced LB populations stained by dyes of different lipophilic chemistries. These lipid body populations are heterogenous on the basis of size (for example Nile Red appears to preferentially stain very small LB, possibly corresponding to the primordial (immature) ER-associated LB seen in adipocytes (Figure 3.7). Control experiments demonstrated (not shown) that the LB structures stained by these dyes were also not overlapping with structures such as the Golgi apparatus, endosomes, lysosomes and ER. The presence of cholesterol and phospholipids in intracellular and the plasma membranes did lead us to identify staining conditions that preferentially highlighted the Insulin-FDI-induced structures. Our data suggest that simple ORO staining significantly underestimates the complexity of LB population in MC.

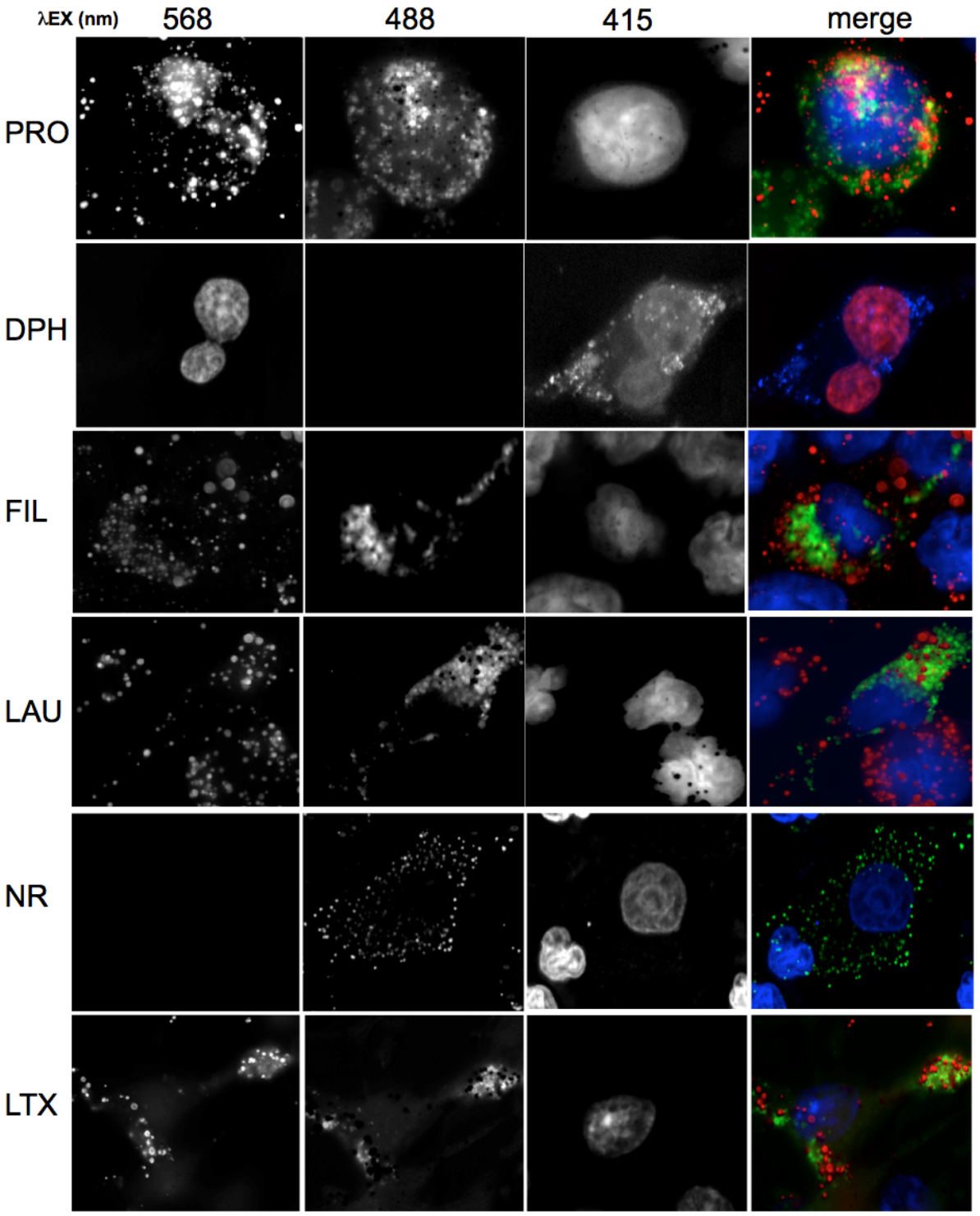
λEX (nm)
568
488
415
merge
PRO
DPH
FIL
LAU
NR
LTX

Figure 3.6. Chronic insulin exposure induces a heterogeneous lipid body population in mast cells. RBL2H3 were plated on glass coverslips in the presence of a stimulus comprising 10% FBS, 0.01mg/ml insulin, 0.25μM dexamethasone and 2.5μM isobutylmethylxanthine (insulin-FDI) for 6 days at 37^{o}C. After PFA fixation, cells were stained with Oil Red O (0.35% w/v), LipidTOX (4μM), Laurdan (2μM), Prodan (2μM), Filipin (10 μg/ml), Nile Red (1μg/ml) or DPH (2μM) and imaged as described in methods. Image overlays (right panels) show the lack of apparent overlap between Insulin-FDI induced lipid-rich structures stained with the various types of dye.

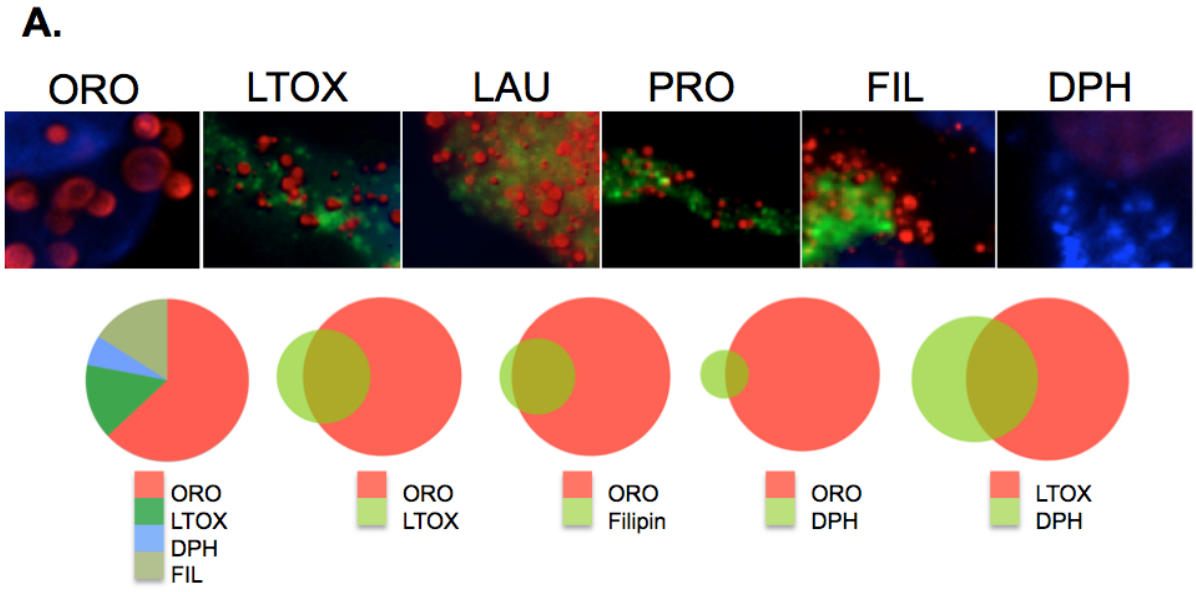
A.
ORO
LTOX
LAU
PRO
FIL
DPH
ORO
LTOX
DPH
FIL
ORO
LTOX
ORO
Filipin
ORO
DPH
LTOX
DPH

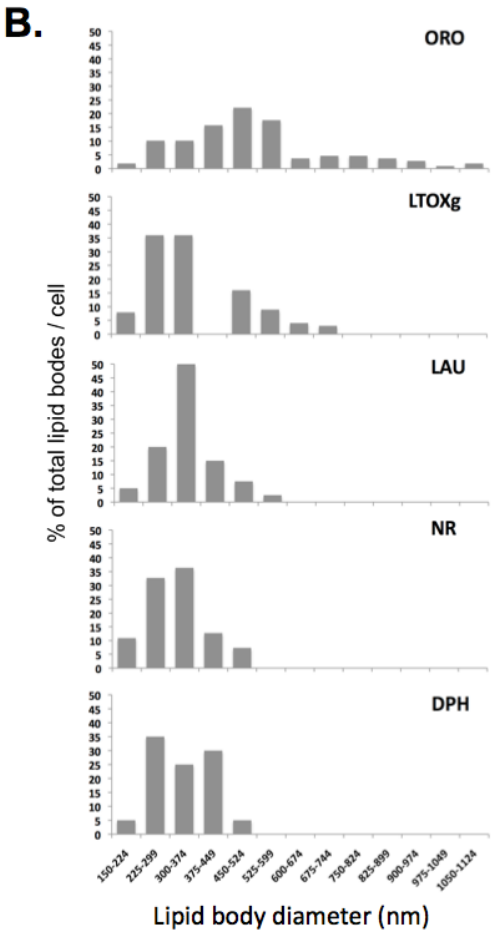
B.
ORO
LTOXg
LAU
NR
DPH
% of total lipid bodes / cell
150-224
225-299
300-374
375-449
450-524
525-599
600-674
675-744
750-824
825-899
900-974
975-1049
1050-1124
Lipid body diameter (nm)

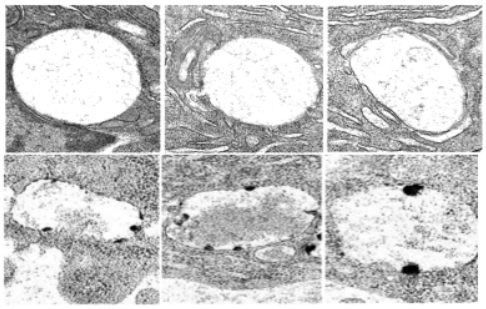
C.

Figure 3.7. Chronic insulin exposure induces a heterogeneous lipid body population in mast cells. A. RBL2H3 were plated on glass coverslips in the presence of a stimulus comprising 10% FBS, 0.01mg/ml insulin, 0.25μM dexamethasone and 2.5μM isobutylmethylxanthine (insulin-FDI) for 6 days at 37^{o}C. After PFA fixation, cells were stained with Oil Red O (0.35% w/v), LipidTOX (4μM), Laurdan (2μM), Prodan (2μM), Filipin (10 μg/ml) or DPH (2μM) as described in methods. Venn diagrams (right panel) represent the percent of cells in a population that contain lipid bodies stained with indicated dye 1, dye 2 or co-localization of both. **B. Quantification of lipid body size distribution.** Each probe is analyzed according to percent of total lipid bodies classified within the indicated size range (nm) distribution measured using ROI in NIS Elements. **C. Example of insulin-induced structures in mast cells.** Electron micrographs were acquired from RBL2H3 cells exposed to the insulin-FDI treatment for 6 days. Higher magnification micrographs show variation in individual lipid body structure. Images are digitally zoomed from an original image captured at a magnification of 5000X.

Dvorak, et al. Diversity of Reported LB Structures in Mast Cells and Basophils

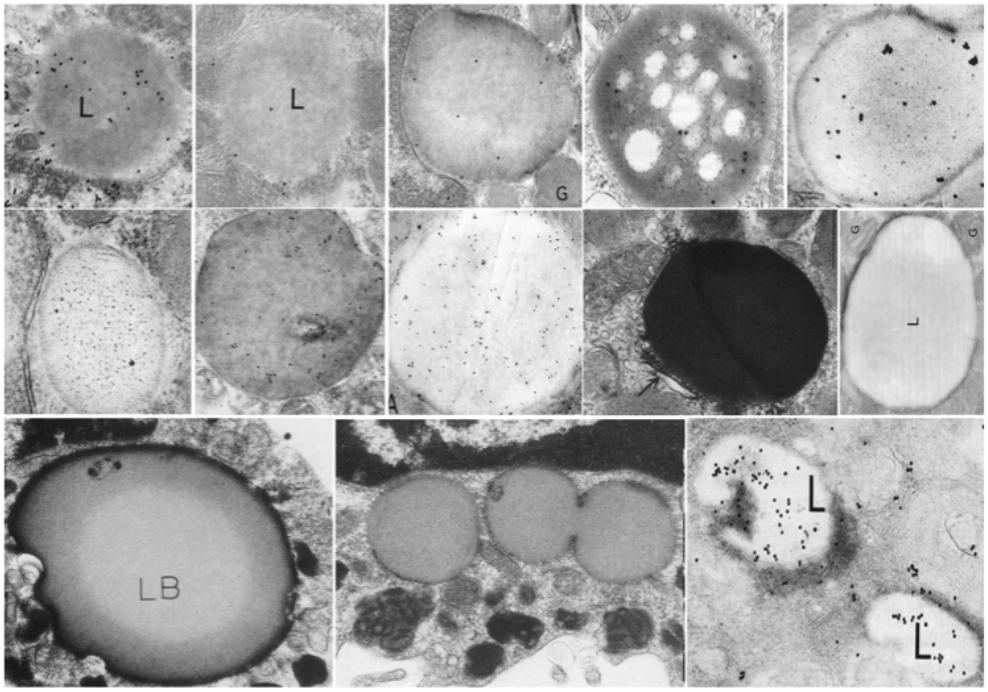

Insulin-FDI induced structures in mast cells

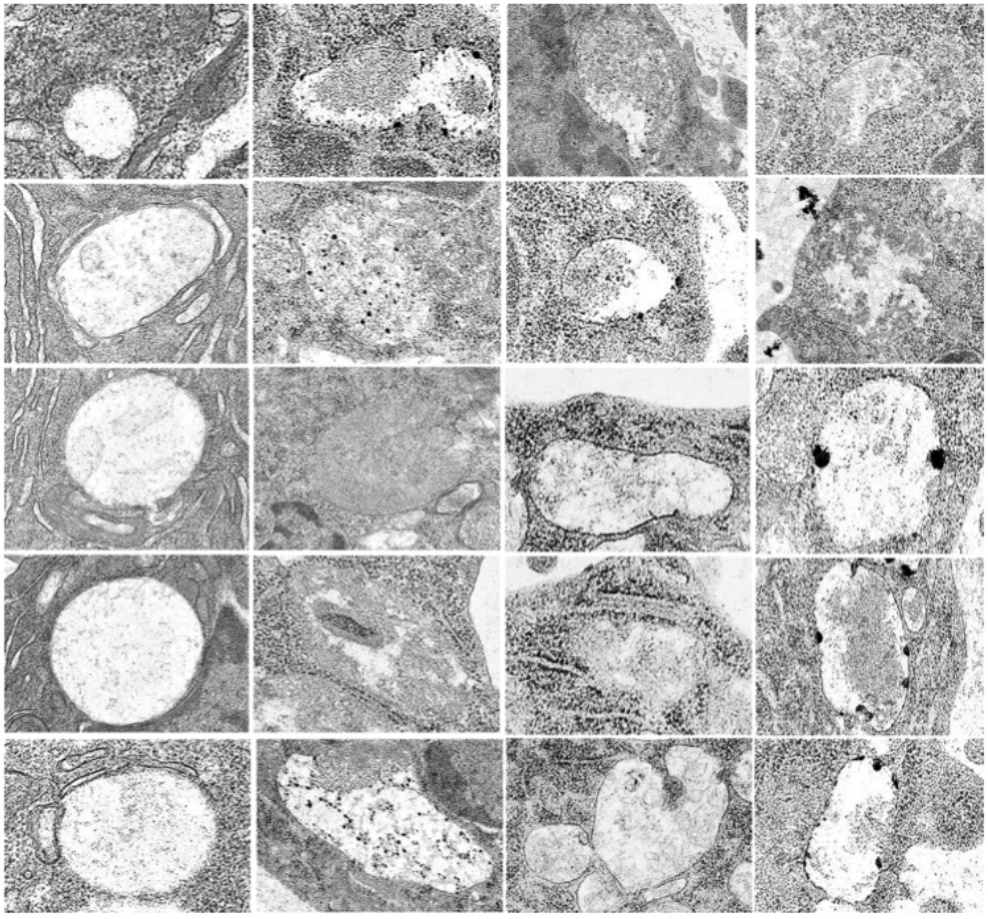

Figure 3.8. Diversity in lipid body ultrastructural appearance revealed by EM. Upper panel. Collation of published images of structures described as lipid bodies by the laboratory of Dr. Ann Dvorak**.** Images are derived from human and rodent mast cells and basophils, imaged with several different contrast techniques and ranging from 250-100nm in diameter (see Dvorak *et al* reference). **Lower Panels.** For comparison, diversity of Insulin-FDI induced structures observed in model rodent mast cells during our analyses (each lower panel is ~1 micron in width). L indicates lipid body.

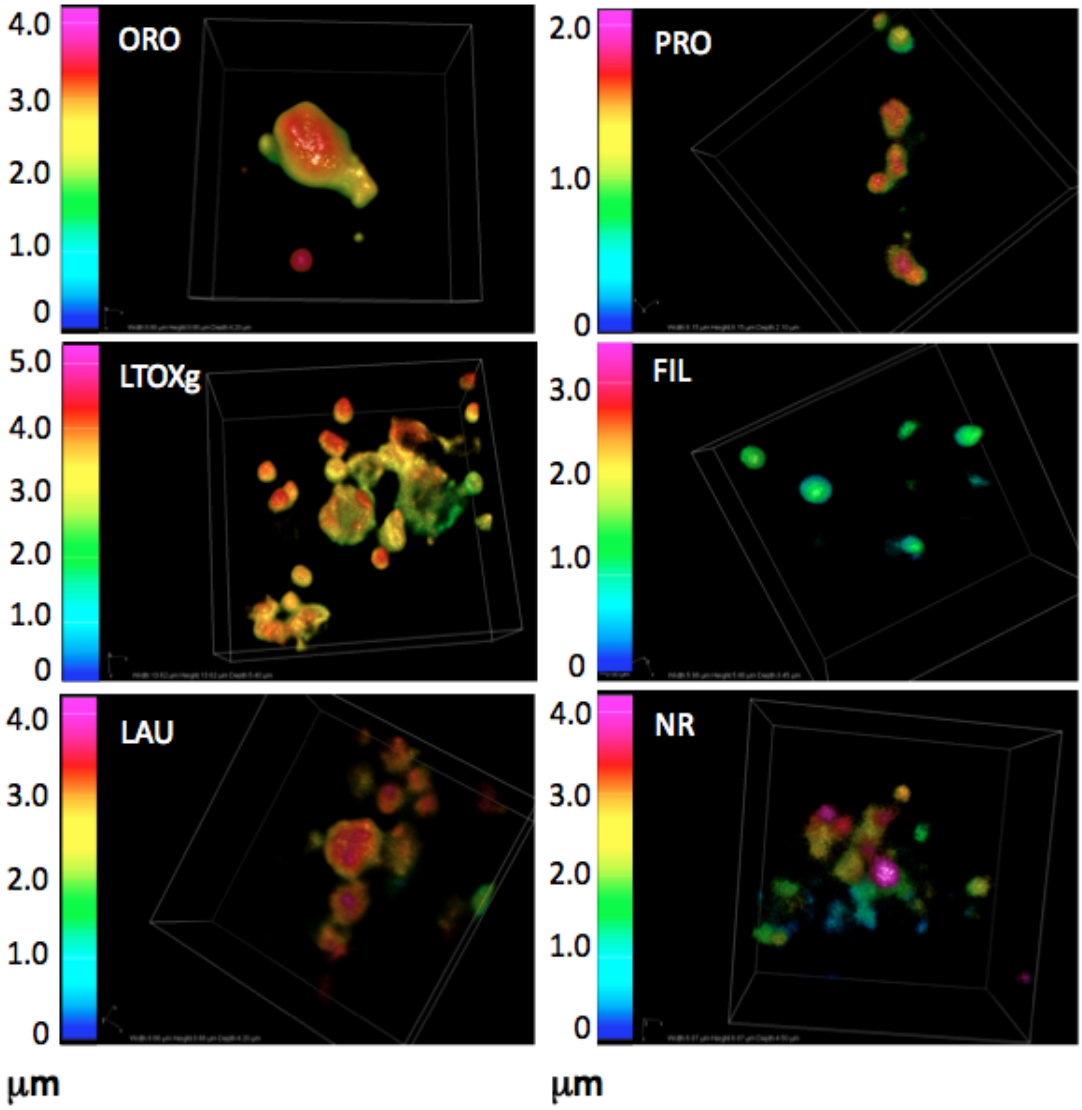

Figure 3.9. 3-D rendered confocal z stacks of individual and clustered lipid bodies in steatotic mast cells.

A. RBL2H3 were plated on glass coverslips in the presence of a stimulus comprising 10% FBS, 0.01mg/ml insulin, 0.25µM dexamethasone and 2.5µM isobutylmethylxanthine (insulin-FDI) for 6 days at 37°C. After PFA fixation, cells were stained with Oil Red O (0.35% w/v), LipidTOX (4µM), Laurdan (2µM), Prodan (2µM), Filipin (10 µg/ml) or NR (1µg/ml) as described in Methods. Lipid bodies were imaged confocally, and after digital deconvolution and reconstruction, images were projected with z-depth color coding corresponding to the look up tables shown at the right of each image (vertical distances in microns).

3.2.3. Lipid body heterogeneity between the adipocyte and mast cell systems: commonalities and contrasts

The data presented above suggest that, within a single cell, lipid bodies exist as subpopulations that are distinct in size and chemistry. Given that these structures are best studied in adipocytes and hepatocytes, where they are viewed as highly homogeneous ORO-positive populations, these data created a need to assess the degree of overall similarity between adipocyte and mast cell lipid bodies. This comparative analysis is presented below.

Lipid body biogenesis in adipocytes is a highly ordered process that is accompanied by hyper-proliferation, and dependent on PPARγ (112-114). Mature lipid bodies have a specific protein content that reflects their function as accessible stores of neutral triacylglycerols (NTG). We assessed several features of lipogenesis in mast cells in comparison with adipocytes. Figure 3.10A shows that chronic insulin exposure does not alter proliferation patterns in the mast cell lines used here. Our data show that insulin is having the hyper-proliferative effect on adipocytes that is suggested by the literature. However, the effect of insulin on RBL2H3 and C57.1 mast cells is that it does not significantly enhance proliferation. Thus in these transformed mast cell lines, we do not see evidence for insulin acting as a growth factor *per se*, which does not preclude such an effect in primary untransformed cells. Moreover, it should be noted that the insulin-FDI treatment used in our experiments to drive high levels of lipogenesis essentially causes both mast cell lines to cease proliferating after 48 hours. Mast cells treated with either insulin-FDI or insulin remain viable. In RBL2H3 treated with insulin or insulin-FDI, 90% of cells are trypan blue negative at 6d, compared to approximately 92% in controls, n=>10) up to at least 144 hours after addition, but if insulin-FDI-treated they show cell cycle arrest and accumulation in G0 and G1 (not shown). Dissection of the insulin-FDI treatment suggested that IBMX (but not dexamethasone) contributes to this proliferation defect.

In adipocytes, upregulation of PPARγ is an essential step in lipogenesis. In mast cells, PPARγ is down-regulated during lipid body biogenesis (Figure 3.10B). In adipocytes, lipid body formation involves multi-protein complexes formed from the PAT family and the upregulation of proteins such as HSL and CD36, which are involved in NTG metabolism (16, 60, 115). In Figure 3.10C, we examined lipid body-associated protein expression in response

to lipogenic stimulation. Expression of PAT family proteins and markers of adipocyte differentiation, both in resting and insulin-FDI-stimulated mast cells, have a distinct profile from that of the adipocyte. Levels of Perilipins A and B increase in adipocytes exposed to insulin-FDI, but are poorly expressed in mast cells and further down-regulated by insulin-FDI. The fatty acid carrier protein TIP47 is predominantly expressed in mast cells in its higher mobility, dephospho-form, and is not upregulated in response to insulin-FDI, in contrast to its upregulation in insulin-FDI-treated 3T3-L1. ADFP (adipophilin) and ATL (adipose tissue lipase) are down-regulated in mast cells in response to insulin-FDI, as opposed to either marked up-regulation or unchanged expression in the adipocyte. HSL is down-regulated as adipocytes enter a lipogenic state, consistent with a decrease in their lipolytic potential. HSL is poorly expressed in mast cells and is not altered by insulin-FDI exposure. CGI-58 levels are slightly decreased after 6 day insulin-FDI treatment in adipocytes and mast cells. In adipocytes, the tetraspan fatty-acid receptor protein CD36 is upregulated by insulin-FDI treatment. Conversely, CD36 is consistently expressed in resting or insulin-FDI-stimulated mast cells (Figure 3.10D). Overall, it appears that proteins involved in the biogenesis of NTG-containing lipid bodies in adipocytes are less critical for the induction of lipid body synthesis that we see in insulin-FDI-treated mast cells.

We assessed the bulk neutral lipid content (using an assay that measures mono-, di- and triglycerides) of RBL2H3 and 3T3-L1 after 6 days of exposure to insulin-FDI. Here, we observe that lipid body biogenesis in 3T3-L1 is associated with a large increase in the cellular pool of conjugated glycerides, consistent with published observations that the major component of the adipocyte lipid body is neutral triglyceride (Figure 3.10E). In contrast, RBL2H3 show only a moderate, and not statistically significant, increase in storage of lipid measured by this assay. These data suggest first that the new pool of lipid induced by insulin-FDI in mast cells is distinct from that in adipocytes, and second, that the primary components of the induced lipid bodies are lipids that are not detected by an assay for conjugated glycerides. Data to be presented in Chapter 5, from a more sophisticated lipidomic analysis, will reinforce this finding.

We have also assembled scanning excitation/emission fluorescence spectra of dye behavior in normal and steatotic mast cells and adipocytes (Figure 3.12 and 3.13) and we note that the spectral characteristics of dyes such as Nile Red and Laurdan reveal that the LB they stain

must have different lipid contents. We focused on Nile Red, for which defined spectral shift properties in varying polarity solvents and within cells have been demonstrated (116, 117).

We designed experiments to look explicitly at spectral properties of all of the dyes above in (a) solvents of varying polarities (Figure 3.11) and (b) adipocytes or mast cells in resting or steatotic states (Figure 3.12 and 3.13). Nine lipophilic dyes were evaluated using 5 distinct excitation wavelengths (350, 420, 470, 520 and 550 nm) and emission was scanned between 350 and 800 nm. Each dye was dissolved in PBS (dielectric constant approaching that of water, ~80, highly polar), dimethylformamide (dielectric content of 38, polar aprotic), ethanol (dielectric constant of 24.55, polar protic) and cyclohexane (dielectric constant of 2.02, non-polar). While we observed some shifts in maxima for Laurdan and Prodan (data not shown), the clearest evidence for altered spectral properties in altered chemical environments was seen in the spectra for Nile Red.

Greenspan's work on Nile Red shows shift in maxima to shorter wavelengths with decreasing polarity solvents (116, 117). Figure 3.11 shows the spectra of Nile Red in various solvents. In response to a fixed excitation (470 nm) we observe Nile Red emission spectra with maxima varying by nearly 200 nm depending on the polarity of the solvent. We also find variations in relative intensity of Nile Red emission (relative fluorescence units, RFU) of Nile Red in these different polar environments. For example, Nile Red analyzed in cyclohexane (CHX), a non-polar solvent, produces an emission spectrum with a peak of ~2200 RFUs. When we compare that to ethanol, a polar protic solvent, we observe an emission spectrum with a peak of ~200, demonstrating a difference of ~2000 RFUs between the two solvents. We interpret these data as indicating that, depending on the polarity of the environment in which Nile Red is located, both the range and height of emission will vary.

We find the behaviour of Nile Red in the adipocyte to be different to that in the mast cell. For example, we find adipocytes treated for 6 days with insulin-FDI to exhibit marked leftward shifts (mean of -24 nm ± 7.5 nm) towards the UV in their emission maxima with higher peak intensities when compared to control, untreated cells. Conversely, we find little or no apparent shift in emission spectra in insulin-FDI treated mast cells (mean of 2.5 nm ± 1.7 nm) and actually observe decreases in peak intensities (see Discussion). In the context of cellular steatosis, these data provide us with a unique biochemical fingerprint and another

level of insight into the compositional heterogeneity of lipid bodies in these two different cell types.

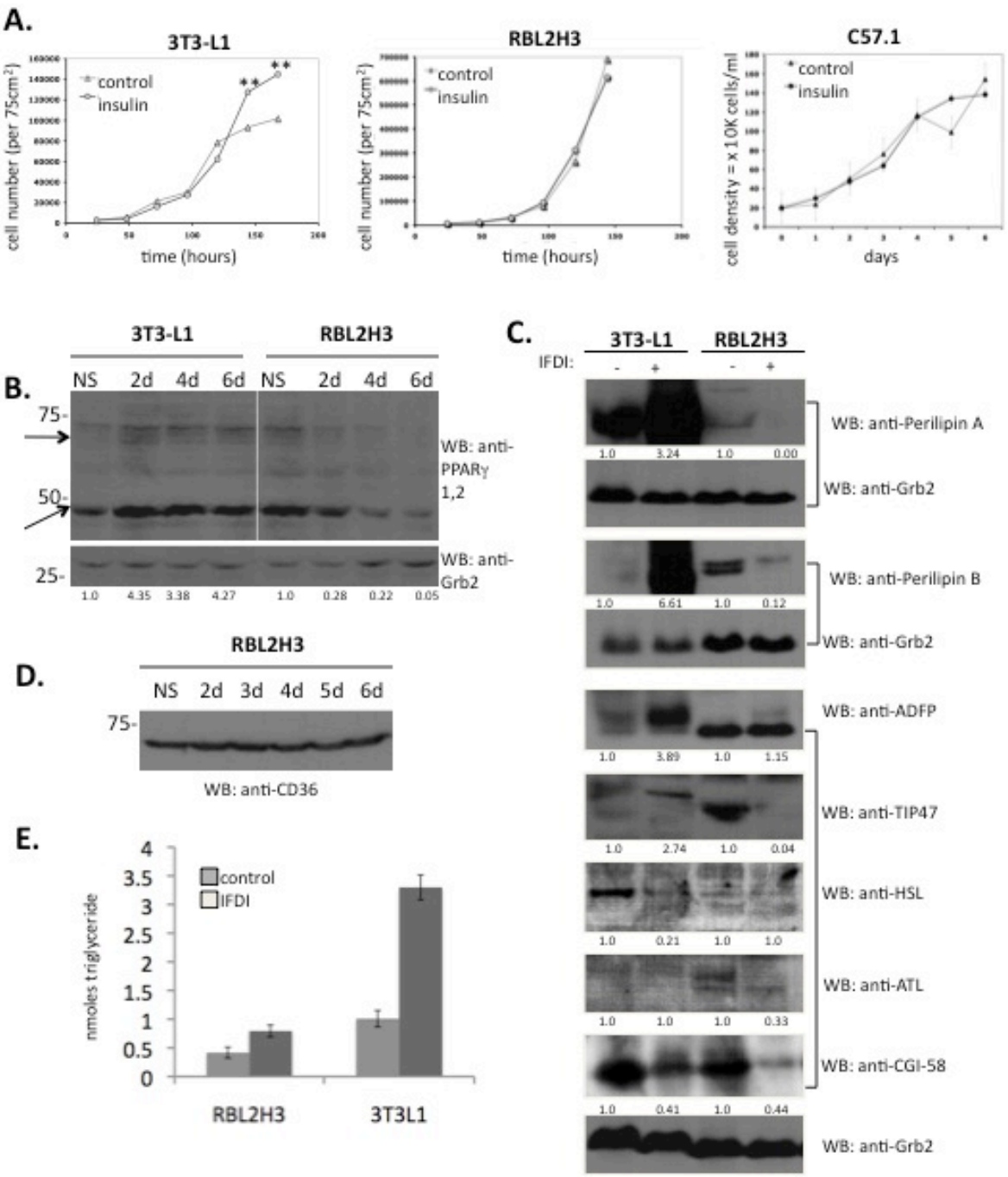
A.
3T3-L1
RBL2H3
C57.1
control
insulin
cell number (per 75cm²)
time (hours)
cell density = x 10K cells/ml
days
B.
3T3-L1
RBL2H3
NS 2d 4d 6d NS 2d 4d 6d
75-
50-
25-
WB: anti-PPARγ 1,2
WB: anti-Grb2
1.0 4.35 3.38 4.27 1.0 0.28 0.22 0.05
C.
3T3-L1
RBL2H3
IFDI: - + - +
WB: anti-Perilipin A
1.0 3.24 1.0 0.00
WB: anti-Grb2
WB: anti-Perilipin B
1.0 6.61 1.0 0.12
WB: anti-Grb2
WB: anti-ADFP
1.0 3.89 1.0 1.15
WB: anti-TIP47
1.0 2.74 1.0 0.04
WB: anti-HSL
1.0 0.21 1.0 1.0
WB: anti-ATL
1.0 1.0 1.0 0.33
WB: anti-CGI-58
1.0 0.41 1.0 0.44
WB: anti-Grb2
D.
RBL2H3
NS 2d 3d 4d 5d 6d
75-
WB: anti-CD36
E.
control
IFDI
nmoles triglyceride
RBL2H3
3T3L1

Figure 3.10. Lipid body biogenesis is mechanistically different in mast cells and adipocytes. A. Effects of insulin on proliferation. 3T3-L1, RBL2H3 and C57.1 BMMC cells were incubated either with insulin alone or untreated for 6 days at 37^{o}C. Live cell numbers were established by trypan blue exclusion assay. **B. PPARγ regulation by insulin-FDI in adipocytes and mast cells.** 3T3-L1 and RBL2H3 were incubated for the indicated time (in days) with insulin-FDI as described. Cell lysates were prepared and Western blotted for the presence of PPARγ using rabbit polyclonal anti-PPARγ (0.1μg/ml for 1h) followed by anti-rabbit IgG secondary. The pan-PPARγ antibody here recognized discrete bands corresponding to PPARγ 1 and 2. Arrowheads indicate PPARγ2 (upper) and PPARγ1 (lower). Expression ratios derived from Image J quantification of the Western are shown below the blot panel. **C. Western blot analysis of lipid body associated proteins in adipocytes and mast cells.** 3T3-L1 and RBL2H3 ($5x10^6$ cells per lane) were stimulated with IDFI for 6 days and protein lysates were prepared as described. Western blot analysis was performed as described in Methods with the following antibodies: anti-perilipin A (5.0 μg/ml); anti-perilipin B (1.0 μg/ml); anti-Adipose Differentiation-Related Protein (ADFP, 0.67 μg/ml); anti-Tail Interacting Protein of 47kDa (TIP-47, 1.2 μg/ml); anti-Hormone Sensitive Lipase (HSL, 2.0 μg/ml); anti-Adipose Triglyceride Lipase (ATL, 0.67 μg/ml); anti-1-acylglycerol-3-phosphate O-acyltransferase (ABHD5, CGI-58, 1.0-2.0 μg/ml). Expression ratios derived from Image J quantification of the Western are shown below the blot panel. Anti-Grb2 Western blots are presented as loading controls. **D. Timecourse of CD36 regulation in response to insulin-FDI.** RBL2H3 ($5x10^6$ cells per lane) were stimulated with insulin-FDI for 6 days and protein lysates were prepared as described. Western blot analysis was performed as described in Methods using anti-CD36. **E. Mono-, di – and tri-glyceride levels in mast cells are not altered by exposure to lipogenic stimuli.** RBL2H3 or 3T3-L1 cells were treated with insulin-FDI for 6 days. Cells ($5.1x10^6$ per sample) were washed, permeabilized and triglycerides were harvested as described in Methods. OD570 was converted to nmoles conjugated glycerides using a standard curve. Values are expressed as mean of triplicates +/- SD. ***Analysis***. *n>3; *p < 0.05; ** p < 0.01; *** p < 0.001; no symbol, p > 0.05.*

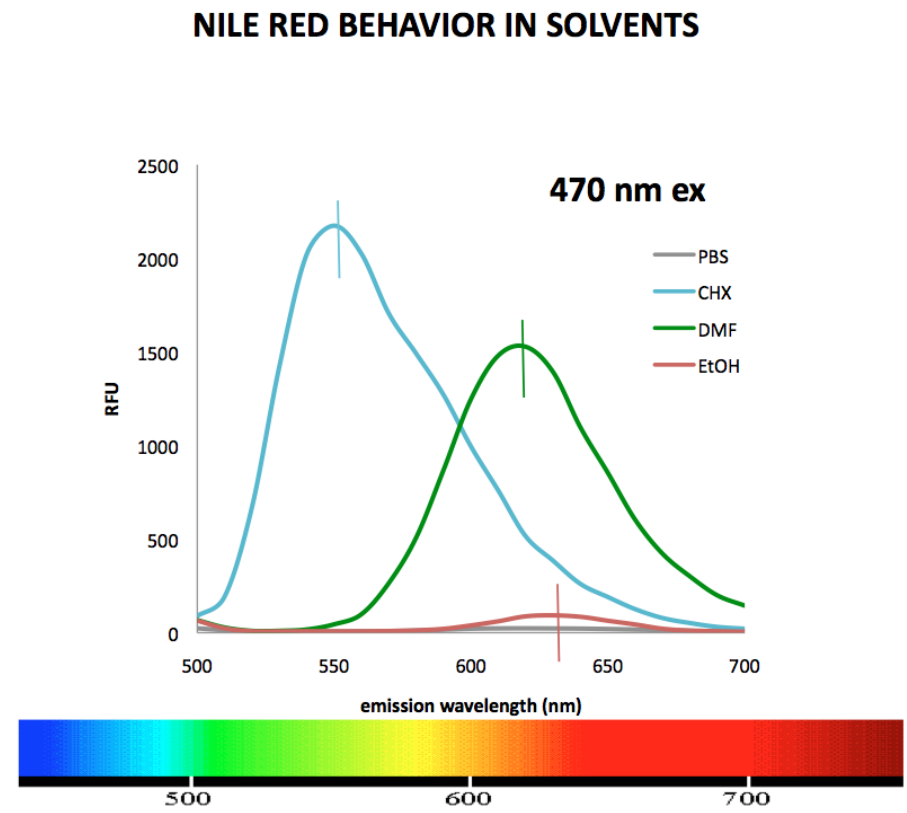

Solvent	Dielectric Constant	Polarity
PBS	~80	Polar
(Water)	(80)	Polar
Dimethylformamide	38	Polar aprotic
Ethanol	24.55	Polar protic
Cyclohexane	2.02	Non-polar

Figure 3.11. Different chemical environments can be resolved by fluorescence emission shifts in the lipophilic dye Nile Red. Nile Red (1μg/ml) was dissolved in 200μl of the indicated solvent and various excitation wavelengths, were used to generate emission spectra scanned between 400 and 800 nm. Shown here is a single 470 nm excitation spectrum scanned for emissions between 500 and 700 nm. Dye is poorly fluorescent in aqueous solution (PBS), but with decreasing polarity the emission spectrum shifts towards the UV end of the spectrum. These data are consistent with previous studies showing that Nile Red fluorescence maxima shift from red towards the yellow-gold in more polar versus neutral lipid environments respectively.

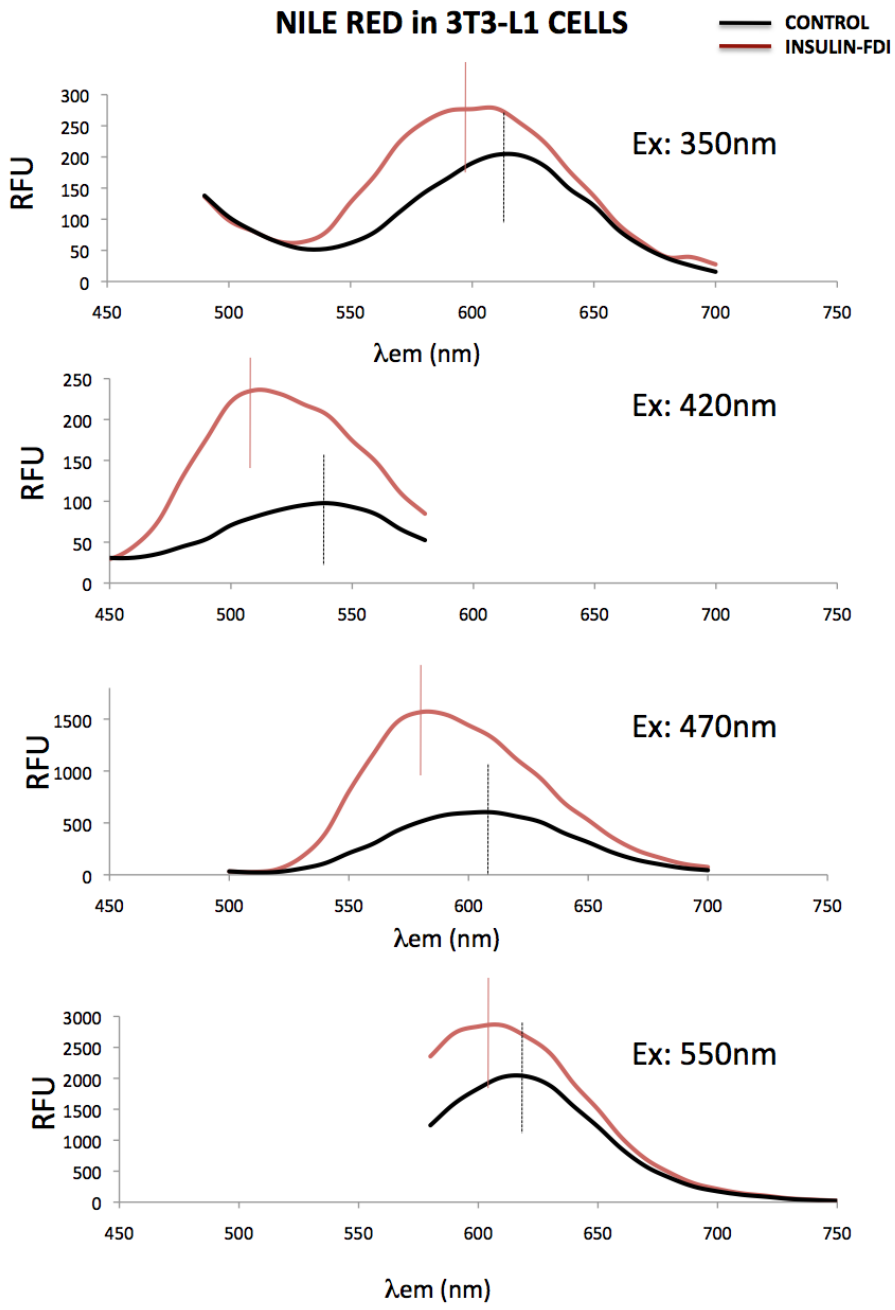

Figure 3.12. Nile Red Emission Spectra in 3T3L-1 adipocytes. 3T3-L1 adipocytes were incubated with Insulin-FDI or vehicle for 6d as described and then labeled with Nile Red. The indicated excitation wavelengths were used to generate emission spectra scanned between 400 and 800 nm. Lines represent averages of triplicate readings at each wavelength.

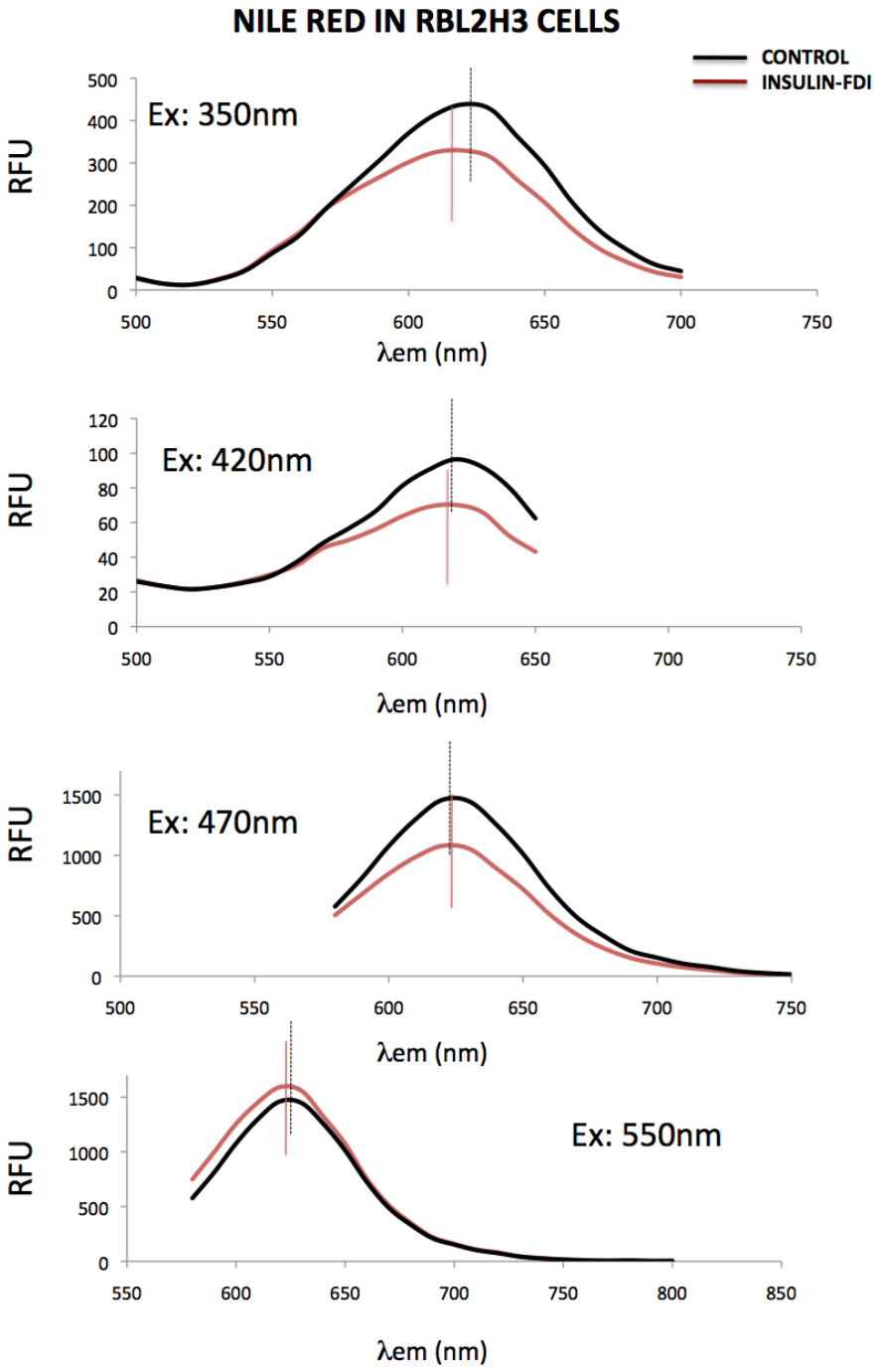

Figure 3.13. Nile Red Emission Spectra in RBL2H3 mast cells. RBL2H3 were incubated with Insulin-FDI or vehicle for 6d as described and then labeled with Nile Red. The indicated excitation wavelengths were used to generate emission spectra scanned between 400 and 800 nm. Lines represent averages of triplicate readings at each wavelength.

3.3. Discussion

The size, number and content of lipid bodies are central markers of metabolic status in cells such as adipocytes and hepatocytes. Lipid accumulation, whether in the form of imported dietary fats or ER-synthesized lipids, results in the accumulation of lipid bodies in the cytosol. In adipocytes and hepatocytes, the primary role of these lipid storage organelles is to act as accessible reserves of anabolic substrates for energy generation, in the form of free fatty acids that can be supplied to closely juxtaposed mitochondria. Lipogenic stimuli, primarily the endocrine hormone insulin, drive the accumulation of these lipid stores. In Chapter 3 we present data that show that the lipogenic, lipid body-inducing role of insulin is not restricted to adipocytes and hepatocytes. Our data show that insulin is necessary and sufficient to drive lipid body accumulation in mast cells. While few major differences between adipocyte and hepatocyte lipid bodies have been noted, our data suggest that in terms of protein content, dye accumulation and mechanism of formation, mast cell lipid bodies are not equivalent to those found in adipocytes and hepatocytes, although there are some commonalities. Finally, our data suggest that even within a single cell type, the lipid body population is highly heterogeneous in terms of size, dye accumulation and internal chemistry, which is again an observation not previously reported in the adipocyte and hepatocyte cell systems.

One of the first goals of the work presented in this thesis was to identify a robust, reproducible, in *vitro* system for the extended study of lipid body biogenesis and function in mast cells. Any *in vitro* system is not without experimental compromises, and while the RBL2H3 mucosal mast cell system has some flaws, it has consistently been a good predictor of signaling and functional responses and regulatory mechanisms in primary cells (96). We validated a set of lipogenic stimuli in the 3T3-L1 adipocyte cell line before translating it to both transformed (RBL2H3) and primary (BMMC) mast cells. In the adipocyte literature, insulin is sufficient to cause lipid body accumulation, but a wider experimental window (more intense responses) has been achieved by co-stimulation with an inhibitor of TNFα production (to oppose lipolysis) and an activator of cAMP generation. We have examined these stimuli components either alone, or in combination, in mast cells, with Oil Red O

staining as a read out. As in the adipocyte, insulin is sufficient to cause lipid body accumulation to high levels with some enhancement of these responses by the addition of the other components of this lipogenic stimulus.

The possibility of insulin being the driving stimulus that establishes lipid body content in mast cells has interesting implications. Building on our *in vitro* data, there are important *in vivo* tests of this hypothesis that need to be performed. In genetic and chemically-induced models of Type I diabetes we would predict a decrease in the lipid body (and hence eicosanoid content) of mast cells in certain tissue locations. Conversely, in hyperinsulinaemic models (e.g. DIO mice) we would predict elevated LB levels in tissue-resident mast cells. Intriguingly, there is one published observation that alludes to histopathology data where mucosal mast cells stain more heavily *in situ* with the lipid body dye Sudan Black in sections from obese than control patients (48). In addition, an unbiased screen for other determinants of lipid body content, especially in a model of mast cell differentiation is important. Our *in vitro* findings have potentially interesting implications under normal physiological conditions, prompting investigation of whether daily fluctuations in insulin levels are able to regulate mast cell lipid body load. Perhaps more likely is the idea that hyper-insulinaemia, associated with the insulin-resistant stage of the progression through obesity and Type II diabetes, could be altering mast cell status.

A role for insulin may suggest that other stimuli (such as leptin, ghrelin, glucagon) may regulate lipid body load in mast cells. A direct stimulus that controls the number of lipid bodies in mast cells has previously not been identified. In other immunocytes (e.g. macrophages), immunological challenge results in an increase in lipid body load, but here we show that insulin may play a key role in determining mast cell lipid body numbers in the absence of challenge. It is not clear what constitutes a ‘normal’ lipid body load in mast cells, or whether under physiological or pathophysiological conditions their number ever increases dramatically. Based on a limited number of published electronmicroscopy studies it appears that the ratio of secretory granules to lipid bodies in primary mast cells is high, with <10 lipid bodies typically observed per cell (84, 92).

The sensitivity of mast cells to insulin is, in a sense, predicted by the fact that insulin receptors have been detected on primary and transformed mast cells, both *in vitro* and *in*

vivo. However, previous studies did not generate a clear picture of the role of insulin in mast cell biology. Surprisingly, given the primary role of insulin as a lipogenic stimulus, previous studies of insulin effects on mast cells did not look at lipid body load or formation. This is a reflection of the degree to which the lipid body has been neglected in studies of the mast cell compared to its counterpart, the histamine-containing secretory granule.

Our data suggest that mast cell and adipocyte lipid bodies are not equivalent by a number of measures. First, there are both commonalities and differences in the levels of PAT family and other lipid body-associated proteins in insulin-treated adipocytes and mast cells. Perhaps most strikingly, PPARγ is not upregulated, either transcriptionally or translationally, in mast cells that are undergoing the accumulation of large numbers of lipid bodies. In adipocytes and hepatocyte, this is a required step in the induction of lipid body biogenesis (114). Our data specifically show that there is no upregulation of PPARγ during chronic insulin exposure. However, there is no downregulation either, and so these data do not exclude the idea that the basal levels of PPARγ in a mast cell are sufficient to accomplish the signaling associated with elevated lipid body biogenesis. Thus we do not exclude a role for PPARγ in mast cell lipid body biogenesis, merely we demonstrate that upregulation of PPARγ levels is not required. Further experiments with knockdown or inhibition of PPARγ pathways would resolve this point.

Considerable effort was placed into establishing fluorescence imaging protocols for the mast cell lipid bodies induced by chronic insulin exposure. Our data in adipocytes closely follow those in the literature, where we observe induction of a homogeneous population of lipid bodies that stain consistently with Oil Red O. In the mast cell, there is strong ORO staining in insulin-FDI treated cells. However, when we embarked on the use of a broader spectrum of lipid dyes, we immediately noted that the lipid body population in mast cells is in fact highly heterogeneous. Each of the dyes used here has previously been used to stain lipid bodies or lipid droplets, but the overlap in populations stained between dyes has never been studied in a systematic fashion, even in the adipocytes. Thus our data may suggest that ORO protocols have led to an underestimation of the complexity and heterogeneity of lipid body populations in adipocytes. This is certainly the case in mast cells, where we observe sub-populations of ORO positive, and ORO negative lipid bodies that can be differentiated on the

basis of dye accumulation, size and (to some extent) subcellular location. For example, Nile Red positive lipid bodies tend to be small structures distributed close to ER concentrations, and in future work we will test the idea that these represent the primordial lipid bodies that are nascently evolving from the ER lamellae.

One of the complications of these analyses is that the dyes themselves are lipids, which are accumulating preferentially in lipophilic environments of, presumably, different internal chemistries. The dyes are not stains in the sense that they are not 'finding' and covalently binding to, an acceptor molecule. Rather we are looking at relative accumulations of dyes in varying locations based on chemical compatibility and preferential localization. Thus we cannot exclude that a dye such as ORO could act to exclude other dyes from a location, and so co-localization studies may be complicated to interpret in this context. A complimentary approach would therefore be to extend the study of lipid body heterogeneity in mast cells to protein-based immunofluorescence, where we would assume that difference in protein localization (e.g. PAT proteins, lipid metabolizing enzymes, ER markers) would be an alternate differentiator of lipid body sub-populations. It is perhaps worth noting that a large body of EM data, generated by Dr. Ann Dvorak's laboratory between the 1970s and 1990s would support the idea that mast cell and basophil lipid bodies are highly heterogenous structures with many different presentations (84, 85, 92, 95, 110, 111, 114, 118). Our own EM data support this, but a real limitation of EM is the lack of associated protein identification data. Again, the addition of a data set looking at protein location using lipid body marker immunogold analysis would strengthen these data sets.

Assuming that the observed sub-populations are not dye artifacts, perhaps the key question that emerges is whether their microscopic heterogeneity is attributable to different lipid content, which in turn, would suggest functional heterogeneity. Our spectral data provide a preliminary indication that at least the lipid bodies in resting, and insulin-FDI treated mast cells provide different chemical environments for the Nile Red probe, reflected in its fluorescence behaviours. Spatially-resolved spectral analysis will be required to test whether this heterogeneity is also found within the insulin-induced lipid body population.

The role of mast cell lipid bodies is still unclear. Our data raise a number of questions. First, it is not clear whether the lipid bodies found in resting mast cells are equivalent to those

induced by insulin-FDI exposure. Thus we do not know whether we have expanded an existing population of lipid bodies or induced the presence of a new type of organelle. A second question that follows from this is whether the primary role of the lipid body is metabolic, or perhaps to store of pro-inflammatory lipid precursors. This question can only be addressed by the extensive lipidomic analysis presented later in this thesis. Finally, the accumulation of lipid bodies on the cytosol of insulin-FDI treated mast cells is a striking phenomenon, and creates the need to assess the functional consequences for the mast cell of this dramatic new phenotype.

Chapter Four

Functional impact of steatosis on mast cell pro-inflammatory function

4.1. Introduction

The data shown in Chapter 3 demonstrate the hyper-accumulation of lipid bodies in mast cells following chronic insulin exposure. The level of LB accumulation is striking, and comparable with that previously observed in macrophage foam cells, adipocytes and hepatocytes. In this Chapter we explore the impact of this acquired phenotype on mast cell function. We compare classical markers of mast cell pro-inflammatory responses (degranulation, eicosanoid release, cytokine gene induction) between control, and steatotic cells. In addition, we compare ER status and calcium signaling dynamics, between control and steatotic cells, since these may provide a mechanistic basis for the impact of LB accumulation on mast cell pro-inflammatory function.

4.1.1 Ectopic lipid deposition and cellular function

As reviewed in Chapter 1, ectopic lipid deposition occurs at the tissue and cellular level. In addition to the well-characterized accumulation of lipid bodies in adipocytes and hepatocytes, cell types such as skeletal and cardiac myocytes, and pancreatic beta cells have been described as accumulating cytoplasmic lipid bodies during obesity (8, 9, 29). Our data (Chapter 3) now provide evidence that this ectopic lipid deposition could extend to cells of the immune system, adding mast cells to the prior descriptions of lipid body accumulation in the macrophage.

The numbers of the LB in the cytosol are striking, and it is hard to believe that they would not dramatically impact the transcytoplasmic signaling pathways that are necessary for cellular function. The sudden presence of such large numbers of lipid structures seems likely to cause dramatic remodeling of the cytoplasm, with subsequent effects on the integrity of cellular signaling pathways. As described in Chapter 1, there are few papers addressing this

issue, but there is intriguing evidence of cytoskeletal remodeling, altered calcium dynamics and uncharacterized signaling changes that result in altered functional responses in steatotic hepatocytes and adipocytes. Thus while cells that exhibit this steatosis have altered functional phenotypes, the mechanistic links between cytosolic LD/LB accumulation and altered cellular signaling and functional responses have not been explored.

4.1.2. Ectopic lipid deposition, the ER and ER stress

The ER is an intracellular organelle that forms an extensive membranous network of interconnected cisternae, tubules and vesicles. The ER is divided into two primary components each responsible for synthesizing its own unique set of biological components. The rough ER is the docking site for ribosomes and is primarily responsible for the synthesis of proteins. In contrast, the smooth ER, in addition to acting as a major storage location for intracellular calcium, is responsible for synthesizing lipids such as fatty acids, triacylglycerols and cholesterol esters. The exact function of the ER can vary substantially from cell-to-cell, which is partially reflected in the abundance of rough to smooth ER found in the cytoplasm.

The ER may present altered functional states initiated by viral infections, nutrient deprivation, oxidative stress or aberrant calcium regulation. Perhaps the best characterized of these ‘altered states’ is the development of an Unfolded Protein Response (UPR) in the ER (69, 119). Stressors can result in the ‘backing up’ of unfolded proteins inside the ER lumen and a cessation of translating new proteins. There is an evolving conceptual framework emerging in regards to the correlation between varying metabolic climates (obesity in particular) and chronic ER stress and the UPR, although the mechanisms reinforcing this relationship are still poorly understood. Studies have recently shown that chronic ER stress and the initiation of the attending unfolded protein response (UPR) results in insulin resistance and type II diabetes. Furthermore, published studies also suggest that alterations in intracellular lipid composition may potentially inhibit SERCA ATPase activity leading to the manifestation of ER stress (120).

The laboratory of Dr. Gokhan Hotamisligil has demonstrated that during obesity, the hepatic ER switches from primarily synthesizing proteins towards primarily synthesizing lipids (71). This transition is associated with decreased protein synthesis, ERAD (endoplasmic reticulum

associated degradation), diminished calcium storage capacity, and activation of some markers of the UPR. There is also evidence in the literature of a morphological change in the obese ER, where distended, possibly lipid-filled cisternae accumulate in the cytoplasm. We based that this transition is likely to be related to lipid body biogenesis and formation, based on the fact that lipid bodies originally arise from the ER. EM experiments on sections from *in vivo* models of diabetes have shown that the integrity of the ER in pancreatic β-cells is dysregulated in diabetic mice (121). This dysregulation has been identified as a consequence of ER stress and is characterized by a thickened nucleoplasmic reticulum membrane and an expanded and highly distended ER. It has also been shown that expression of certain transcription factors (for example XBP1) are activated during ER stress and that XBP1 stimulates lipid biosynthesis and enlarges the ER lumen in both B lymphocytes and fibroblasts (69). We do not currently understand the relationship between ELD, ER stress and their functional consequences in the mast cell system.

These data provide a foundation for our model that ER dysregulation, suppression of protein synthesis and enhancement of lipid synthesis, lipid body formation and the backing up of a lipid-laden and distended ER could all be progressively and causally linked to metabolic dysregulations attributable to chronic exposure to the insulin-FDI treatment, although the order of events remain to be elucidated.

4.1.3. Potential impacts of steatosis on pro-inflammatory functions of the mast cell

At the cellular level, ectopic lipid deposition manifests as the accumulation of lipid droplets in the cytosol, in high numbers. It seems likely that occlusion of the cytosol with large numbers of lipid structures would impact the cell in numerous ways, from cytoskeletal rearrangement/disruption, to repositioning of organelles and potentially altered behaviour of signaling molecules and second messengers. Moreover, a stressed and ‘re-programmed’ ER would impact the cell in a potentially vast number of ways from altered integrity and capacity of the ER calcium store to defective synthesis and production of almost all cellular proteins. Surprisingly this is a little studied area in the steatosis literature, and it is completely unstudied in mast cells.

Previous studies evaluating ER stress in mast cells have been limited to observations of functional characteristics that are associated with ER stress such as defective ER calcium

signaling. But no explicit studies of ER stress or the UPR have been carried out. Currently, there have been no studies in mast cells investigating ER stress in the context of metabolic dysregulation

In mast cells, the generation of a calcium signal is an essential requirement for an array of physiological functions including the production of eicosanoids, the optimal induction of cytokine gene transcription and degranulation in response to antigens or other stimulants. From the mobilization of intracellular stores to the opening of calcium channels in the plasma membrane, the mobilization of this potent second messenger is a vital step in the transmission of intracellular signalling (122-125). We hypothesize that the accumulation of lipid bodies observed in the insulin-FDI treated mast cell may act as a barrier to the progress of a cytoplasmic calcium signal. The biophysical impact lipid bodies may have on signaling by second messengers in the cytoplasmic soluble phase has not been studied. Moreover, the potential for these bodies to act as potential calcium stores, calcium sinks or to exclude calcium has only been alluded to in the literature.

4.1.4. Experimental Approach: Exploring the phenotype of steatotic mast cells

In this Chapter we explored the functional impact of the steatotic accumulation of lipid bodies on mast cell degranulation, cytokine gene induction and the production of bioactive eicosanoid lipids. We evaluated two fundamental mechanisms by which the steatotic accumulation of lipid bodies may alter the phenotype of mast cells, through the dysregulation of intracellular calcium signaling and the induction of endoplasmic reticulum stress and reprogramming.

4.2. Results

4.2.1. Altered mast cell granularity phenotype in response to chronic insulin exposure

Based on our findings in Chapter 3, we sought to characterise the phenotype of mast cells that had been exposed to insulin-FDI and have developed the highly lipid body-rich state shown above. Using flow cytometry, we compared insulin-FDI treated cells to controls initially evaluating forward scatter (FSC) and side scatter (SSC) characteristics. Figure 4.1 shows that control mast cells divide into $SSC^{hi}FSC^{lo}$ and $SSC^{lo}FSC^{hi}$ sub-populations. With insulin-FDI treatment or insulin alone, there is an increase in the number of cells in the $SSC^{lo}FSC^{hi}$ population (Figure 4.1A). The secretory granule load of mast cells is reflected in their scatter properties assayed by flow cytometry (126, 127), with high granularity conferring high side scatter (SSC) properties. As a population, insulin-FDI-treated mast cells decrease in SSC and increase in forward scatter (FSC) in comparison to controls. We hypothesized that this shift in scatter properties could reflect alterations in functional capability of mast cells.

4.2.2. Degranulation is suppressed in mast cells chronically-exposed to insulin

We asked whether lipogenic stimuli had any effect on the degranulation response and secretory granule population in mast cells. Figure 4.1B and 4.1C show that degranulation responses are suppressed in insulin-FDI treated mast cells in response to both pharmacological and antigenic stimulation of mast cells.

4.2.3. Altered enzyme expression in the eicosanoid synthesis pathways and altered eicosanoid production in insulin-exposed mast cells

There is some evidence that the proximal synthetic enzymes for leukotrienes and prostaglandins are located within the lipid body, leading to the proposal that lipid bodies represent a possible secondary site for eicosanoid synthesis in addition to the recognized cytosolic PLA2-dependent pathway (84, 92, 94, 128). Indeed, both phospholipid-derived and triglyceride pools of arachidonic acid have been described in macrophages, and lipid bodies are thought to contain a unilamellar layer of phospholipid that may be a PLA2 substrate. We asked whether mast cell levels of cyclo-oxygenase (COX) and lipoxygenase (LO) enzymes

were regulated during lipogenesis. Insulin-FDI induces downregulation of COX2 (Figure 4.1D) and a striking upregulation of 5-LO and LTC4 synthase (Figure 4.1F), indicating a transition towards the eicosanoid synthesis program. Quantifications of these data are presented in Figure 4.1E. The COX2 downregulation is, predictably, highly dexamethasone dependent (data not shown), while LTC4 synthase upregulation is accomplished by insulin in the absence of dexamethasone (Figure 4.1G).

We asked whether the upregulation in eicosanoid synthetic enzymes noted above translated to an increase in the release of their eicosanoid products in response to mast cell stimulation. Mast cells incubated with lipogenic stimuli for 6 days exhibit elevated basal LTC4 levels, and when stimulated via the FcεRI receptor, release significantly more LTC4 than untreated cells (Figure 4.1H). These data suggest that the upregulation in leukotriene synthesis enzymes during lipogenesis is functionally significant for mast cells.

4.2.4. Cytokine gene expression in insulin-exposed mast cells

The third arm of the mast cell response to stimulation (in addition to degranulation and eicosanoid production) is the *de novo* production of cytokines and chemokines (42). In the context of metabolic disease, mast cell-derived IL-6 and IFNγ have been shown to directly promote adipose inflammation and angiogenesis, promoting obesity. Moreover, IL-4 production by adipose resident Th2, macrophages and potentially mast cells, could alter the inflammatory status of adipose tissue (see Chapter 1). We performed a broad assessment of cytokine gene transcriptional status in mast cells in the absence and presence of insulin-FDI exposure. A panel of cytokines assessed by microarray revealed few alterations in response to insulin-FDI-exposure, with the exception being a marked downregulation in basal levels IL-3 transcripts and some slight upregulation in the Th2 cytokines IL2, IL-6 and IL-10 (data not shown). No change was noted in basal IL-4 levels. For this broad panel of cytokines we did not ask whether antigen-induced transcriptional activation was altered in insulin-FDI exposed versus control cells. Rather, we performed a more focused analysis on IL-6, for which a direct link between mast cell production of the cytokine and adipose inflammation has been demonstrated (45, 129).

Mast cell derived IL-6 has been suggested to play a causative role in diet-induced obesity and glucose intolerance, and our data suggest that basal IL-6 levels are upregulated by chronic

exposure to lipogenic stimuli in mast cells (Figure 4.1I), and the degree of IL-6 transcriptional activation in response to subsequent antigen stimulation is also significantly enhanced in insulin-FDI-exposed mast cells.

A.

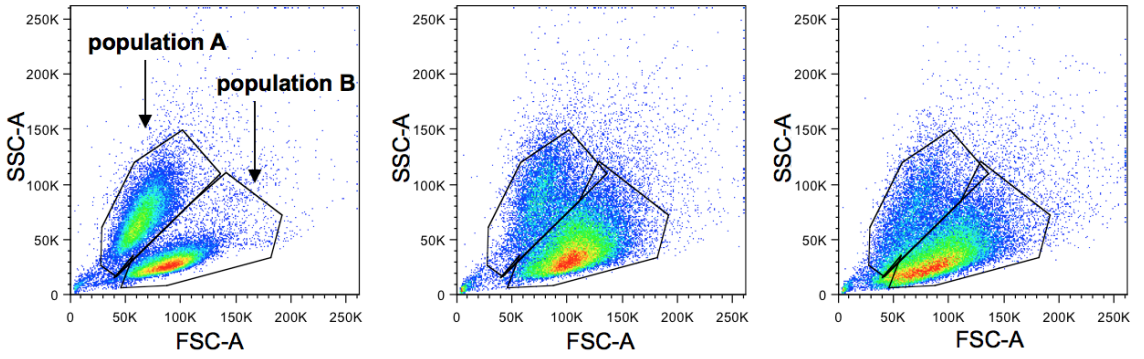

% cells	SSC MPI	FSC MPI
A: 41.8	A: 69,545	A: 64,554
B: 54.5	B: 28,017	B: 88,788

% cells	SSC MPI	FSC MPI
A: 17.2	A: 85,876	A: 77,778
B: 77.3	B: 40,564	B: 107,000

% cells	SSC MPI	FSC MPI
A: 17.5	A: 68,180	A: 66,679
B: 73.9	B: 33,996	B: 92,839

B.

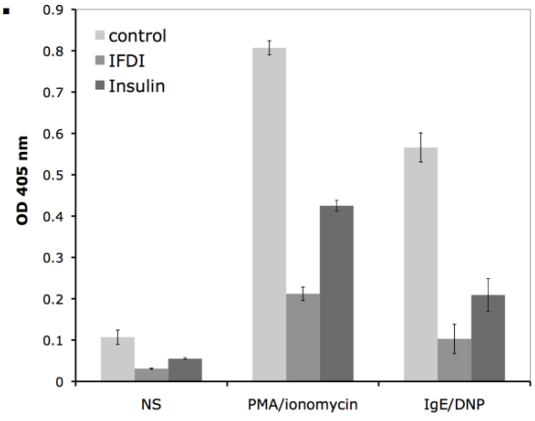

C.

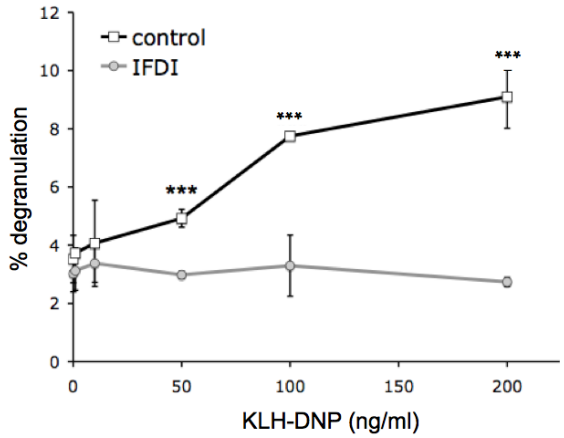

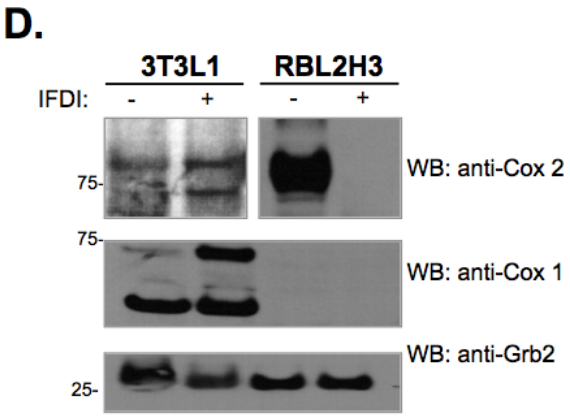

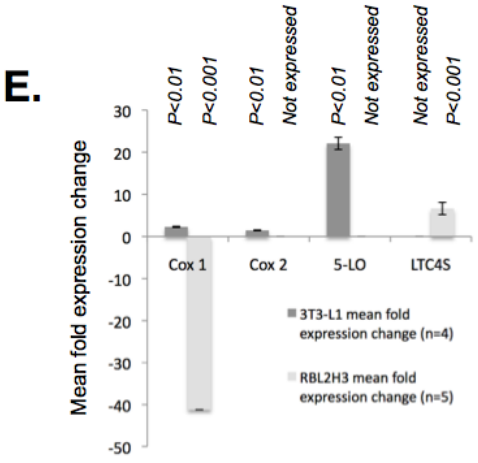

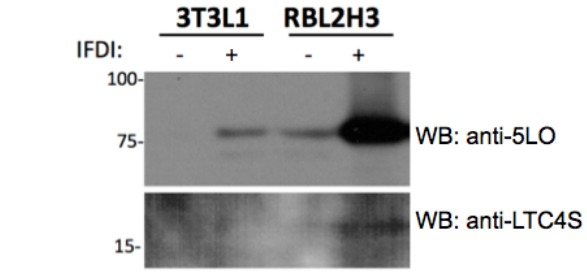

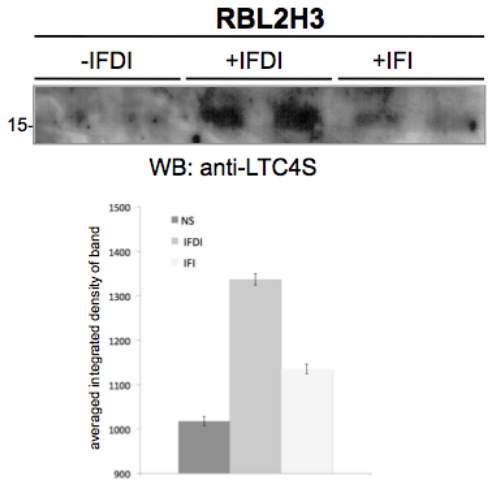

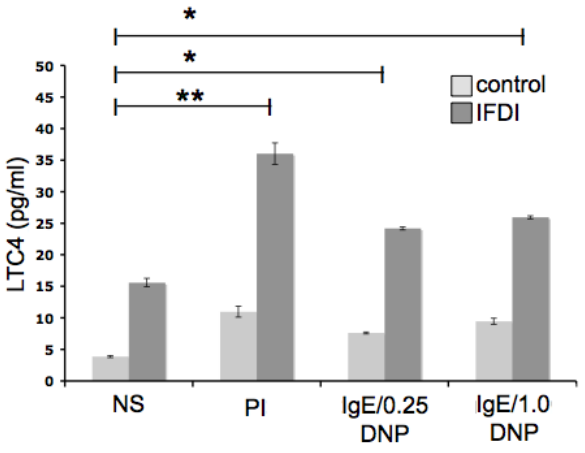

	Untreated	IFDI
Maximum releaseable LTC4 per 1x10^6 cells	2.5 (± 0.035) pg	8.2 (±0.15) pg
Basal releaseable LTC4 as % maximum	35.2%	50.9%
FcεRI-induced releaseable LTC4 as % maximum	80.5%	72.0%

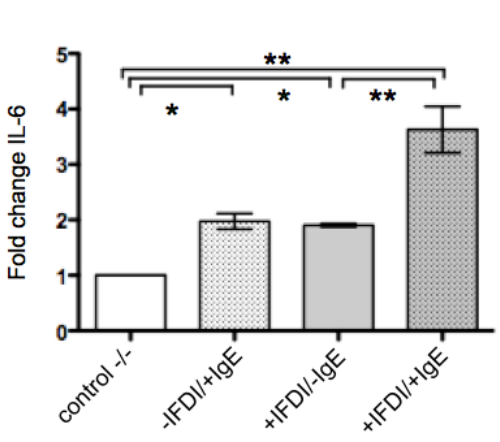

Figure 4.1. Insulin-containing lipogenic stimuli induce phenotypic change in mast cell granule content. A. Scatter profile of control and insulin-FDI-treated mast cells. RBL2H3 cells were incubated with insulin-FDI treatment, insulin-FBS, or left untreated, for 6 days at 37^{o}C. Cells (5 x 10^{5}) per sample were harvested and fixed in PFA before assessed for cell size (FSC) and granularity/membrane complexity (SSC) using a BD FACSAria. Based on FSC and SSC, two distinct sub-populations (A and B) can be distinguished. **B, C. Insulin-containing lipogenic stimuli suppress degranulation of mast cells in response to antigenic and pharmacological activation.** RBL2H3 cells were incubated with insulin-FDI treatment, insulin alone or left untreated for 6 days at 37^{o}C. Cells were either exposed to phorbol-12-myristate-13-acetate and ionomycin (B) for 60 minutes or primed overnight with 1 μg/ml IgE and stimulated with the indicated doses of KLH-DNP for 20 minutes (B, C). Degranulation was quantified using a beta-hexosaminidase assay. **D. Cyclo-oxygenase regulation in mast cells and adipocytes following insulin-FDI exposure.** 3T3L1 and RBL2H3 (5x10^{6} cells per lane) were stimulated with insulin-FDI for 6 days and protein lysates were prepared as described. Western blot analysis for the indicated proteins was performed as described (anti-COX1 2.5 μg/ml, anti-COX2 0.17 mg/ml). **E. Quantification of Western blot analyses for fold change in expression of Cox 1, Cox 2, 5-LO and LTC4-S. F, G. LTC4S and 5-LO regulation in 3T3L1 and RBL2H3**. Cells (1x10^{7} cells per lane) were treated with insulin-FDI or insulin/FBS/IBMX (IFI) for 6 days and lysates were Western blotted as described using anti-LTC4S (2.0 μg/ml) and anti-5LO (0.4 μg/ml). Lower panel in H presents quantification of LTC4S expression changes in response to insulin-FDI and insulin-FI. **H. LTC4 assay in control and insulin-FDI-treated mast cells.** RBL2H3 were exposed to insulin-FDI or vehicle for 6 days. After 15 min stimulation at 37^{o}C with either vehicle or PMA/ionomycin (PI, 1μM/1μM) or via FcεRI (IgE 1μg/ml for 16h followed by 0.25 or 1.0 μg/ml KLH-DNP), LTC4 levels were assayed. LTC4 concentrations were calculated by reference to a standard curve and are expressed as mean +/-SD of triplicate samples. **I. IL-6 transcript levels in mast cells exposed to lipogenic stimuli.** mRNA was isolated from control and insulin-FDI-treated cells that were either unstimulated or activated via FcεRI. qPCR analysis of IL-6 transcript levels was performed as described in Methods. Average of IL-6 fold-change was made of two independent experiments. ***Analysis****. n>3; *p < 0.05; ** p < 0.01; *** p < 0.001; no symbol, p > 0.05.*

4.2.5. Characteristics of the $SSC^{lo}FSC^{hi}$ insulin-induced population in model mast cells

The data presented above suggest that there are marked distinctions between insulin-FDI treated cells and untreated RBL2H3. We further explored the properties of the $SSC^{lo}FSC^{hi}$ population, which is expanded in the insulin-FDI-treated cells. Mast cell secretory granules are autofluorescent due to their serotonin content. We examined the intrinsic autofluorescent properties of both sub-populations, and noted that the $SSC^{hi}FSC^{lo}$ population (referred to here as Population A) is characterised by higher autofluorescence, reflecting higher content of secretory granules (data not shown). Moreover, this population loads more intensely with the granule-staining dye Berberine Sulphate (Figure 4.2A, B). Moreover, using FITC autofluorescence as a measurement of granule content, we noted that the stimulus-induced loss in this parameter, as well as mean peak fluorescence intensity (MPI), was more pronounced in the $SSC^{hi}FSC^{lo}$ population than in the $SSC^{lo}FSC^{hi}$ cells (Figure 4.2C, D).

We used a flow cytometric assay for lipogenesis in mast cells to compare the level of lipid accumulation in the $SSC^{hi}FSC^{lo}$ and $SSC^{lo}FSC^{hi}$ cells. In the flow cytometric application, we found Nile Red to be a preferable stain to ORO, although it should be noted that subsequent staining data performed two years after these flow experiments (Chapter 3) suggests that NR may preferentially stain immature lipid bodies and does not overlap completely with Oil Red staining. In adipocytes and mast cells, Nile Red staining is nevertheless detectable above autofluorescence levels and increases further in response to the lipogenic insulin-FDI treatment (Figure 4.2E, F). Figure 4.2E shows that the insulin-FDI-induced increase in NR accumulation (reflecting lipid body load) is more pronounced in the $SSC^{lo}FSC^{hi}$ cells, while more cells become NR^{+} after insulin-FDI treatment in population B than population A (Figure 4.2F).

The large increases in 5-LO and LTC4 synthase levels that we observe at the whole population level (Figure 4.2G, H) are more pronounced in population B than in population A (Figure 4.2H). These data are consistent with observations from other cell systems, such as neutrophils, which suggest that the lipid bodies that we see preferentially accumulating in population B are reservoirs of eicosanoid metabolizing enzymes. Together, these data indicate that the insulin-exposed mast cell population becomes biased towards a functional

phenotype where bioactive lipid production is enhanced but degranulation responses are compromised.

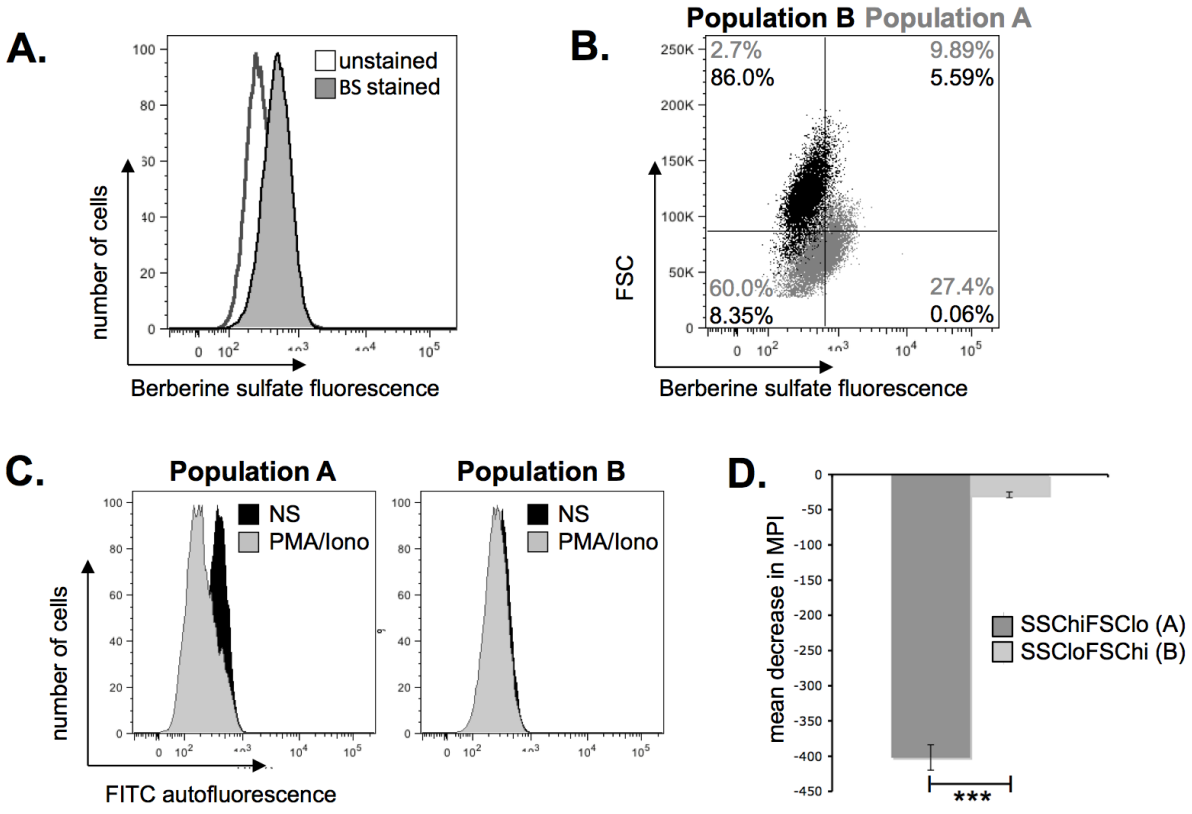
A.
unstained
BS stained
number of cells
Berberine sulfate fluorescence
B.
Population B
Population A
2.7%
86.0%
9.89%
5.59%
60.0%
8.35%
27.4%
0.06%
FSC
Berberine sulfate fluorescence
C.
Population A
Population B
NS
PMA/Iono
number of cells
FITC autofluorescence
D.
mean decrease in MPI
SSChiFSClo (A)
SSCloFSChi (B)
***

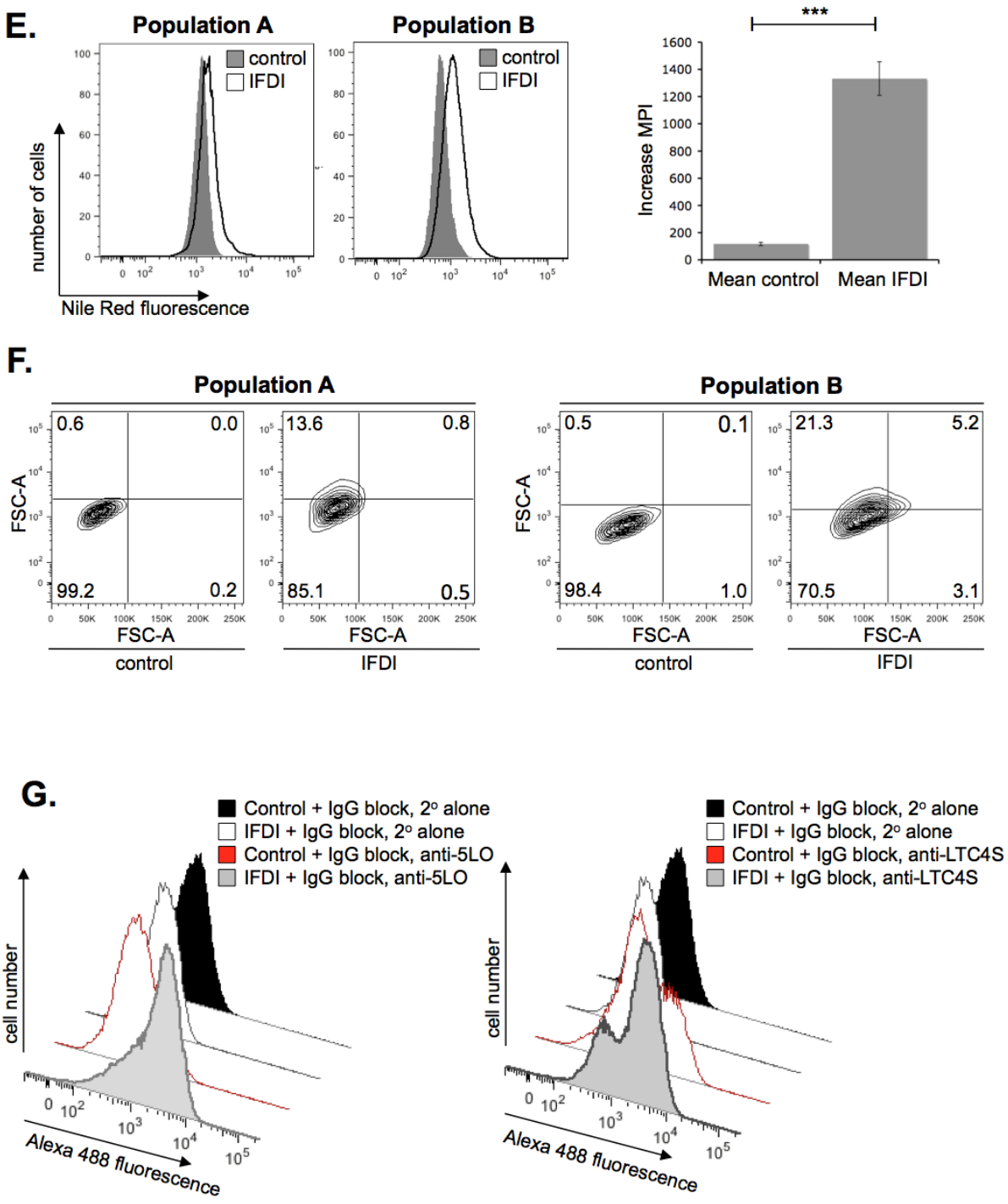
E.
Population A
Population B
control
IFDI
number of cells
Nile Red fluorescence
***
Increase MPI
Mean control
Mean IFDI
F.
Population A
Population B
0.6
0.0
99.2
0.2
13.6
0.8
85.1
0.5
0.5
0.1
98.4
1.0
21.3
5.2
70.5
3.1
FSC-A
control
IFDI
G.
Control + IgG block, 2° alone
IFDI + IgG block, 2° alone
Control + IgG block, anti-5LO
IFDI + IgG block, anti-5LO
Control + IgG block, anti-LTC4S
IFDI + IgG block, anti-LTC4S
cell number
Alexa 488 fluorescence

H.

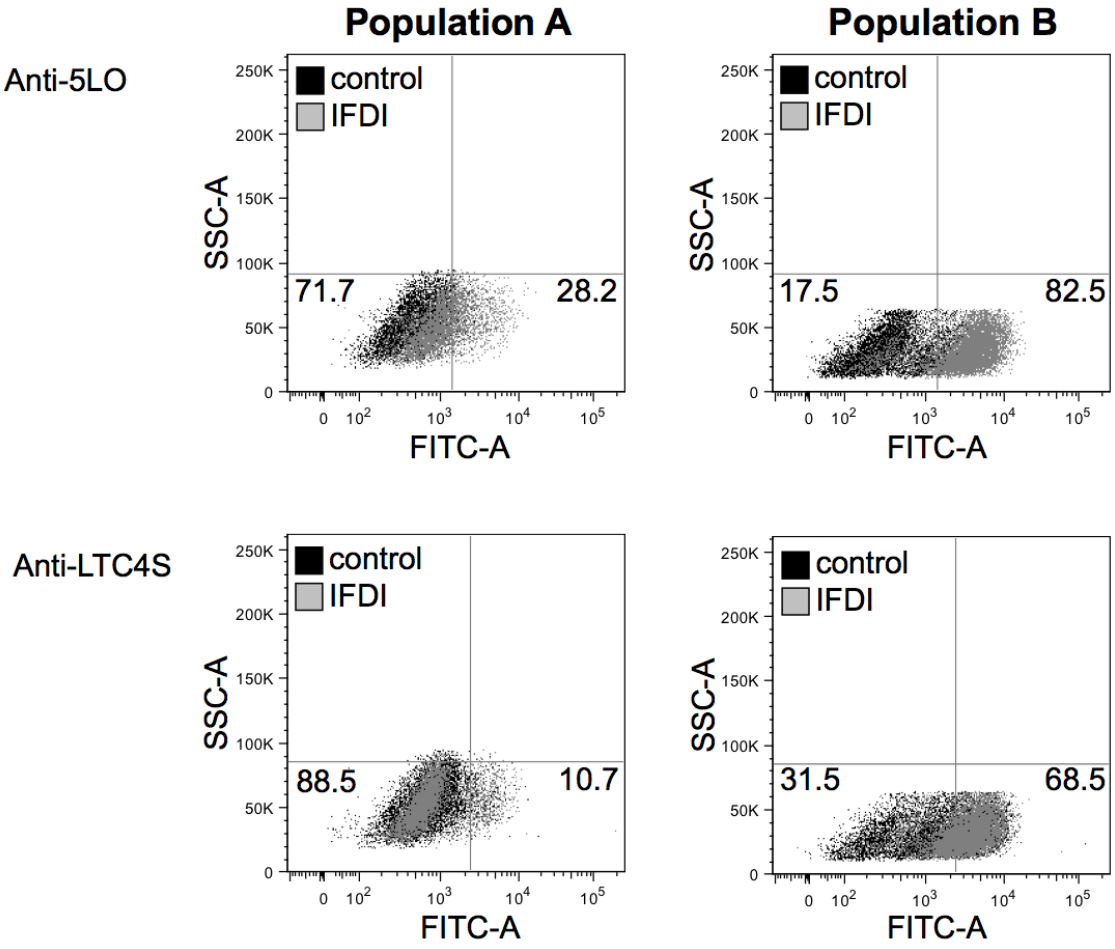
Population A
Population B
Anti-5LO
Anti-LTC4S
control
IFDI
SSC-A
FITC-A
71.7
28.2
17.5
82.5
88.5
10.7
31.5
68.5

Figure 4.2. Characterization of insulin-FDI-induced sub-populations in mast cells. A, B. Berberine sulfate staining is enhanced in the insulin-FDI-induced $SSC^{lo}FSC^{hi}$ subpopulation. RBL2H3 were treated with insulin-FDI for 6 days as described. Staining with Berberine sulfate was performed as described in Methods (left panel). Sub-populations of insulin-FDI-treated cells were assessed for levels of BS accumulation *(right panel)*. **C. $SSC^{hi}FSC^{lo}$ cell sub-population is diminished and loses autofluorescence after stimulation of mast cell degranulation.** RBL2H3 cells were treated with insulin-FDI for 6 days as described. Cells were exposed to vehicle or PMA/ionomycin for 20 minutes. Post-stimulation, cells (5×10^5) were harvested, immediately fixed in PFA and analyzed using a BD FACSAria cell sorter for autofluorescence levels. **D. Quantification of fluorescence loss.** Normalized decrease in MPI in response to PMA/ionomycin stimulation of control and lipid body-enriched mast cells (data averaged from 3 experiments). **E, F. Nile Red accumulation is preferentially localized to $SSC^{lo}FSC^{hi}$ mast cell sub-population.** RB2H3 were analyzed for NR accumulation as described after 6 days exposure to vehicle control or insulin-FDI. The increase in NR fluorescence intensity (E, *left panel*) and number of NR^+ cells in response to insulin-FDI (F) are greater in population B than A. Fluorescence gain (normalized increase in MPI) in response to insulin-FDI treatment of RBL2H3 in populations A and B was averaged from 3 experiments (E, right panel). **G, H. Upregulation in eicosanoid metabolizing enzymes are preferentially localized to $SSC^{lo}FSC^{hi}$ mast cell sub-population.** Upregulation in 5-LO and LTC4 synthase levels following insulin-FDI treatment of RBL2H3 was measured using flow cytometry. **G.** Anti-5LO and LTC4S synthase staining in whole population of RBL2H3. **H.** Increase in positively staining cells in populations A and B, respectively following insulin-FDI treatment. ***Analysis***. *$n>3$; *$p < 0.05$; ** $p < 0.01$; *** $p < 0.001$; no symbol, $p > 0.05$.*

4.2.6. Suppression of FcεRI-induced calcium fluxes in insulin-exposed mast cells

Mast cells drive inflammation in a multi-faceted manner. Antigen or secretagogue stimulation results in degranulation of pre-formed mediators (serotonin, histamine), *de novo* synthesis of bioactive lipids (leukotriene C4, prostaglandin D2), and induction of cytokine gene transcription. Mast cell activation is absolutely dependent upon a biphasic intracellular calcium response, where calcium release from Inositol (1,4,5) P3-gated calcium stores followed by activation of the I_{CRAC}/Orai1 influx pathway (122-125). We proposed that altered calcium signaling could provide a mechanism for the suppression of secretory responses, and sought to examine the dynamics of calcium signaling in a cytosol that is largely occluded with lipid bodies.

FcεRI-induced calcium fluxes are compromised in insulin-FDI treated cells (Figure 4.3 and 4.4). Analysis of initial rates in the absence of extracellular calcium indicates (Figure 4.3A, B) that the progress of initial InsP3-dependent calcium signals (ER store release) is dramatically suppressed in lipid-body enriched cells, and subsequent CRAC-dependent influx is also suppressed. The ER is physically-altered in insulin-FDI treated cells (Figure 4.3C, D). We noted that while that in EM analysis the ER appears structurally distended, the actual size of the calcium store that is InsP3-sensitive is decreased in insulin-FDI-treated cells.

We asked if the alterations in calcium signal intensity that we see in insulin-FDI treated cells were sufficient to cause a change in the downstream outcomes of calcium signaling, for which we used the phosphorylation status of the calcium-dependent transcription factor NFATC1 as a marker (130, 131). In response to antigenic stimulation, NFATC1, which is basally phosphorylated in the cytosol, becomes dephosphorylated and translocates to the nucleus in a calcium-dependent manner. This dephosphorylation and translocation is suppressed in insulin-FDI treated cells, which is consistent with a defect in calcium signaling (Figure 4.4B).

4.2.7. Calcium signal dynamics in insulin-treated mast cells

As we describe in Figure 4.3 and 4.4, there is a suppression in calcium responses (both store release and influx) in Insulin-FDI treated mast cells. This suppression is evident at both the population and single cell levels. Deficiencies in store release in steatotic liver cells have been attributed to the fact that a distended, lipid engorged ER is, for some reason, an ineffective calcium store. We asked whether altered expression of calcium handling proteins, or altered propagation of calcium signals across the cytosol, could also play a role in the suppressed calcium signaling phenotype that we observe.

Figure 4.5 shows mRNA and Western blot analysis of expression of various calcium-handling proteins in control and insulin-FDI treated mast cells. Protein levels for the type I Ins (1,4,5) P3 receptor were not altered between control and treated cells. We noted altered expression of the type II and III Ins (1,4,5) P3 receptor proteins, the former of which was apparently strongly upregulated at the protein level. These data could represent the expansion of stores gated by type II InsP3R, with the concurrent shrinkage of stores gated by Type III (132, 133). Looking at calcium influx channels, the ORAi1 CRAC channel is upregulated, despite the apparent diminution in calcium influx across the plasma membrane. In turn, the intracellular calcium pumps, which regulate uptake of calcium into various intracellular store compartments were also assessed. While SERCA2A expression did not change, the protein levels for SERCA2B were down-regulated. Again, these data could reflect the shrinkage of a store that expresses SERCA2B, or a widespread downregulation of the protein levels of this pump across all of the intracellular calcium storage compartments. The plasma membrane ATPase (PMCA) pump, regulating calcium efflux into the extracellular milieu, was also down-regulated. While our data did highlight disconnects between mRNA and protein expression regulation, it is clear from these Western blots that Insulin-FDI treated cells do display some alterations in the levels of calcium handling proteins that could contribute to alterations in calcium signals that we observe.

We used a number of methods to begin to examine the dynamics of calcium signal propagation in the cytosol of cells with steatotic levels of lipid bodies. In Figure 4.5 we compare the time resolved movement of calcium in a steatotic area of cytosol compared to a non-lipid body containing area. We assayed a live cell in nominally calcium-free external

media. There is a notable difference in the calcium signal that develops around a nearby Oil Red positive lipid body cluster, compared to the path of the calcium signal that is taken through cytosol that is not occluded by a lipid body cluster. In this instance and ~20 similar observations (data not shown), a propagating calcium signal appears to move around a lipid body cluster suggesting that these may provide some impedance to trans-cytoplasmic signaling.

We compared averaged calcium signals from regions of the cytosol that were designated as either discrete intracellular stores, non-store cytosol or lipid body clusters. While we cannot exclude the presence of some calcium sinks (e.g. mitochondria) in the 'non-store' regions of interest (ROI) analyzed, we do discern different patterns of behaviour between the lipid body enriched and other areas of cytosol. Figure 4.5C shows that during antigen receptor stimulation, an intracellular calcium store sequentially is depleted in a biphasic fashion and then refills. Conversely, the non-store areas of cytosol show modest increases in calcium levels consistent with depletion of intracellular stores into the cytoplasm, followed by a striking influx response that is mediated by store-dependent operation of the CRAC calcium channel in the plasma membrane. The calcium signals in the Oil Red O-positive lipid body structures display a discrete pattern, and our observations are summarized as follows:

(i) The starting Fluo-4 intensity for 130 ORO positive ROI versus 150 areas of non-store cytosol ranged from 0.06-1.28x that of surrounding cytosol. Of 130 ROI studied, 86 had resting Fluo-4 levels at or exceeding that of ROI drawn in the surrounding cytosol. Also 14 of these had no appreciable Fluo-4 in resting cells, suggesting that in some situations Fluo-4 is actively excluded from areas of ORO accumulation.

(ii) On average (Figure 4.5C) ORO positive structures diminish in Fluo-4 signal and then increase, during the first 10-20 s of antigen stimulation, a timecourse comparable with ER store depletion. During the influx phase, the Fluo-4 fluorescence increased dramatically, presumably indicating calcium accumulation in the ORO positive structure;

(iii) We identified two distinct types of ORO positive structure in terms of their calcium signaling (Figure 4.5D). Both populations display an overall accumulation of Fluo-4 fluorescence across the timecourse of FcεRI-induced elevations in intracellular calcium levels. However, in some of the ORO^{+} structures this rise is preceded by a slight drop in

fluorescence intensity, possibly corresponding to calcium efflux form the LB itself. This latter phenomenon is exemplified in Figure 4.6. Over a 12s time course the Fluo-4 signal in the ORO positive structure diminishes slightly, while in two immediately juxtaposed areas we see a concomitant elevation in Fluo-4 fluorescence.

(iv) We occasionally observed a calcium store closely positioned to a lipid body, and we carried out a series of analyses to compare them to non-LB associated stores. With some consistency we noted that stores close to LB depleted and refilled with a sharper kinetic that capacity-matched stores that were not located next to LB.

(vi) Large (>1 micron diameter) ORO+ structures were large enough to z stack in their own right, and were imaged as a 120nm deep z disc in two fluorescence channels corresponding to Fluo-4 and ORO. While the latter remained fairly constant (completely constant in analyses where we compensated for the slight movement of the lipid bodes during stimulation), the Fluo-4 signal in this lipid body z disc increased over time, and notably the increase was from the periphery of the z disc inwards. Indicating movement of calcium towards the center of the disc (not shown).

A.

Fc(eps)R1 response in 0mM [Ca $^{2+}$] ext	Area under the Curve (AUC)	Maximum Initial rate *d*Ca/*dt*
Control	335.1	1.843
Insulin-FDI	148.8	0.676

C.

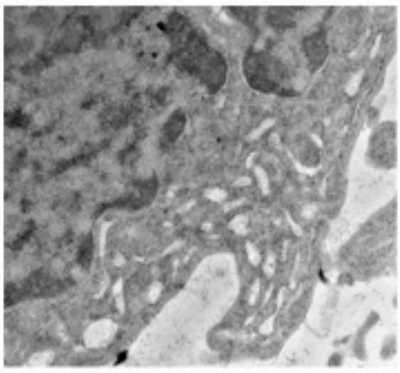

B.

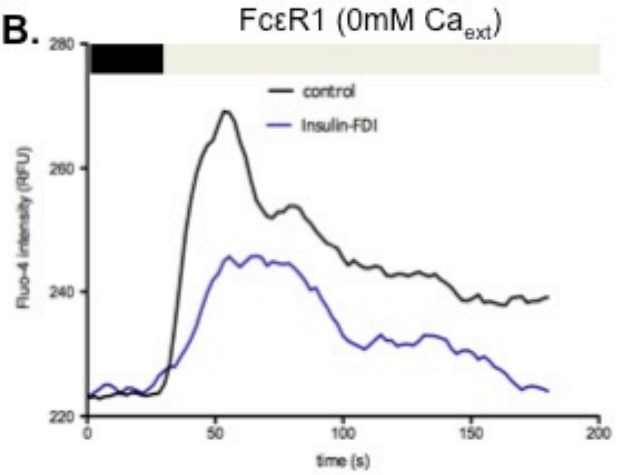

D.

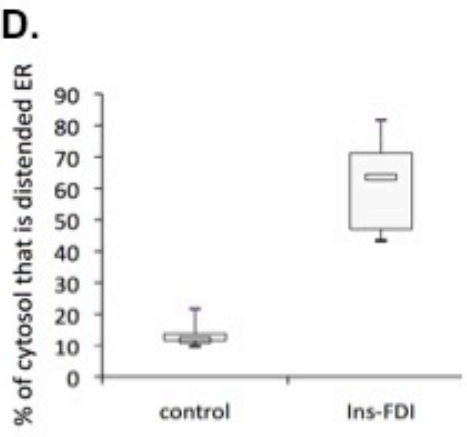

Figure 4.3. Suppression of calcium signaling and ER phenotypic alterations in lipid body-enriched mast cells. Calcium signaling is suppressed in insulin-FDI treated RBL2H3. A. Analysis of AUC and initial rates of calcium mobilization in control and insulin-FDI treated RBL2H3**.** Values are shown as mean of 3 experiments +/- SD. Experiments were performed in nominally calcium free (0mM $CaCl_2$ + 1mM EGTA) Ringer solution. **B.** FcεRI-induced calcium fluxes in control and 6-day insulin-FDI treated RBL2H3. Experiment was performed in 0mM external calcium. RFU, Relative fluorescence units; *d*Ca/*dt*, rate of change in calcium signal over time. **ER phenotypic alterations in insulin-FDI treated RBL2H3. C.** Electron micrographs were acquired from RBL2H3 cells exposed to the insulin-FDI treatment for 6 days. Micrographs show variation in ER structure. Images are digitally zoomed from an original image captured at a magnification of 5000X. **D.** Quantitation (NIH Image J) from EM of % cytosol that is apparent ER in control and 6d insulin-treated mast cells (n=12).

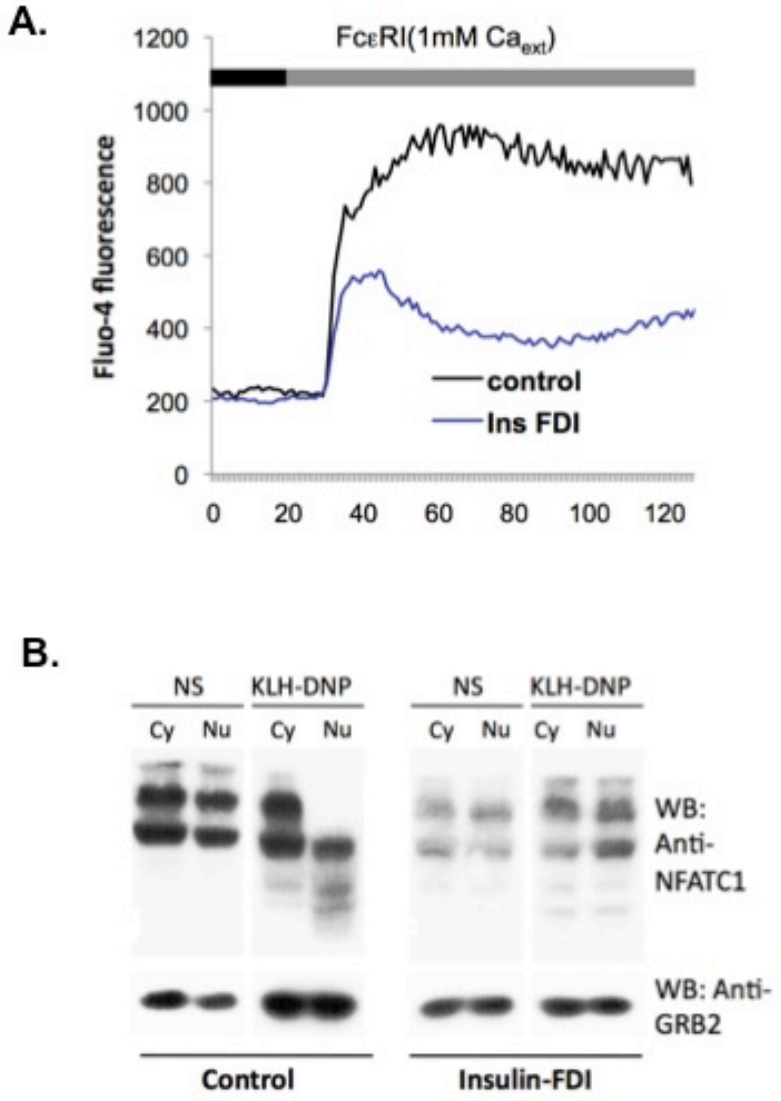

Figure 4.4. Suppression of calcium signaling and downstream targets in lipid body-enriched mast cells. **A.** Population based measurements of calcium flux in FcεRI-stimulated control or insulin-treated mast cells. Experiment was performed in 1mM external calcium. **B.** Western blot analysis of NFATC1 dephosphorylation in cytoplasmic and nuclear fractions from control and antigenically-stimulated RBL2H3. NS: non-stimulated, KLH-DNP: antigenically-stimulated.

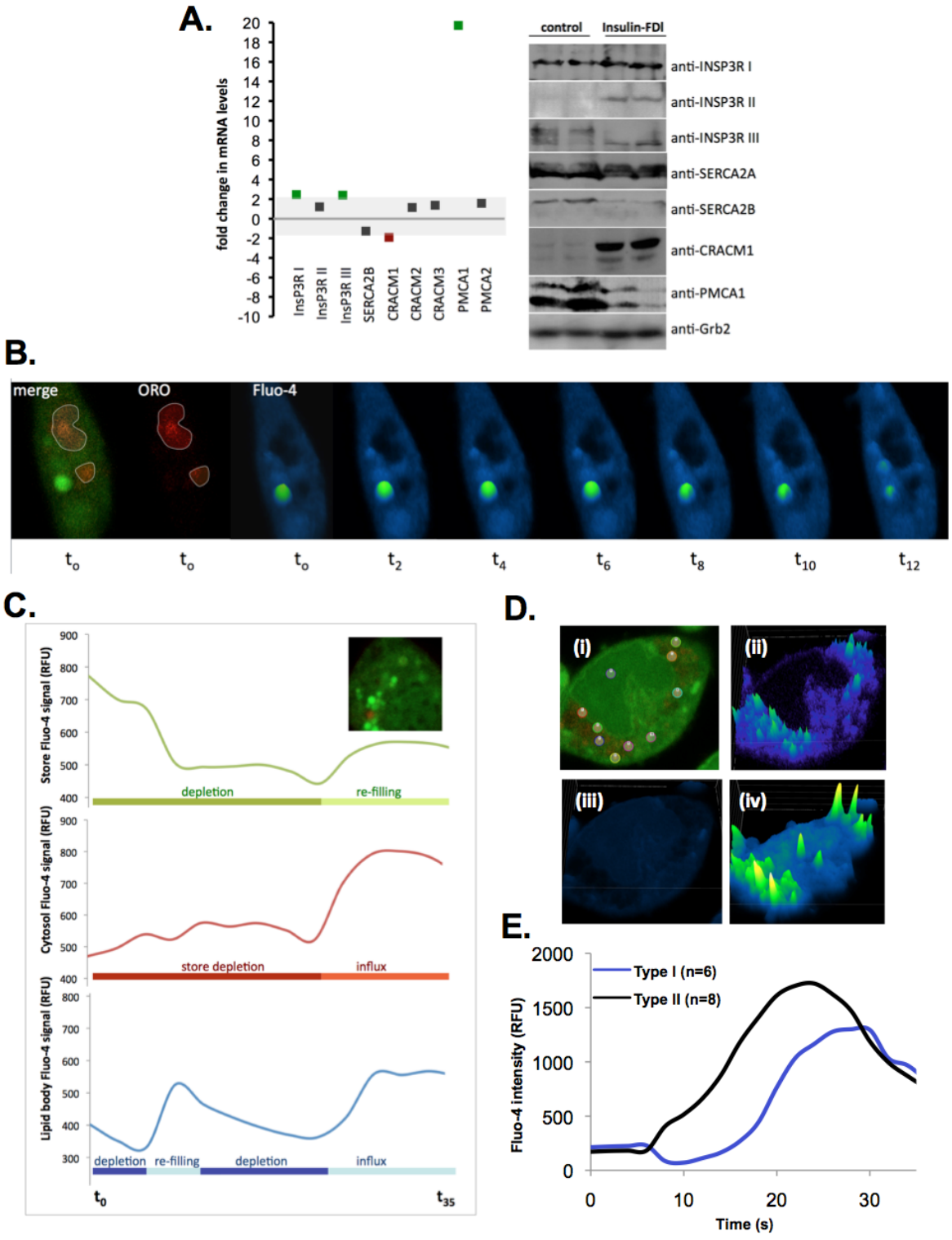
A.
fold change in mRNA levels
InsP3R I
InsP3R II
InsP3R III
SERCA2B
CRACM1
CRACM2
CRACM3
PMCA1
PMCA2
control
Insulin-FDI
anti-INSP3R I
anti-INSP3R II
anti-INSP3R III
anti-SERCA2A
anti-SERCA2B
anti-CRACM1
anti-PMCA1
anti-Grb2
B.
merge
ORO
Fluo-4
C.
Store Fluo-4 signal (RFU)
depletion
re-filling
Cytosol Fluo-4 signal (RFU)
store depletion
influx
Lipid body Fluo-4 signal (RFU)
depletion
re-filling
depletion
influx
D.
(i)
(ii)
(iii)
(iv)
E.
Type I (n=6)
Type II (n=8)
Fluo-4 intensity (RFU)
Time (s)

Figure 4.5. Calcium dynamics in cytosol and lipid bodies within insulin-exposed mast cells. A. mRNA expression fold change measured by microarray analysis (left) and protein expression (right) of calcium handling proteins in insulin-FDI treated mast cells. Western blot concentrations are as follows: Anti-ITPR1 (1:500), ITPR2 (1:500), ITPR3 (1:500), anti-SERCA2a (1:100), anti-SERCA2b (1:500), anti-PMCA1 (1:500), anti-CRACM1 (1:500). **B.** Depletion of an individual calcium store skirting a lipid body in an antigenically-stimulated mast cell labeled with Fluo-4 and Oil Red O. **C.** Averaged analyses of calcium dynamics in matched area ROI in stores (top panel n =13), cytoplasm (middle panel, n=10) and lipid bodies (lower panel, n=7) during an antigen receptor induced calcium response in the presence of external calcium. ROI were gathered from 4 separate cells. **D.** Example of localization of initial (i, iii) and stimulated (iv) Fluo-4 calcium intensity in 6d insulin-exposed mast cells. (ii) visualization of ORO staining (lipid body location) in resting mast cell. **E.** Averaged calcium signals from two types of lipid body observed in antigen-stimulated, 6d insulin-exposed mast cells.

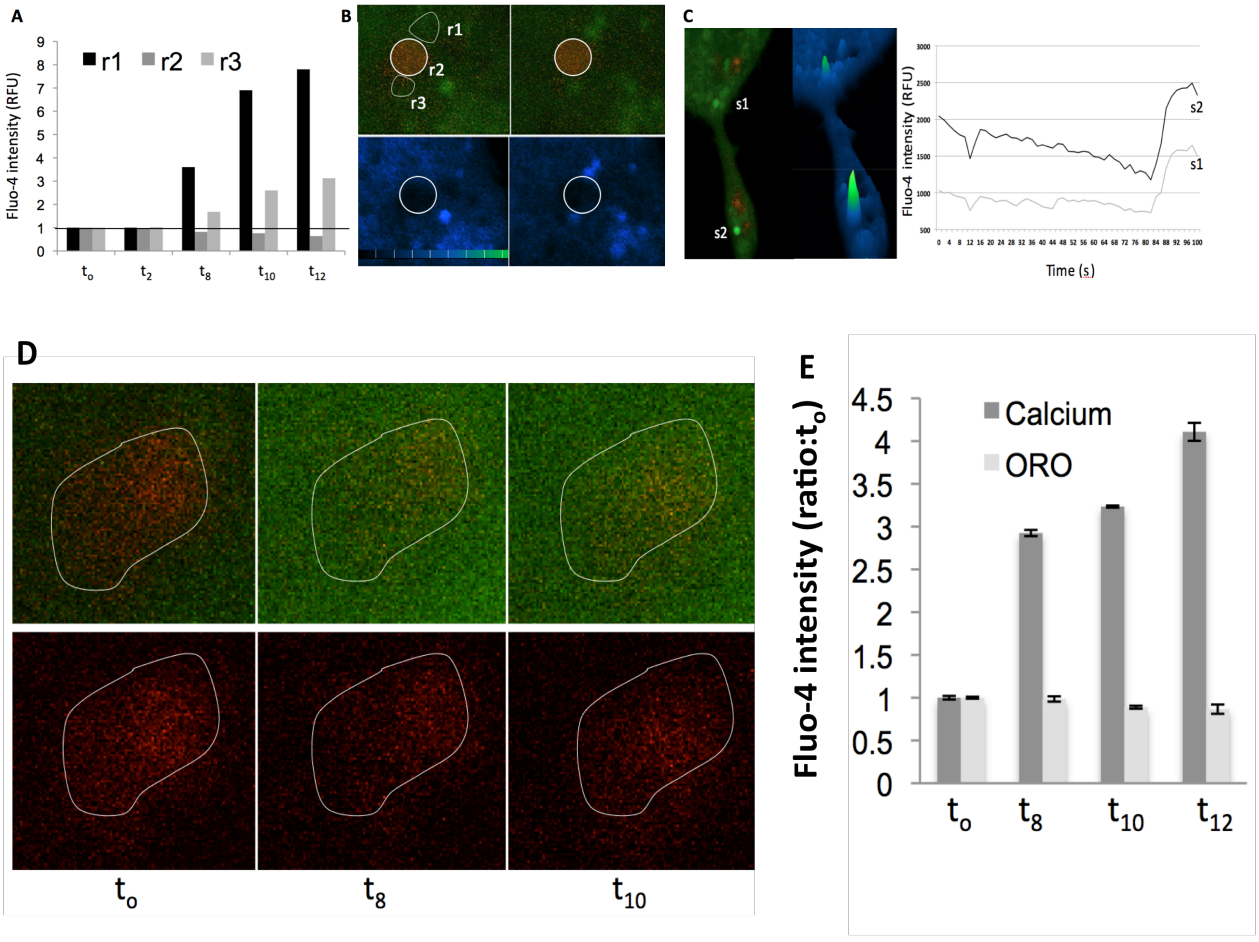

Figure 4.6. Calcium dynamics in cytosolic stores and lipid bodies within antigen stimulated, insulin-exposed, mast cells. A, B. Fluo-4 intensity in lipid body and two discrete calcium stores that emerge during antigen activation of a mast cell in the presence of external calcium. r1, r2 and r3 represent various regions of interest. **C.** Time-resolved analysis of two calcium stores (s1 and s2) that were either distant from (s1) or closely juxtaposed to (s2) a lipid body during the course of an antigen induced calcium flux in an insulin-FDI treated mast cell. **D, E.** ORO and Fluo-4 dynamics across one vertically-centered *z* disc of a cytoplasmic lipid body during an ongoing calcium flux in an antigen-stimulated, 6d insulin-exposed cell.

4.2.8. Endoplasmic reticulum remodeling, reprogramming and stress in insulin-treated mast cells

LB are believed to derive from the ER, thus the status of the ER is likely to be intimately linked to the steatotic process. The Hotamisligil laboratory has shown elegantly that the ER is dysfunctional in hepatocytes derived from obese liver (71). Steatosis of these cells is associated with diminished ER protein production and a switch ('re-programming') to ER lipid synthesis, upregulation of ER stress markers and diminished capacity of the ER calcium stores. Moreover, others have suggested that the ER becomes structurally distended in steatotic cells, as elevated ER lipogenesis exceeds the capacity of the cell to form new storage LB. Our data show that the hyper-accumulation of LB in insulin-treated MC resembles this phenotype closely. The ER in insulin-FDI treated cells is indeed physically distended but has a diminished calcium storage capacity (Figure 4.3). We therefore asked whether the ER in insulin-treated cells exhibits hallmarks of ER stress and the UPR.

(a) ER distension

It has been demonstrated that inducing metabolic stress in pancreatic β-cells leads to morphological alterations, primarily a marked distension of the ER lamellae (121). EM micrographs show striking alterations in the morphology of the ER in mast cells chronically exposed to insulin-FDI (Figure 4.3C). Instead of the condensed and streamlined appearance of the ER normally observed at the cellular level, we find the ER in insulin-FDI treated mast cells to be distended. This increase in ER size coupled with the atypical appearance of the ER bears a striking similarity to the distended ER found in the aforementioned metabolically stressed pancreatic β-cells.

(b) Induction of ER stress and UPR pathways

It is well documented in the context of metabolic dysregulation that nutrient excess, subsequent ectopic lipid deposition and the inflammatory dysfunction that ensues are all causally linked to stress at the tissue, cellular and sub-cellular level. One form of cellular stress involves the ER and cellular attempts to rectify this type of stress require the activation of the unfolded protein response (UPR). Several activation indicators of the UPR have been

identified and we hypothesized, given the steatotic conditions observed in insulin-FDI treated mast cells, that we may observe activation of this pathway. Initial activation of the UPR leads to the upregulation of 3 distinct ER resident proteins associated with 3 distinct canonical pathways; PERK, IRE1α and ATF6 (69). We find that insulin-FDI treated mast cells express higher levels of all 3 UPR associated markers compared to control cells (Figure 4.7) Furthermore, we observe an upregulation in Jun-N-terminal kinase (JNK), a stress-associated protein kinase component of the UPR JNK regulates inflammatory genes and has been implicated in the dysregulation of the insulin receptor through its capability to alternatively phosphorylate insulin receptor-associated proteins including insulin receptor substrate-1 (IRS1) (see Figure 4.7).

Chronic dysregulation of the insulin receptor leads to an inability to translocate glucose transporter type 4 (GLUT4) to the plasma membrane and a subsequent decrease in the ability to sequester glucose from the extracellular milieu (12). We find GLUT4 to be downregulated in insulin-FDI treated mast cells, in addition to both IRS1 and IRS2. Lastly, we find glucose transporter type 5 (GLUT5), a fructose transporter implicated in type II diabetes, to be largely upregulated, which may be a compensatory mechanism for the downregulation of GLUT4. These data support the idea that chronic insulin-FDI treatment in mast cells and the attending ectopic lipid deposition are associated with an upregulation in proteins associated with ER stress. Furthermore, these data indicate a relationship between ER stress and the status of the insulin receptor pathway in steatotic mast cells.

(c) AMPK and ACC regulation in Insulin-FDI treated mast cells

Originally documented as a protein kinase with activity associated with acetyl-CoA carboxylase (ACC) and HMG-CoA reductase, the two rate-limiting regulatory enzymes for fatty acid and cholesterol synthesis respectively, AMP-activated protein kinase (AMPK) has since been established as the master ‘switch’ of cellular metabolic regulation (134). AMPK controls anabolic pathways such as fatty acid, triglyceride, cholesterol synthesis, protein synthesis and transcription but also has the capacity to ‘switch’ on catabolic pathways such as fatty acid oxidation and glycolysis. Dysregulation in AMPK has been implicated in such disease states as hypertension, cardiovascular disease, cancer, obesity and the metabolic syndrome and we sought to determine the status of AMPK signaling in insulin-FDI treated

mast cells.

It has been demonstrated in genetic models of rodent obesity that AMPK levels are reduced in peripheral tissues such as heart, skeletal muscle, and liver. However, in animals made obese by a high-fat diet, which may more closely mimic the development of human obesity and insulin resistance, it appears that AMPK activity is not altered in skeletal muscle or the hypothalamus (134). Observations of AMPK activity in settings of mast cell steatosis have not been documented. AMPK is a highly conserved heterotrimeric complex composed of a catalytic α subunit and regulatory β and γ subunits. AMPK is activated by an elevation in the ratio of AMP to ATP (AMP:ATP), most commonly caused by cellular and environmental stress. Activation of AMPKα is dependent on phosphorylation at Thr172 and phosphorylation at Ser108 of the β1 subunit seems to be required for the activation of the AMPK enzyme. Our data show an increase in the phosphorylation at Thr 172 of AMPKα, in addition to a clear upregulation in Ser108 of the β1 subunit in mast cells chronically exposed to insulin-FDI for 6 days (Figure 4.7). Interestingly, we find little to no change in the phosphorylation status of ACC1 at serine 79, a known phosphorylation target of AMPK, or the expression of ACC in insulin-FDI treated mast cells even in the presence of AMPK activation. These data suggest that fatty acid biosynthesis and the production of fatty acids may somehow be compromised, independent of the activation status of AMPK in mast cells chronically exposed to insulin.

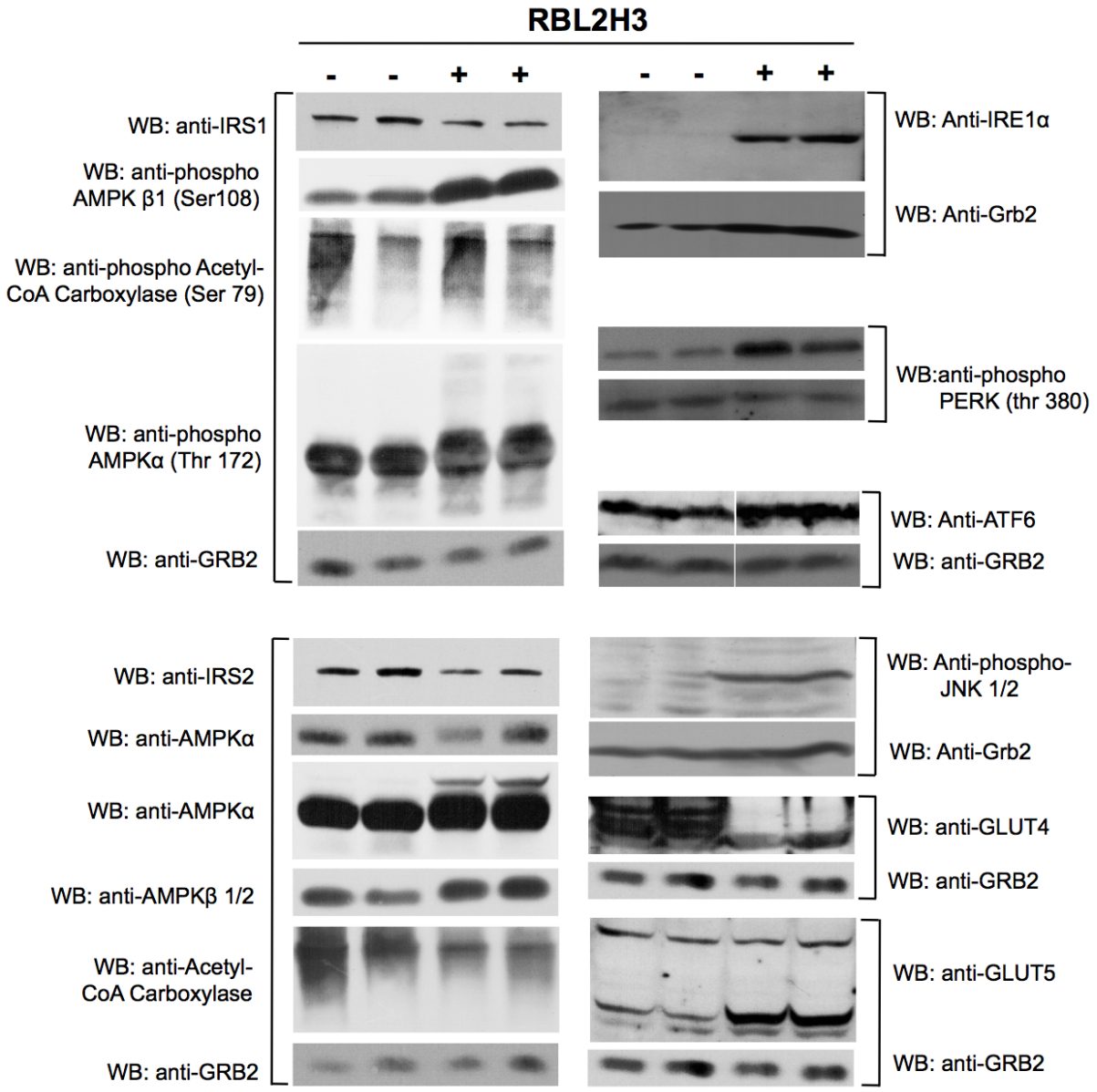

Figure 4.7. Chronic insulin exposure induces ER stress and altered metabolism in RBL2H3 mast cells. A. RBL2H3 cells were treated with insulin-FDI for 6 days and protein lysates were prepared as described. Western blot analysis for the indicated proteins was performed as described: anti-phospho PERK-thr380 (1:1000), anti-phospho JNK1/2 (1:1000), anti-IRE1α (1:850), anti-ATF6 (2.5µg/ml), anti-phospho AMPKβ1-ser108 (1:850), anti-phospho Acetyl-CoA Carboxylase-ser79 (1:850), anti-phospho AMPKα-thr172 (1:850), anti-AMPKα (1:850), anti-AMPKβ1/2 (1:850), anti-Acetyl-CoA Carboxylase (1:850), anti-GLUT4 (1:1000), anti-GLUT5 (1:500), anti-IRS1 (1:850), anti-IRS2 (1:850) and anti-GRB2 (1:7500).

(c) Diminished ER protein synthesis and altered Golgi structure in insulin-FDI-treated cells

It has been demonstrated *in vivo* that there is a shift in the proteomic profile of the ER in the obese liver in response to a high-fat diet. Here, Hotamisligil showed that ER-reprogramming is associated with elevated lipid synthesis and concomitantly suppressed protein synthesis (71). Given that our data mirror Hotamisligil's findings of ER distension, defective calcium signaling and ER stress, we asked if the mast cells similarly exhibit diminished protein production from this reprogrammed ER. In order to evaluate the protein synthesis status of mast cells treated for 6 days with insulin-FDI, we revisited a data set that had been generated early in our work. We had performed a 2 dimensional-differential in gel electrophoresis (2D-DIGE) analysis to examine the differential protein expression between control and steatotic mast cells. Examination of these data in Figure 4.8 A and B show the evaluation of approximately 700 proteins and we find significant alterations in the regulation of the proteins in this data set. Of the evaluated proteins, over 500 proteins were expressed at a lower level in insulin-FDI treated than control mast cells. Conversely, only 150 proteins were expressed at a higher level in insulin-FDI treated than control mast cells. Moreover, the protein content of 6d insulin-FDI treated cells measured by BCA assay was ~68% of that in control cells. Similarly, BCA assay of the ER/microsomal fraction isolated from 6d insulin treated cells by sucrose gradient ultracentrifugation showed a 60% reduction in the protein content of the ER (Figure 4.8C). We also noted that the Golgi apparatus is distended and there is a significant decrease in the appearance of late Golgi (trafficking) vesicles in the Insulin-FDI treated cells, which may again reflect a general suppression of protein synthesis and trafficking (Figure 4.8D).

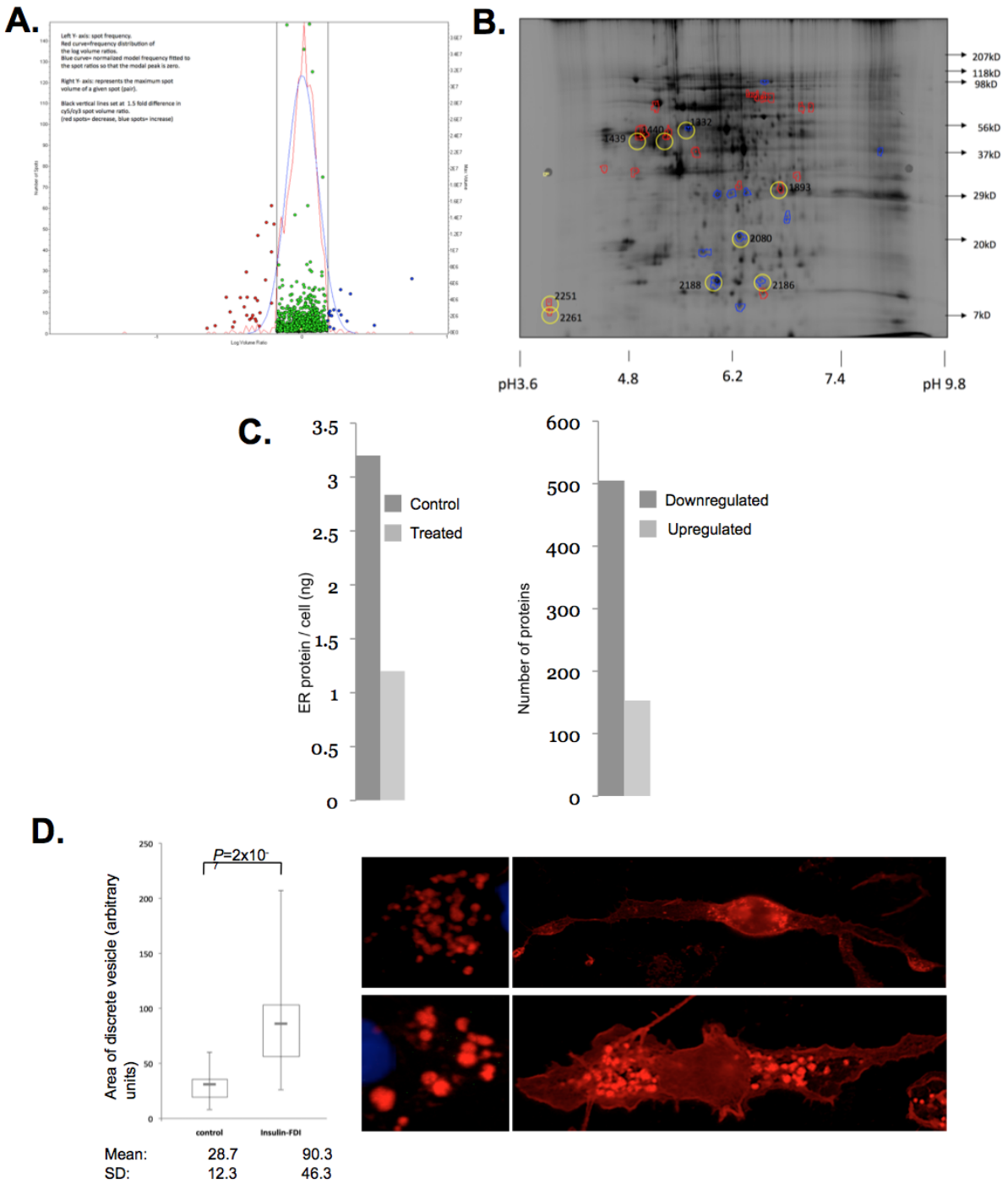
A.
B.
207kD
118kD
98kD
56kD
37kD
29kD
20kD
7kD
1439
1440
1332
1893
2080
2188
2186
2251
2261
pH3.6
4.8
6.2
7.4
pH 9.8
C.
ER protein / cell (ng)
Control
Treated
Number of proteins
Downregulated
Upregulated
D.
Area of discrete vesicle (arbitrary units)
P=2x10
control
Insulin-FDI
Mean: 28.7 90.3
SD: 12.3 46.3

Figure 4.8. Proteomic analysis and golgi trafficking in insulin-FDI treated mast cells. RBL2H3 were treated with insulin-FDI for 6 days as described. **A. Distribution in protein expression from a 2D-DIGE analysis in insulin-FDI treated mast cells.** Insulin-FDI cells were subjected to a 2D-DIGE analysis performed by the Keck Institute at Yale University. Red curve represents the frequency distribution of the log volume ratios. Blue curve represents normalized model frequency fitted to the spot ratios so that the model peak is zero. Vertical black lines are set at a 1.5 fold difference in cy5/cy3 spot volume ratio. Red spots indicate a decrease in protein expression, blue spots indicate an increase in protein expression and green spots indicate no change in protein expression within the defined 1.5-fold change range. **B.** Spot choices for specific protein identification in the performed 2D-DIGE analysis. Red and blue colors are consistent with (A). Yellow circles and the associated serial number represent identified and reported proteins (n=9). **C.** Quantitative analysis of total protein concentrations (BCA assay) of isolated ER per cell (*left*) and differences in protein expression from a 2D-DIGE analysis of ~700 proteins (*right*) in insulin-FDI treated mast cells. **D. Evaluation of Golgi trafficking in insulin-FDI treated mast cells.** Insulin-FDI treated mast cells were stained using 100μg/ml concanavalin A and discrete vesicle formation were quantified (left) and fluorescently imaged (right) in control (top right panels) and insulin-FDI treated (bottom right panels).

(d) Altered ER lipidome in insulin-FDI treated cells

In addition to the proteomic alterations observed in the ER of the obese liver in response to high fat diet, it has also been demonstrated *in vivo* that there are substantial lipidomic alterations that occur concomitantly (71). The ER is the major site of cellular lipid synthesis and it has been speculated that alterations in lipid profiles may have implications in various disease pathology. Furthermore, many of the bioactive mediators that make up pro-inflammatory molecules are derived from various isoforms of long-chain fatty acids, particularly polyunsaturated fatty acids such as arachidonic acid. We assessed the lipidomic landscape of isolated ER in mast cells chronically exposed to insulin-FDI. The ER/microsomal fraction was isolated using density gradient centrifugation and validated by Western blot analysis (data not shown).

Our data show significant alterations in treated compared to control cells evaluated from several vantage points. First, we find a redistribution in the relative abundance of individual fatty acids in our analysis (Figure 4.9C). We observe changes in all degrees of saturation including saturated, mono- and poly-unsaturated fatty acids (Figure 4.9B). More specifically, of the saturated fatty acid species studied here (n=7) we observed that 70% decreased in relative abundance. All of the monounsaturated fatty acids measured (n=5) decreased in abundance in response to chronic insulin-FDI exposure. All of the polyunsaturated fatty acids in mast cells chronically treated with insulin-FDI increased in relative abundance (n=3). As previously mentioned, polyunsaturated fatty acids such as arachidonic acid provide the molecular framework for the production of a large subset of bioactive pro-inflammatory and pro-thrombotic factors such as the eicosanoids. The biosynthetic pathway leading to the production of AA (which is described in more detail in chapter 5), starts with linoleic acid, which, in addition to AA we find to be upregulated in insulin-FDI treated mast cells as demonstrated in Figure 4.9A. Finally, although the conversion of eicosatrienoic acid (an omega-3 fatty acid) to AA is less likely to physiologically occur, it is possible and we observe an upregulation in this specific fatty acid as well (Figure 4.9A). These data provide evidence of lipidomic reprogramming of the ER in insulin-FDI treated mast cells. Our data show that mast cells chronically treated with insulin-FDI leads to a reprogramming of the ER to a more ‘pro-inflammatory’ state providing the mast cell with a higher abundance of precursor molecules for eicosanoid synthesis. This data suggest that, in situations of high

insulin/high fat diet, the mast cell may potentially act as a major source and/or reservoir for the production of eicosanoids. Furthermore, these data may lead to an alternative intervention site in the treatment of inflammatory dysregulation.

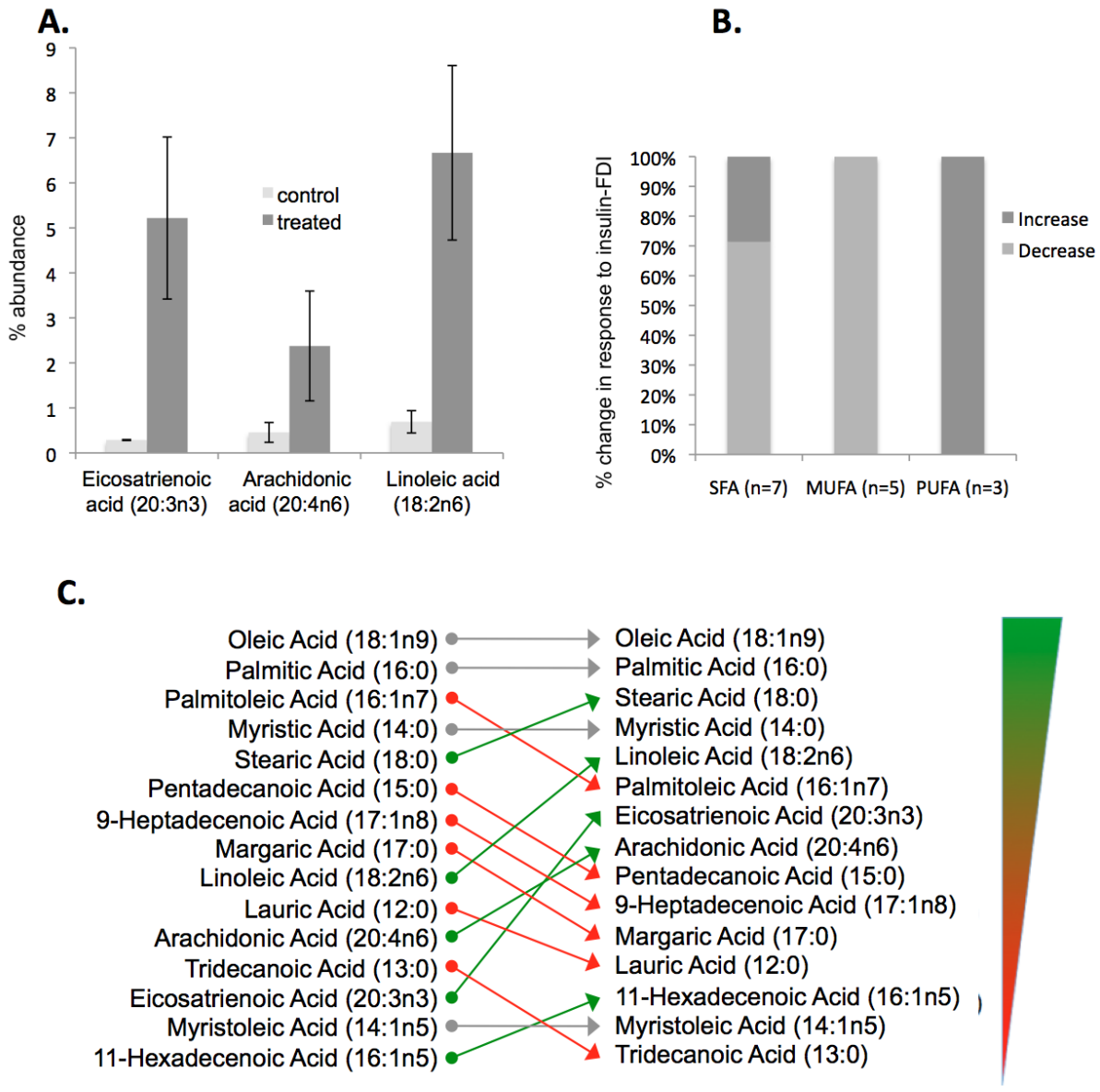

Figure 4.9. Characterization of the ER lipidomic landscape in insulin-FDI treated mast cells. A-C. RBL2H3 were grown for 6 days with insulin-FDI as described. Cells were harvested and the ER was isolated as described in methods and analyzed by GC/MS**.** Variations in resident ER lipid species were evaluated in response to insulin-FDI and organized according to abundance by degree of unsaturation (B), by expanding a single class of unsaturation (A) or by overall abundance relative to control cells (C).

4.3. Discussion

In Chapter 4 we sought to assess the impact of steatosis on the ability of a mast cell to initiate the suite of pro-inflammatory responses that are initiated by antigenic ligation of the high affinity receptor for IgE, FcεRI. This focus arose from our observation that the cytosol of mast cells become heavily occluded with lipid bodies in the presence of chronic insulin exposure, and follows from *in vivo* data suggesting that hyper- or hypo-insulinaemic conditions affect the outcome of inflammatory responses at the whole animal level. We identified a number of parameters that we would assess to gain a picture of the functionality of steatotic mast cells. First, we evaluated the three major types of pro-inflammatory event that are typically viewed as following FcεRI activation: secretory granule release (degranulation), the production of bioactive lipid messengers such as the eicosanoid leukotriene C4 and cytokine gene induction. Secondly, based on existing observations in situations of metabolic dysregulation, it was important for us to understand and assess the integrity of calcium signaling pathways in insulin-FDI induced steatotic mast cells in response to both antigenic and pharmacological activation. And lastly, we sought to evaluate the status of the ER due to the fact that the ER is the major site of intracellular calcium storage.

Our early observations suggested that the mast cell population exhibits a different phenotype following chronic insulin-FDI (or insulin alone, not shown) exposure. Resting mast cells distribute between two equal populations that can be differentiated on the basis of side and forward scatter properties. Insulin-FDI treatment resulted in enrichment of an $SSC^{lo}FSC^{hi}$ population of larger cells that we showed by several methods to be less granular (i.e. lower content of secretory granules). Thus the FACS data presented suggest that insulin-FDI treatment is causing the mast cell population to have less potential for secretory responses. These data are borne out by our functional assays of degranulation responses. This inability to degranulate may have physiological implications. A particularly distinct side-effect in long-term battles with diabetes is an inability to properly heal wounds. Given that mast cells play a primary role in innate wound healing and that diabetic patients have dysregulations in

insulin signaling pathways, we believe that insulin responsiveness in mast cells may contribute to improper wound healing in diabetic patients.

While the insulin-FDI treatment seems to be associated with a clear loss of function (diminished secretory capacity), it is clear that the $SSC^{lo}FSC^{hi}$ population also has some gains in function. The $SSC^{lo}FSC^{hi}$ population contained mast cells, which stained more robustly with lipophilic dye Nile Red indicating that this sub-population of cells contained mast cells with more pronounced lipid body loads. Bulk assays analysing the ability of insulin-FDI treated mast cells to secrete lipid-derived mediators such as LTC4 show that upon antigenic or pharmacological stimulation, mast cells increase their basal and stimulable amounts of LTC4. We also observe altered expression of enzymes responsible for the catalysing of arachidonic acid, the lipid-derived molecular backbone for a wide spectrum of leukotrienes, prostaglandins, prostacyclins and thromboxanes. More specifically, we find 5LO and LTC4 synthase, enzymes associated with leukotriene production to be upregulated in insulin-FDI treated mast cells, which we find to be localized to the same lipid enriched sub-population of mast cells. These data are consistent with EM findings from the Dvorak laboratory demonstrating the presence of these enzymes in lipid bodies, although we have not been able to demonstrate confocally, colocalization of these enzymes with the induced lipid bodies. This may be due to staining technicalities arising from immunofluorescently staining the lipid body core. It is well documented that increases in adiposity coinciding with the transition toward an obese phenotype lead to increased densities of mast cells in growing adipose tissue depositions and that this adipose tissue is inflamed. Our data suggest that mast cells in this setting may be an enhanced source of the inflammatory mediators (such as the eicosanoids) that can act to exacerbate adipose tissue inflammation and vascularization.

In Chapter 4 we attempted to assess the impact of steatosis on calcium signaling dynamics and the status of the ER. Bulk calcium assays in insulin-FDI treated mast cells show that, in response to antigenic stimulation, calcium signaling both initiates at a slower rate and decreases in intensity when compared to controls. This work arose from the very simplistic idea that calcium waves may be disrupted by the packing or occlusion of the cytosol with large numbers of lipid bodies. Indeed, there is evidence in the cardiomyocyte literature indicating that ELD accompanies a disruption in calcium flux following a voltage clamp assay. Further analysis of calcium flux at the single cell level in insulin-FDI treated mast

cells provide further insight into the interaction of calcium in the context of a lipid filled cytosol. We find some evidence that lipid bodies behave as a partition in the face of an approaching calcium flux initiated by antigenic stimulation. This occlusion of the cytosol with lipid bodies may explain the delay or local disruption in calcium signaling observed at the single and whole cell level. We also find that there are certain instances where lipid bodies act as calcium sinks, or intermediate calcium stores, which may also participate in the delay on calcium through the cytosol.

Ectopic lipid deposition, as observed in the context of metabolic dysregulation, have been demonstrated to be accompanied by ER stress. This observation has been documented in such systems as the pancreas during beta-cell dysregulation and the obese liver (71). ER stress has been shown to be consistent with a downregulation in protein transcription, an upregulation in lipid synthesis and cause aberrations in calcium signaling all of which we find to be present in insulin-FDI treated mast cells. The implications of ER stress in the mast cell system have yet to be identified, however we propose that this observed stress may partially explain the effects on mast cell function. It is still not clear the exact relationship between the formation of lipid bodies and the ER distension apparent in the context of ER stress and whether lipid body formation is a cause or an effect of this stress.

The high levels of lipid body formation that are induced in this study are accompanied by a marked suppression of secretory responses. At least under the experimental conditions employed here, these data suggest that insulin can bias the outcome of mast cell activation by promoting a poorly secretory but pro-eicosanoid phenotype. It is interesting to consider this idea in light of observations that mast cells from different tissue locations can be differentiated on the basis of functional phenotypes. Initial studies on mast cell subsets focused upon receptor heterogeneity, protease expression differences and cytokine profile, but there is also evidence of differential ability to produce histamine secretion and bioactive lipids (35, 79, 135-140). Our data suggest that these phenotypes may be plastic, in the sense that they can be dynamically regulated in non-proliferating cells, and that signals such as insulin may play a role in establishing the local phenotype of mast cells.

Chapter Five

Impact of steatosis on the mast cell lipidome

5.1. Introduction

The data in Chapters 3 and 4 show that insulin exposure causes mast cells to accumulate lipid storage structures. This steatotic phenotype is associated with marked changes in mast cell functionality. Moreover, the steatosis itself is complex, since our data suggest that the lipid body population is not structurally or chemically homogeneous. These data created a need to understand the exact lipid composition of the mast cells and the lipid bodies that are induced by chronic insulin exposure. In Chapter 5 we describe the lipidomic analysis of normal, and steatotic mast cells, and describe efforts to assemble a lipidome of isolated, purified lipid bodies.

5.1.1. Fat and cellular lipid classes

The word ‘fat’ is a rather ambiguous umbrella term used to define a diverse subset of cellular components ranging from biomolecules and second messengers to adipose tissue and lipid bodies. Typically, fat refers to adipose, which, compositionally, is a collection of adipocytes, connective tissue and other cells in the stromo-vascular fraction. Adipocytes have been catalogued according to their ability to sequester several distinct types of what are properly termed lipids, and are considered to be a large group of naturally occurring molecules such as fat-soluble vitamins, waxes and cholesterol. Lipids are divided into 8 distinct categories: fatty acids, glycerolipids, glycerophospholipids, sphingolipids, prenol lipids, saccharolipids, polyketides and sterol lipids.

Every cell in the human body contains a plasma membrane and this membrane alone, on average, contains 10 billion lipid molecules per cell. This calculation is independent of the lipid-bilayer associated with subcellular organelles, lipid stores and lipid bodies or lipid-derived signaling molecules. Lipids influence membrane rigidity and fluidity, provide scaffolding for cell-signaling proteins, post-translationally modify proteins and act directly as inter- and intra-cellular signaling molecules. Therefore, it seems reasonable to assume that alterations in lipid species at the cellular and tissue level may evoke broad effects.

Additionally, alterations in these lipid species may play a role in the pathogenesis and a variety of disease models as observed in diseases of lipid abundance such as coronary artery disease, diabetes, obesity and the metabolic syndrome.

5.1.2. Lipidomes – cellular lipid fingerprints

In comparison to biomolecules such as proteins, the structural complexity of lipids is relatively simple, however, there are actually 9,000–100,000 defined lipid species (141-143). This leads to a lipid-based fingerprint (a 'lipidome') at the cellular and tissue level with the potential to be quite complex. Currently, the mechanisms that control compositional complexity of cellular lipids and the effects on cellular function and homeostasis are largely unknown and poorly understood. The ability to isolate and quantify the absolute lipid complement at the organism, tissue, cellular and subcellular level has been termed 'lipidomics.' This approach is carried out using highly sensitive technology, for example high-performance liquid chromatography (HPLC) and mass spectrometry (MS), aimed to quantify and characterize large-scale lipidomes. This arm of the 'omics' revolution, in addition to other systems biology fields such as proteomics and transcriptomics, is being recognized for its potential role in investigating various aspects of molecular medicine, cellular biology and pathogenesis.

There have been several advances in lipidomic analysis over the past decade. First, the use of tandem MS (MS/MS) spectroscopy allows for high throughput quantitation with very small sample volumes required for analysis (143). Secondly, several large collaborative groups have taken the initiative (i.e. LIPID MAPS) to develop and centralise lipidomic aproaches, which has led to the development of more robust internal standards and a bioinformatic approach to the resulting data sets. A recent focus has been the need to measure absolute amounts of these lipids as opposed to relative fold change. The evolution of high-resolution instrumentation has led to the identification of glycerophospholipids, providing another level of insight into lipid variability, which can then be analyzed as mentioned above. Additionally, advances in software tools designed to analyze and visualize large data sets have led to a more comprehensive understanding of the data and an ability to observe data from a broader vantage point (144).

5.1.3. Prior studies of lipidomes in steatosis and immunocytes

The accumulation of adipose tissue in situations such as obesity have been causally linked to the development of a variety of pathologies, including type II diabetes and atherosclerosis. The expansion of adipose tissue is primarily driven by the accession of lipids sequestered and stored within adipose-resident adipocytes. Various major lipid species and their associated fatty acid profiles have been shown to play a major role in pathogenesis of metabolic disease. That being said, there is an interest in understanding the lipidomic profile of these adipocytes and more so, understanding differences in these lipid profiles between lean and obese subjects. *In vivo* data have evaluated the lipidomic landscape of adipose tissue-resident adipocytes in lean and obese mice (145). These studies show large increases in absolute triglyceride values with dynamic changes in the triglyceride content between lean controls and obese mice, including the loss of saturation and the gain of unsaturation in triglyceride associated fatty acids. This upregulation in unsaturation includes the polyunsaturated precursor molecules used for the biosynthesis of the eicosanoids.

In addition to the increase in absolute lipid content found in the obese pathology, there is a well-established inflammatory dysregulation associated within adipose tissue in obese subjects. During the progression toward an obese pathology, immune cells such as macrophages are recruited to these adipose depots (above basal levels) to sequester an array of lipid derivatives such as cholesterol in an attempt to ameliorate nutrient overload (141, 142). Lipidomic characterization of these adipose tissue macrophages (ATMs) in lean control and obese mice reveal increases in free cholesterol and cytotoxic saturated triglycerides with decreases in the accumulation of polyunsaturated fatty acids in obese mice. Interestingly, these ATMs also show decreased total phospholipid levels in ob/ob mice and alterations in membrane phospholipid associated lipid profiles (141, 142). Taken together, these data indicate in various cell systems that lipidomic alterations ensue when faced with increased intracellular lipid loads in obesogenic situations.

Mast cells are drivers of the inflammatory response capable of releasing a potent burst of proinflammatory mediators both pre-formed and synthesized *de novo* from lipid precursors. Mast cells have also been shown to occupy obese adipose tissue in increased densities above

basal levels (146) and produce a wide array of mediators known to exacerbate the obese pathology. For example, *in vivo* studies using mast cell deficient mice or pharmacologically stabilizing mast cells have shown marked outcomes in obesity, atherosclerosis, insulin sensitivity, and glucose tolerance (45). Adipose resident mast cells are exposed to the same extracellular milieu to that of the adipocyte and the macrophage in obesigenic situations, both of which present higher degrees of lipid loading. However, a lipidomic analysis of these cells has not been performed.

5.1.4. Experimental Approach: Lipidomics in steatotic mast cells

We studied the lipidomic profile of steatotic, insulin-FDI treated mast cells and control cells. Our focus in this study was to evaluate major lipid species and their respective fatty acid conjugations. More specifically, we explored the biosynthetic pathway associated with the production of arachidonic acid (AA), the precursor molecule for leukotrienes, prostaglandins, prostacyclins and thromboxanes.

5.2. Results

5.2.1. Whole cell lipidome of steatotic and control mast cells

Our lipidomic evaluation quantified and analyzed 342 distinct lipid molecules consisting of 38 fatty acids in 9 major lipid species. Whole cell lipid extracts from mast cells treated for 6 days with insulin-FDI show significant alterations in major lipid species and associated fatty acid composition in respect to fold change (Figure 5.1) and relative abundance (Figure 5.2). Of the 9 major lipid species examined, we find free fatty acids (FFA) and lysophosphotidylcholine (LYPC) increase in absolute fold change above a 2-fold threshold with values of 2.35-fold and 2.5-fold respectively, in mast cells treated with insulin-FDI for 6 days. Although we do observe slight increases in 4 of the other major lipid classes (CE, TAG, PS, FC), these lipids do not increase over 1.5-fold in response to insulin-FDI. Decreases in absolute fold change with insulin-FDI treatment occur in major lipid species cardiolipin (CL) and phoshotidylcholine (PC). On average, FFA show the most significant increases in individual fatty acids across the class with 3.71-fold followed by LYPC with 3.02-fold. A negative average is observed in the CL class with a value of a -0.71 fold change.

A survey of individual fatty acids show the largest increase in eicosatetraenoic acid (20:4n3)

with a 16.3-fold change and the largest decrease occurring in palmitoleic acid (16:1n7) with a 8.9-fold change. We find several omega-3 fatty acids to be upregulated over 10-fold, eicosatetraenoic acid (20:4n3) and docosapentaenoic acid (22:5n3), both of which were detected in the FFA category. On average, di-homo-gamma-linolenic acid (20:3n6), the immediate precursor molecule for AA increased the most across all major lipid species at 5.85 fold next to eicosapentaenoic acid (20:5n3) at 5.15 fold.

Taking a look at absolute abundances in our lipidomic analysis, we find the most marked alterations to exist in docosahexaenoic acid (22:6n3) with a 24.7 % increase in absolute abundance. This finding is consistent with our fold change analysis, which demonstrates the largest increase to exist in the immediate precursor molecule for AA. The second largest increase in absolute abundance we observe is in AA with a 13.8% increase. We find our most profound decrease in absolute abundance to exist in oleic acid (18:1n9) at -26.3%.

We detect significant alterations in the degree of unsaturation in individual fatty acids (Figure 5.3B). Using a cut-off threshold of a 2-fold change, we observe that the insulin-FDI treatment resulted in a significant upregulation of the polyunsaturated fatty acids (PUFAs), specifically the omega-3 and omega-6 PUFAs. PUFAs, in particular the 18-20 carbon long omega-6 PUFAs, constitute the precursor molecules required for AA synthesis. AA can be enzymatically catalyzed, as described in more detail below, leading to the production of eicosanoids such as prostaglandins, prostacyclins, thromboxanes and leukotrienes.

Figure 5.3C indicates the metabolic steps involved in the biosynthesis of AA with the enzymes involved in each catalytic step labeled in red. The first step in the pathway involves the conversion of linoleic acid (18:2n6), an essential fatty acid acquired solely through dietary means, to α-linolenic acid (18:3n6) by the addition of a double bond achieved by the enzymatic activity of delta-6-desaturase. The second step involves the elongation of α-linolenic acid to di-homo-α-linolenic acid (20:3n6). The final step in the biosynthetic pathway is catalyzed by the action of delta-5-desaturase leading to the production of AA (20:4n6). With the exception of 18:3n6 (a metabolite recognized to be short lived in this biosynthetic pathway) our data show an upregulation ranging from approximately 1.5-9-fold of each fatty acid in all 9 major lipid species (Figure 5.4). As expected, absolute quantities of these specific lipid species follow the same pattern with increases in 3 of the 4 metabolites

directly involved in this pathway (Figure 5.5). Interestingly, AA is the fatty acid with the most marked increase in this biosynthetic pathway with no less than a 3-fold increase in 7 of the 9 major lipid classes. Variations of these fatty acids in their respective major lipid species can be observed in Figure 5.6.

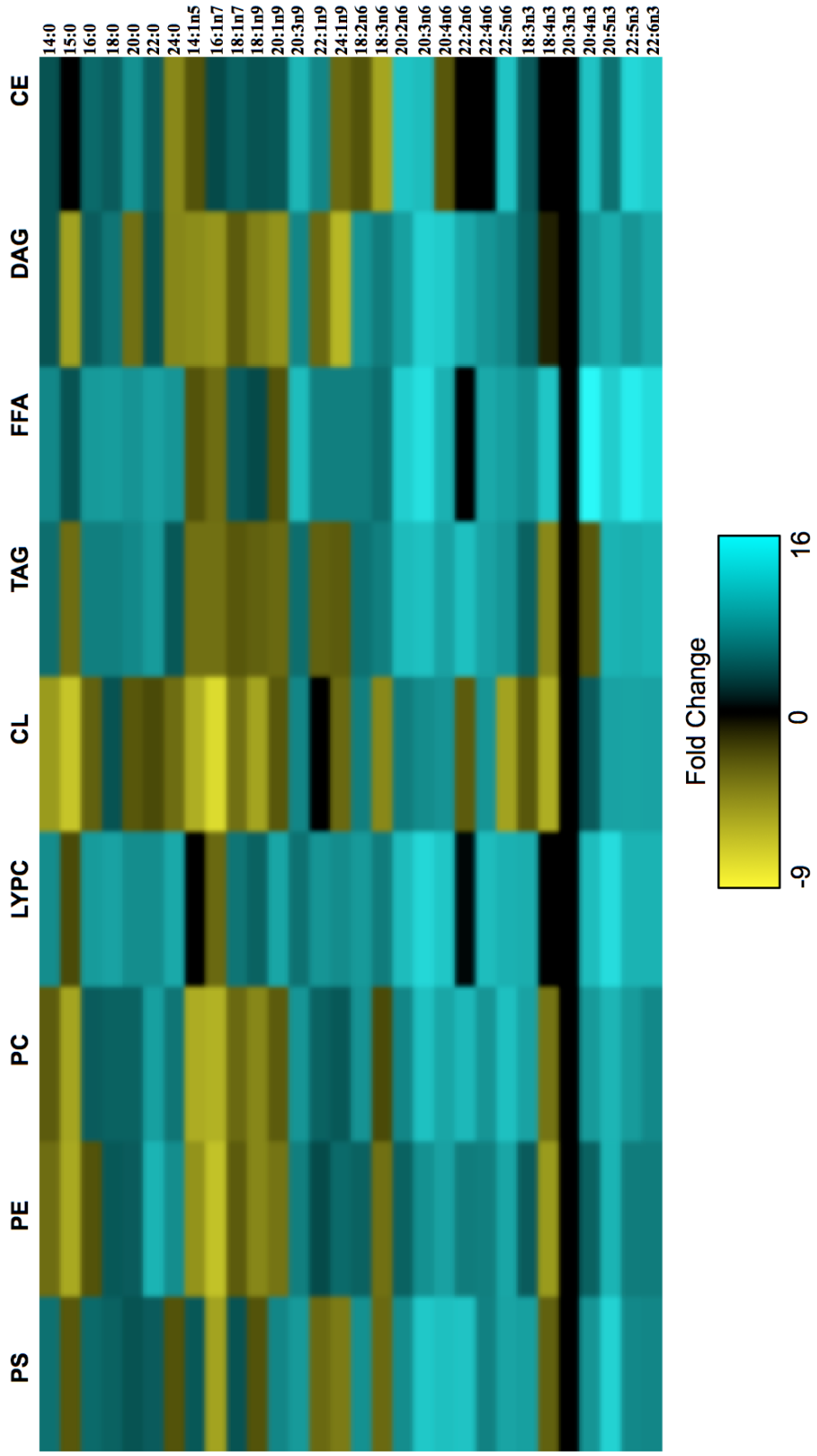
14:0
15:0
16:0
18:0
20:0
22:0
24:0
14:1n5
16:1n7
18:1n7
18:1n9
20:1n9
20:3n9
22:1n9
24:1n9
18:2n6
18:3n6
20:2n6
20:3n6
20:4n6
22:2n6
22:4n6
22:5n6
18:3n3
18:4n3
20:3n3
20:4n3
20:5n3
22:5n3
22:6n3
CE
DAG
FFA
TAG
CL
LYPC
PC
PE
PS
Fold Change
16
0
-9

Figure 5.1. Lipidomic characterization (fold change) of insulin-FDI treated mast cells. RBL2H3 were grown for 6 days with insulin-FDI. Cells were harvested, pelleted and prepared for analysis as indicated in methods. Individual major lipid species were separated by high performance liquid chromatography (HPLC) and fatty acid methyl esters from each class were produced and subsequently analyzed by GC/MS. Variations in lipid species were quantified and organized into a heatmap according to observed fold change (nmol/billion cells) relative to control cells. Each row indicates a specific fatty acid labeled as follows: the carbon length (the number to the left of the colon), the number of double bonds in the molecule (the number on the immediate left of the 'n') and the starting location of those double bonds (the number on the immediate right of the 'n'). *Abbreviations: Cholesterol Ester (CE), Cardiolipin (CL), Triacylglycerol (TAG), Diacylglycerol (DAG), Free Fatty Acid (FFA), Phosphotidylserine (PS), Phosphotidylcholine (PC), Phosphotidylethanolamide (PE), Lysophoshotidylcholine (LYPC)*.

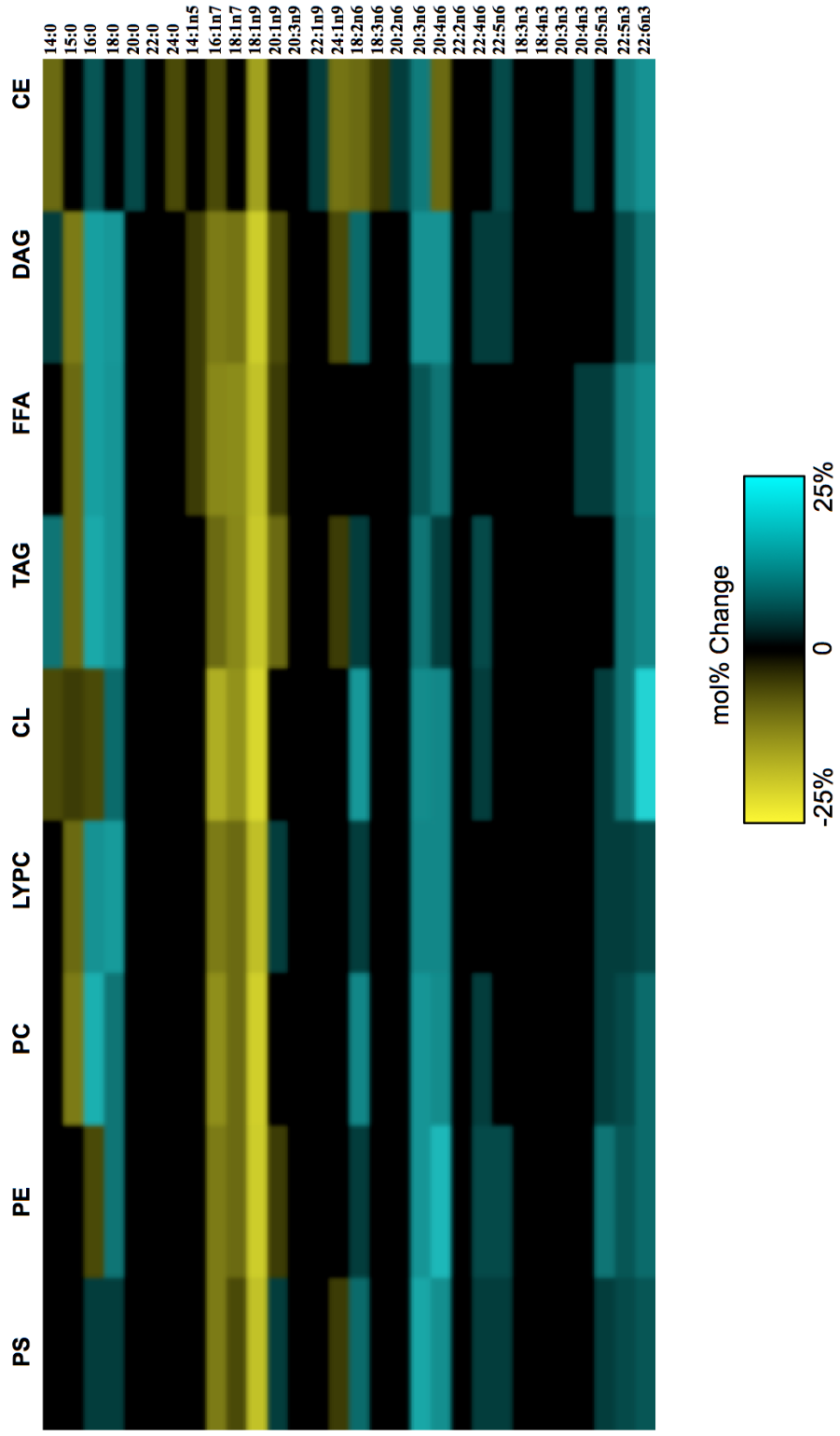
14:0
15:0
16:0
18:0
20:0
22:0
24:0
14:1n5
16:1n7
18:1n7
18:1n9
20:1n9
20:3n9
22:1n9
24:1n9
18:2n6
18:3n6
20:2n6
20:3n6
20:4n6
22:2n6
22:4n6
22:5n6
18:3n3
18:4n3
20:3n3
20:4n3
20:5n3
22:5n3
22:6n3
PS
PE
PC
LYPC
CL
TAG
FFA
DAG
CE
mol% Change
25%
0
-25%

Figure 5.2. Lipidomic characterization (percent change) of insulin-FDI treated mast cells. RBL2H3 were grown for 6 days with insulin-FDI. Cells were harvested, pelleted and prepared for analysis. Individual major lipid species were separated by high performance liquid chromatography (HPLC) and fatty acid methyl esters from each class were produced and subsequently analyzed by GC/MS. Variations in lipid species were quantified and organized into a heatmap according to the observed percent change in moles of fatty acid as a percentage of the total moles of fatty acid in the specified lipid class relative to control cells. Each row indicates a specific fatty acid labeled as follows: the carbon length (the number to the left of the colon), the number of double bonds in the molecule (the number on the immediate left of the 'n') and the starting location of those double bonds (the number on the immediate right of the 'n'). *Abbreviations: Cholesterol Ester (CE), Cardiolipin (CL), Triacylglycerol (TAG), Diacylglycerol (DAG), Free Fatty Acid (FFA), Phosphotidylserine (PS), Phosphotidylcholine (PC), Phosphotidylethanolamide (PE), Lysophoshotidylcholine (LYPC)*.

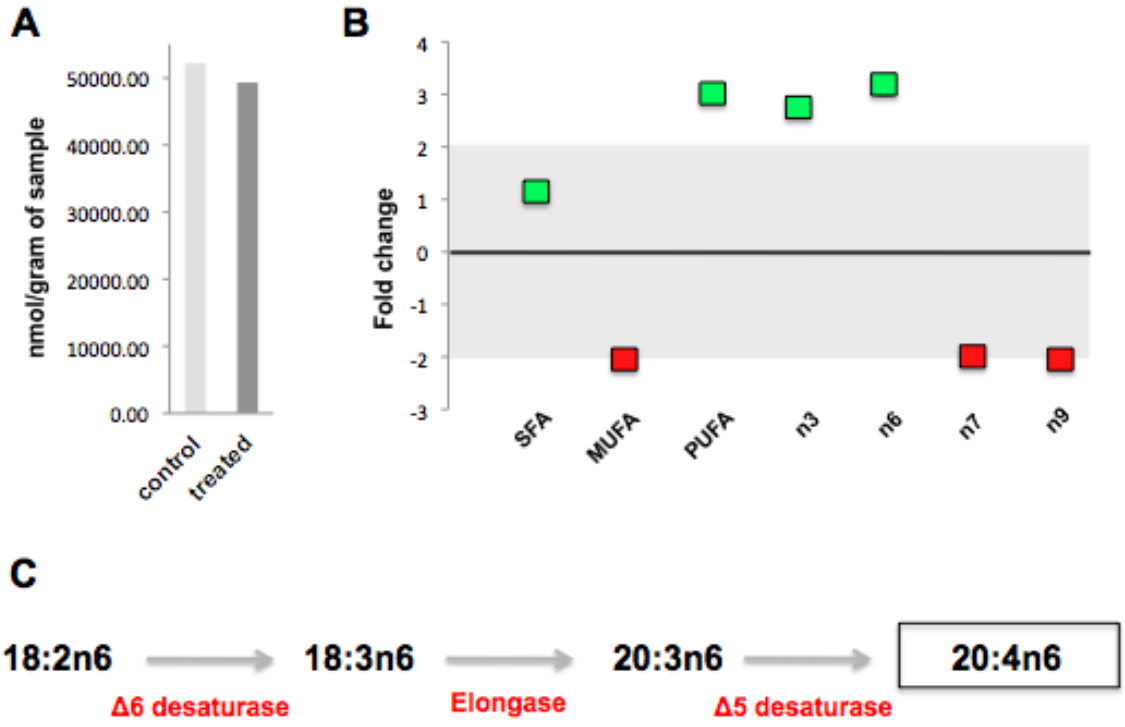

Figure 5.3. Insulin containing lipogenic stimulus alters fatty acid class presentation in mast cells. RBL2H3 mast cells were treated for 6 days with insulin-FDI. **A.** Absolute cellular lipid content was analyzed in Insulin-FDI treated mast cells. **B**. Overall comparison as a function of fold change in major lipid classes of RBL2H3 mast cells chronically exposed to insulin-FDI for 6 days**. C.** Schematic diagram representing the biosynthetic pathway in the conversion of linoleic acid (18:2n6) to arachidonic acid (20:4n6), including the major enzymes (red) involved. *Abbreviations*: *Saturated Fatty Acid (SFA), Monounsaturated Fatty Acid (MUFA), Polyunsaturated Fatty acid (PUFA), n3 (omega-3 polyunsaturated fatty acid), n6 (omega-6 polyunsaturated fatty acid), n7 (omega-7 polyunsaturated fatty acid), n9 (omega-9 polyunsaturated fatty acid), 18:3n6 (α-linolenic acid) and 20:3n6 (di-homo-α-linolenic acid).*

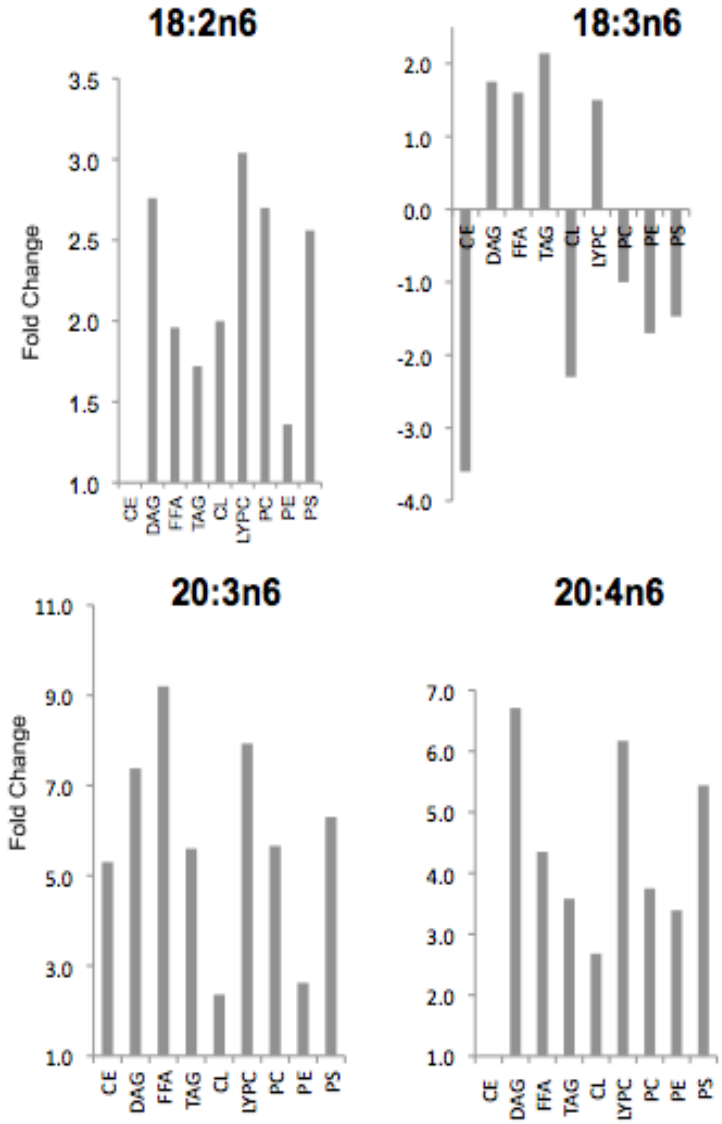

Figure 5.4. Insulin containing lipogenic stimulus alters precursor molecules associated with the arachidonic acid biosynthetic pathway in mast cells. RBL2H3 mast cells were treated for 6 days with insulin-FDI. After initial separation by HPLC, individual fatty acids directly involved in the arachidonic biosynthetic pathway were evaluated and quantified according to their respective major lipid class. Fold change was calculated based on response to insulin-FDI in treated compared to control mast cells. *Abbreviations: 18:2n6 (linoleic acid), 18:3n6 (α-linolenic acid), 20:3n6 (di-homo-α-linolenic acid), 20:4n6 (arachidonic acid), Cholesterol Ester (CE), Cardiolipin (CL), Triacylglycerol (TAG), Diacylglycerol (DAG), Free Fatty Acid (FFA), Phosphotidylserine (PS), Phosphotidylcholine (PC), Phosphotidylethanolamide (PE), Lysophoshotidylcholine (LYPC).*

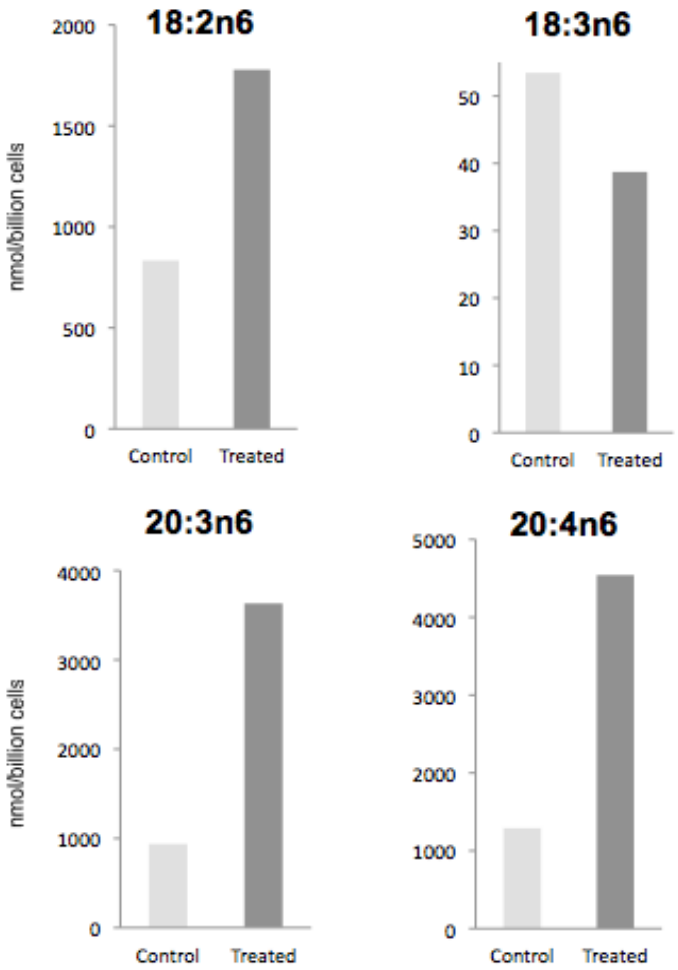

Figure 5.5. Insulin containing lipogenic stimulus alters absolute concentrations of precursor molecules associated with the arachidonic acid biosynthetic pathway in mast cells. RBL2H3 mast cells were treated for 6 days with insulin-FDI. After initial separation by HPLC, individual fatty acids directly involved in the arachidonic biosynthetic pathway were evaluated and absolute cellular concentrations were quantified. Quantification is in terms of absolute concentration (nmol/billion cells) based on the response to insulin-FDI in treated compared to control cells. *Abbreviations: 18:2n6 (linoleic acid), 18:3n6 (α-linolenic acid), 20:3n6 (di-homo-α-linolenic acid) and 20:4n6 (arachidonic acid).*

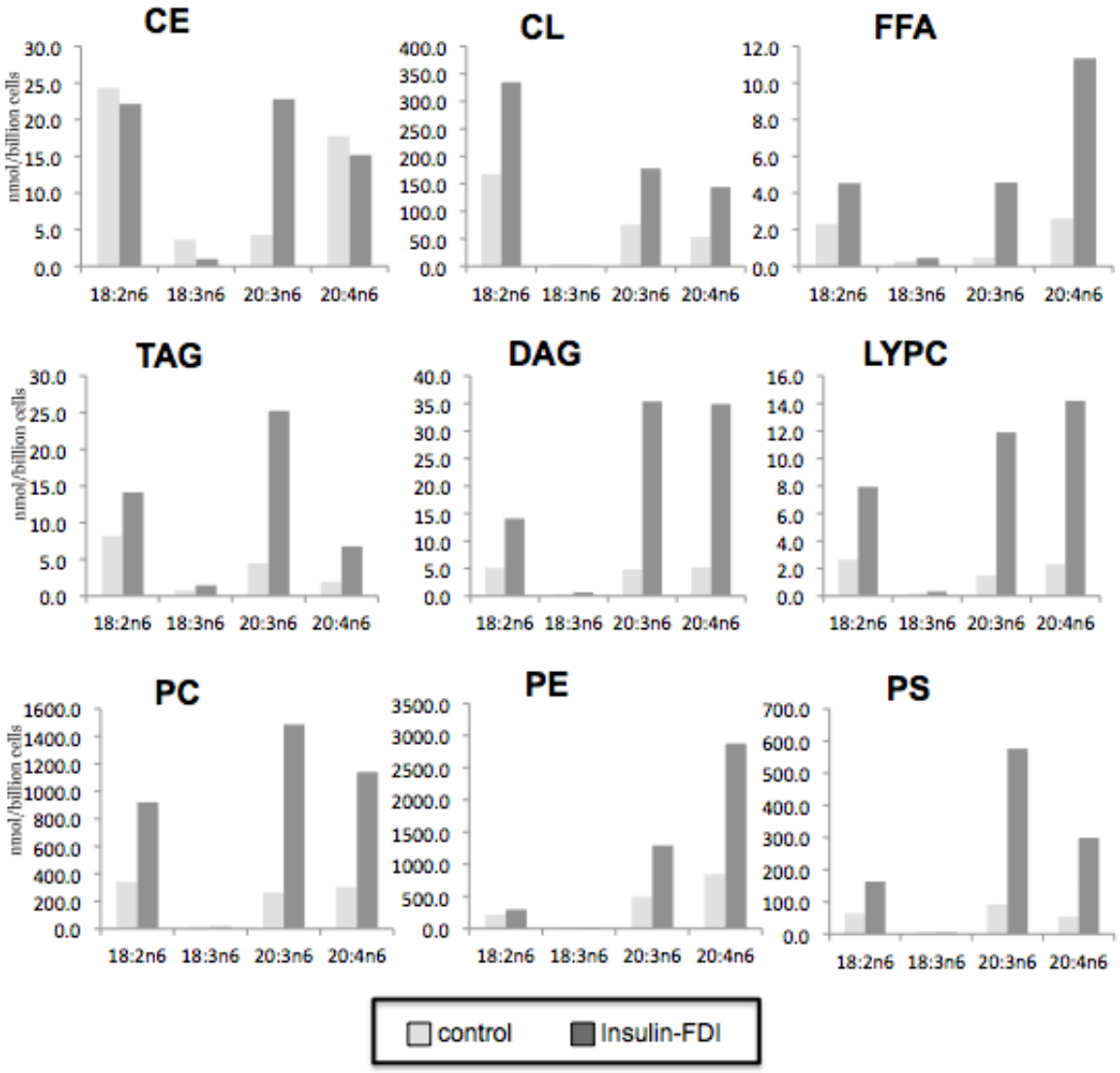

Figure 5.6. Insulin containing lipogenic stimulus alters absolute concentrations of precursor molecules associated with the arachidonic acid biosynthetic pathway in mast cells. RBL2H3 mast cells were treated for 6 days with insulin-FDI. After initial separation by HPLC, individual fatty acids directly involved in the arachidonic biosynthetic pathway were evaluated and quantified according to their respective major lipid class. Quantification is in terms of absolute concentration (nmol/billion cells) based on the response to insulin-FDI in treated compared to control mast cells. *Abbreviations: Cholesterol Ester (CE), Cardiolipin (CL), Triacylglycerol (TAG), Diacylglycerol (DAG), Free Fatty Acid (FFA), Phosphotidylserine (PS), Phosphotidylcholine (PC), Phosphotidylethanolamide (PE), Lysophoshotidylcholine (LYPC), 18:2n6 (linoleic acid), 18:3n6 (α-linolenic acid), 20:3n6 (di-homo-α-linolenic acid) and 20:4n6 (arachidonic acid).*

5.2.2. Lipidome of lipid bodies purified from normal and steatotic mast cells using ultracentrifugation

The whole cell lipidome described above represents a significant advance in our understanding of the lipid distribution in both resting and steatotic mast cells, and begins to paint a picture of the changes that are associated with steatosis in the cellular lipid profile. However, these data present an integrated picture of every lipid location in the cell, not just the lipid bodies. The data in Figures 5.1-5.6 include membrane, organellar and lipid body lipids. We therefore sought to harvest a more purified lipid body sample from the steatotic cell, in order to analyse, in a more targeted fashion, the exact composition of the lipid bodies themselves. We view this as a key data set since (1) in its absence we cannot make predictions as to the contributions of the lipids stored in these LB to mast cell function, and (2) it will advance the field as the first data set of its type.

There are published ultracentrifugation protocols for the isolation of LB from leukocytes, and we followed the method developed in Dr. Peter Weller's laboratory (109). This immediately presented two challenges. First, as a density-based separation method, we have limited available ways to validate the purity of the fraction, since it will presumably contain other organelles and structures of similar Svedberg co-efficients (e.g. microsomal vesicles, endosome) and lipid body associated structures (mitochondria, ER lamellae). Second, the abundance of lipid bodies in control cells is so low (typically 1-2 structures per cell) that securing sufficient sample for a valid comparison with steatotic cells could be an issue. Moreover, control and steatotic lipid bodies may be qualitatively different, so they may not sediment similarly. Finally, the low abundance of LB in control samples may lead to a higher ratio of contaminant to LB in the control samples. In order to move forward, we did perform the LB ultracentrifugation and validate the presence of lipid bodies in a given fraction by performing a parallel extraction (which could not be sent for analysis due to the presence of dye) in cells that had been labeled with ORO. Given the limitations of this system we chose simply to develop a fingerprint of the lipid body fraction from steatotic (6d insulin-FDI) treated) cells, rather than seek a potentially flawed comparison with fractions from control cells.

Steatotic mast cells were lysed and lipid body fractions were harvested by ultracentrifugation

as described in Methods. Figure 5.7 depicts the relative abundance of each fatty acid and the associated major lipid species to which it is conjugated in isolated lipid bodies from insulin-FDI treated mast cells. We observe the most abundant fatty acids to be the saturated fatty acids, specifically Palmitic (16:0) and Stearic (18:0) acid, followed immediately by the monounsaturated fatty acids, which are known to be *bona fide* products of *de novo* lipogenesis in the liver (71). Interestingly, when we compare PUFA abundance in isolated lipid bodies we observe larger abundances of the omega-6 PUFAs than the omega-3 PUFAs, which are largely considered to be anti-inflammatory.

Assessing the LB fingerprint generated by our LB analysis, we noted marked differences between these profiles and that of whole cell analyses shown earlier (Figure 5.2). The most abundant lipid species detected in our isolated lipid body fraction exhibit marked contrast to our whole cell lipidomic data but similarity to our ER lipidomic data. We observe the most abundant fatty acids in our lipid body isolation to be palmitic acid (16:0), stearic acid (18:0) and oleic acid (18:1n9), which are the same 3 fatty acids with the highest abundance analyzed from our ER fractions in mast cells treated for 6 days with insulin-FDI. These data suggest the contents of the observed lipid bodies bear a similar lipidomic profile to that of the ER in insulin-FDI treated mast cells.

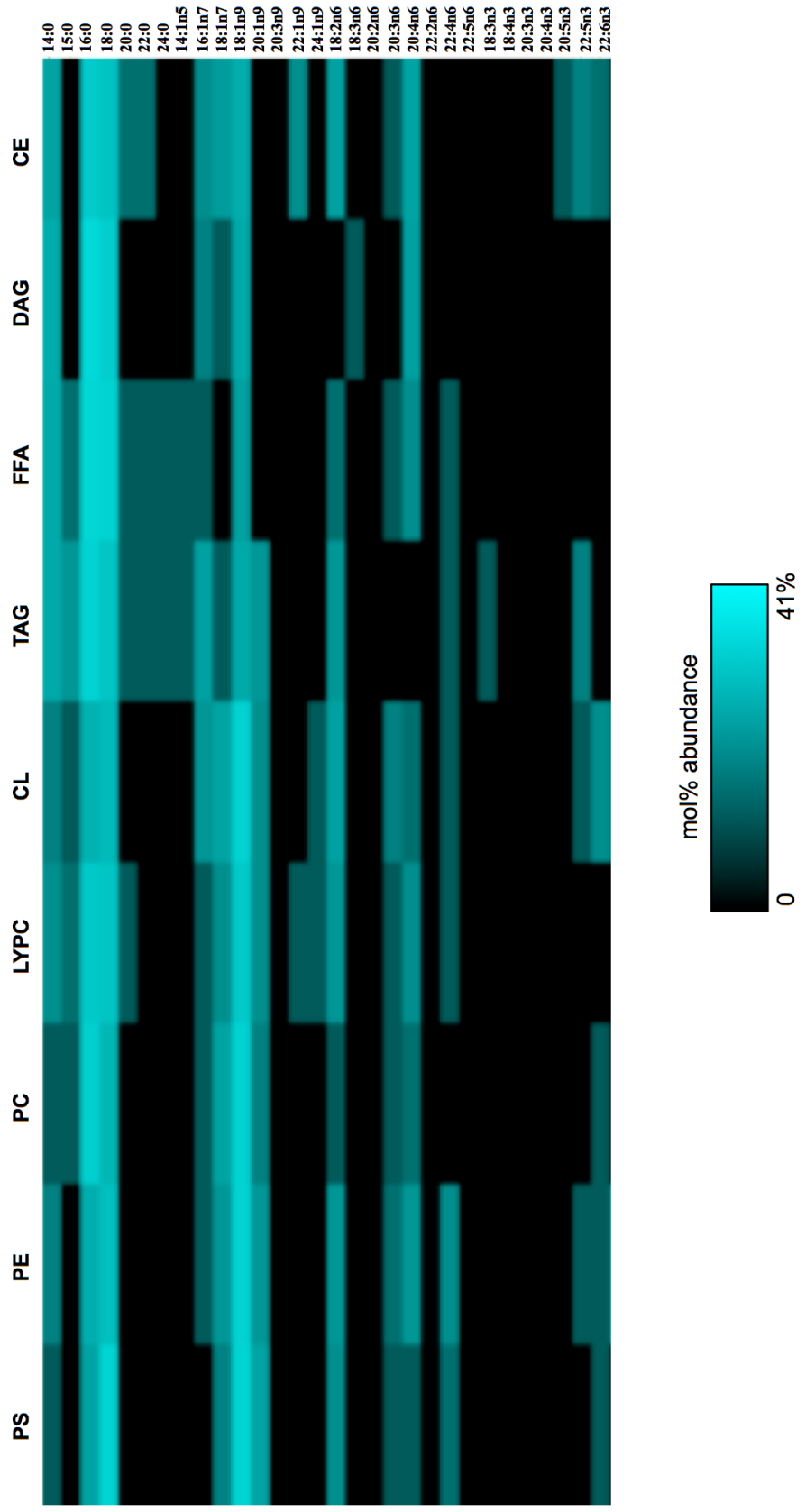
14:0
15:0
16:0
18:0
20:0
22:0
24:0
14:1n5
16:1n7
18:1n7
18:1n9
20:1n9
20:3n9
22:1n9
24:1n9
18:2n6
18:3n6
20:2n6
20:3n6
20:4n6
22:2n6
22:4n6
22:5n6
18:3n3
18:4n3
20:3n3
20:4n3
20:5n3
22:5n3
22:6n3
PS
PE
PC
LYPC
CL
TAG
FFA
DAG
CE
mol% abundance
41%
0

Figure 5.7. Lipidomic characterization (relative abundance) of insulin-FDI treated lipid bodies in mast cells. RBL2H3 were grown for 6 days with insulin-FDI. Cells were harvested, pelleted and lipid bodies were fractioned by ultracentrifugation as described in methods. Individual major lipid species were separated by high performance liquid chromatography (HPLC) and fatty acid methyl esters from each class were produced and subsequently analyzed by GC/MS. Abundance of lipid species in insulin-FDI treated mast cells were quantified and organized into a heatmap according to the observed percentage of the total moles of fatty acid in the specified lipid class. Each row indicates a specific fatty acid labeled as follows: the carbon length (the number to the left of the colon), the number of double bonds in the molecule (the number on the immediate left of the 'n') and the starting location of those double bonds (the number on the immediate right of the 'n'). *Abbreviations: Cholesterol Ester (CE), Cardiolipin (CL), Triacylglycerol (TAG), Diacylglycerol (DAG), Free Fatty Acid (FFA), Phosphotidylserine (PS), Phosphotidylcholine (PC), Phosphotidylethanolamide (PE), Lysophoshotidylcholine (LYPC)*.

5.2.3. Development and testing of a microaspiration technique to highly purify lipid bodies

Protocols designed to isolate lipid bodies from other cellular lipids require the use of sucrose gradients and several ultracentrifugation cycles cumulatively designed to separate subcellular organelles according to their respective size and mass. However, one of the unique characteristics of lipid bodies is that they can be found in sizes ranging from sub micron to nearly 100µm with respective differences in individual mass (19, 20, 59). Clearly, this distribution in size and density may prove problematic in such lipid body isolation protocols, especially in cell systems such as the mast cell, which at rest lack large numbers of lipid bodies. Our second issue with ultracentrifugation protocols is the likely presence of contaminants (see above). Furthermore, there is an overarching assumption in these protocols, that lipid bodies retain their structure under such stringent conditions, which, given some of our preliminary lipid body micromanipulation data in insulin-FDI treated mast cells (data not shown), we consider to be unlikely. Physical manipulation of lipid bodies in insulin-FDI treated mast cells show that they are fragile and easily disturbed, losing their native spherical structure with very little agitation.

We designed and assembled an intracellular lipid body microaspiration apparatus with the intended capability of isolating lipid bodies directly from cells. This apparatus consists of a TransferMan NK2 micromanipulator (Eppendorf) and a CellTram Vario (Eppendorf) for pressure control, equipped with an ICSI TransferTip micropipette (Eppendorf). We initially sought to perform a proof-of-concept experiment to establish whether lipid body microaspiration was a viable approach. For this proof-of-concept we chose the 3T3-L1 cell line. The abundance and bright-field visibility of adipocyte lipid droplets is higher than the corresponding structures in mast cells. In order to generate quantitative results, it was essential to meet the sensitivity requirements of HPLC and GC/MS. We aspirated approximately 15,000 lipid bodies from nearly 1000 cells equating to approximately 60ng sample from 3T3-L1 cells exposed to insulin-FDI for 6 days. Figure 5.9 (upper and middle panel) show a time lapse over 2 slides (top to bottom) of an individual lipid body being aspirated into a micropipette. Aspirated lipid bodies were intentionally collected in small

numbers (~10-100 at a time) and immediately deposited into a Target I-D vial with a polyspring insert (National Scientific) containing ~150 µl of hexane in an attempt to preserve native lipid isoforms and prevent lipid peroxidation.

We analyzed microaspirated lipid bodies from 3T3-L1 cells treated for 6 days with insulin-FDI using HPLC and GC/MS. Figure 5.8 indicates a summary of our analysis in terms of the major lipid class triacylglycerol. Note that other lipid classes were below the limit of detection (LOD) for the full lipidomic profile shown in previous Figures. This indicates the necessity for more sample, and establishes the scale of the effort needed to gather sufficient sample for full-scale analyses.

We present the absolute amount of each fatty acid in Figure 5.8A and the absolute amount of fatty acids with various degrees of saturation in Figure 5.8C. Similarly, we quantified the percent abundance of each fatty acid in Figure 5.8B and the percent abundance of fatty acids with various degrees of saturation in Figure 5.8D. Palmitic acid (16:0) is the most abundant saturated fatty acid found naturally in animal cells and we observe Palmitic Acid to be the most abundant fatty acid conjugated to TAG in our analysis. The second most abundant fatty acid we find in insulin-FDI treated adipocytes is Oleic acid (18:1n9), an omega-9 monounsaturated fatty acid, which is a direct biosynthetic product of Palmitic acid. Oleic acid is the most abundant fatty acid found in adipose tissue and the most common unsaturated fatty acid produced *de novo* by humans. Additionally, we find a much higher percentage of saturated fatty acids compared to mono- and poly-unsaturated fatty acids in insulin-FDI treated adipocytes. These data from our microaspirated lipid bodies are consistent with published lipidomic findings in adipose using traditionally accepted methods. We believe that this analysis proves that the presented isolation technique is adequate in acquiring, and preserving lipid species for lipidomic analysis.

A. nmol/µg of sample

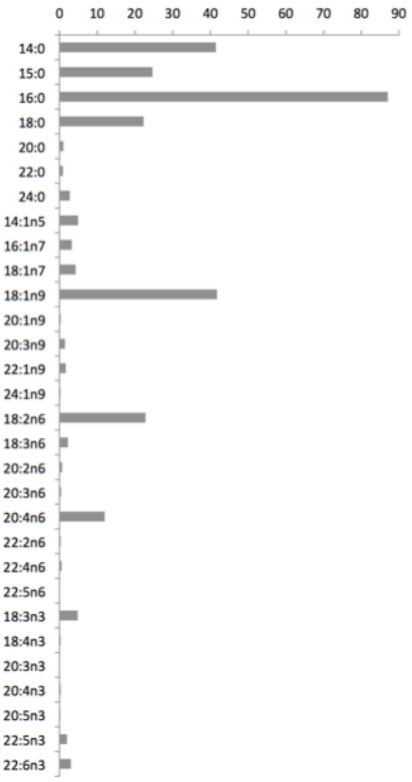

B. moles as a % of total moles

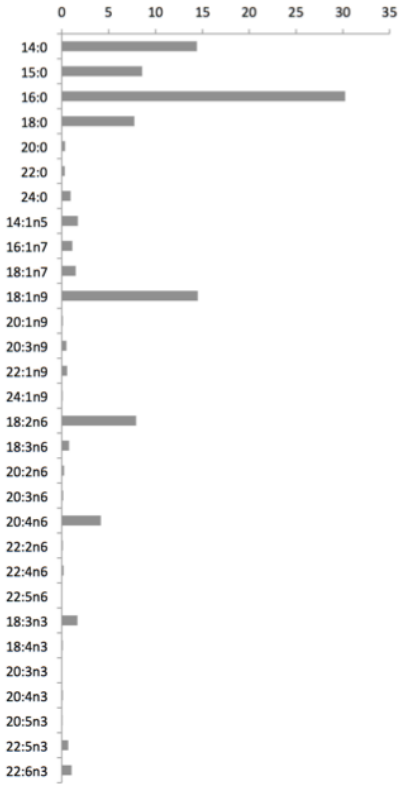

C. nmol/gram of sample

TFA	SFA	MUFA	PUFA	n3	n6	n7	n9
287.9	180.1	56.5	51.2	10.7	39.1	7.5	43.5

D. moles as a % of total moles

%TFA	%SFA	%MUFA	%PUFA	%n3	%n6	%n7	%n9
100	62.6	19.6	17.8	3.7	13.6	2.6	15.8

Figure 5.8. Novel lipidomic characterization of microaspirated lipid bodies from insulin-FDI treated adipocytes. 3T3-L1 cells were grown for 6 days with insulin-FDI on glass bottom dishes. Cells were imaged under a 100X objective and individual lipid bodies were microaspirated from the cytosol and collected in hexane. Individual major lipid species TAG were separated by high performance liquid chromatography (HPLC) and fatty acid methyl esters from TAG were produced and subsequently analyzed by GC/MS. Absolute values were quantified for individual fatty acids (**A**) and degrees of saturation (**C**). Percent abundances were quantified for individual fatty acids (**B**) and degrees of saturation (**D**). Each row in Figure A and B indicates a specific fatty acid labeled as follows: the carbon length (the number to the left of the colon), the number of double bonds in the molecule (the number on the immediate left of the 'n') and the starting location of those double bonds (the number on the immediate right of the 'n'). Abbreviations: TFA (total fatty acid), SFA (saturated fatty acid), MUFA (monounsaturated fatty acid), PUFA (polyunsaturated fatty acid), n3 (omega-3 polyunsaturated fatty acid), n6 (omega-6 polyunsaturated fatty acid), n7 (omega-7 polyunsaturated fatty acid) and n9 (omega-9 polyunsaturated fatty acid).

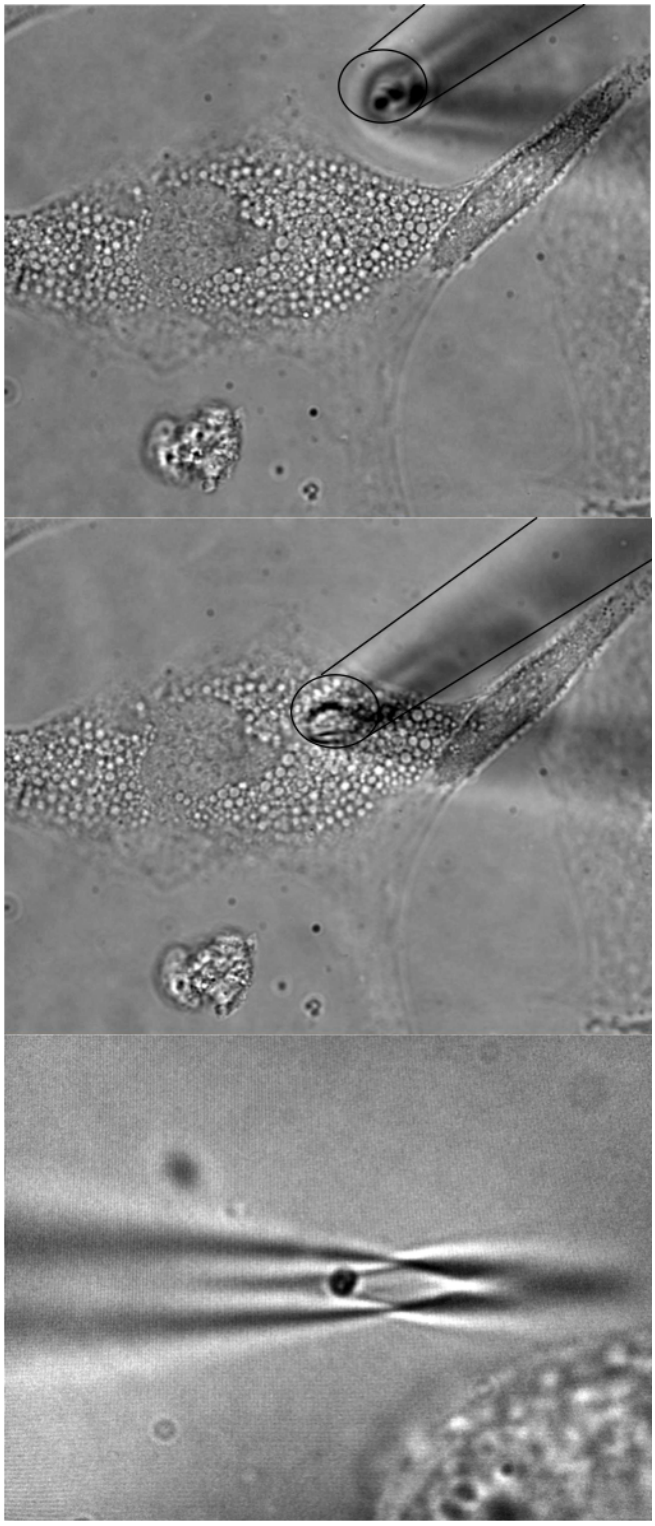

Figure 5.9. Development of a novel microaspiration technique for isolating cytoplasmic lipid bodies.

3T3-L1 and RBL2H3 (not shown) cells were grown for 6 days with insulin-FDI on glass bottom dishes. Cells were viewed under a 100X objective and individual lipid bodies were microaspirated from the cytosol and deposited into hexane. **Upper panel.** Microaspiration (ICSI transfer) needle approaching steatotic 3T3-L1 cell. **Middle panel.** After penetration of the cell membrane, application of ~100 psi suction pressure (Eppendorf Vario system) starts to extract lipid bodies. **Lower panel.** Highly zoomed image of a single lipid body in a microaspiration piptette from an RBL2H3 mast cell.

5.3. Discussion

The central goal of the experiments in Chapter 5 was to measure the lipid content of resting and steatotic mast cells, and to develop methodology that allowed us to measure the lipid content of purified lipid bodies. Here, we provide the first lipidomic analysis of resting mast cells, and of a steatotic mast cell induced by chronic insulin exposure over a 6-day timecourse. Both the resting and induced data sets have value, since the mast cell lipidome has not previously been published. In addition to providing insight into the basic lipid chemistry of this cell type, these data establish a baseline for the study of induced alterations in lipid profile, here studied in response to chronic insulin, but which could be extended to the response to antigenic and other mast cell-activating stimuli.

Our data suggest that mast cells chronically exposed to insulin *in vitro* have marked alterations in their lipidomic landscape. Mast cells have been linked to a variety of pathologies defined by an underlying inflammatory component, and the role of mast cell derived lipid messengers (leukotrienes, prostaglandins, thromboxanes, etc.) in these pathologies is clear (42). The physiological roles of mast cells in wound healing, regulation of smooth muscle tone and vasoregulation are also dependent upon these lipid messengers (42, 43). However, the exact contribution of the mast cell is largely unexplored. As we have previously demonstrated, chronic insulin exposure drives the formation of lipid bodies in mast cells, however, the contents of these lipid bodies or the collateral effects the production of these lipid bodies have on the whole cell lipidome have yet to be investigated.

It has been shown in the obese liver that excess levels of ectopic fat deposition, for example during hepatosteatosis, can drive the liver into a re-programming, altering the composition of the hepatocyte lipidome (71). Consistent with the findings in the liver, we also find that treating mast cells with insulin for 6 days and inducing steatosis drives the mast cell into a lipidomic reprogramming. There are changes in the absolute abundance of a large number of lipids, thus it is clear that the changes in lipid profile engendered by the addition of large numbers of lipid bodies to mast cells are sufficient to cause shifts in the whole cell's lipid signature.

There are commonalities and differences between the insulin-induced lipid profile changes in mast cells and those previously observed in the obese liver or adipocyte systems. There are three major data sets that we compared to our findings; the lipidome of obese adipose tissue (multiple cell types including adipocytes, mesenchyme and immunocytes), the lipidome of resting and lipogenically-stimulated isolated adipocytes, and the lipidome of macrophages isolated from obese adipose (142, 145, 147).

Isolated adipocytes from obese tissue show large increases in PUFA and TAG levels (147). Similarly, adipose tissue as a whole, and the macrophages isolated from it show increased PUFA levels in the obese setting and elevated TAG (145). Our analysis suggest that under the hyperinsulinaemic conditions mimicked in our experiments, mast cells show dramatic increases in PUFA but no overall increase in TAG. This latter observation is worthy of some discussion, since it would speak to a distinct, not primarily energy storage role for mast cell lipid bodies when compare to those from other cell types. Moreover, the only other lipid analysis of mast cell lipid bodies (from the Kovanen laboratory) suggest that TAG are stored in mast cell LB (83). We also detect TAG in mast cell lipid bodies but they are not conserved under the condition used here and so that role of the LB is not being expanded in the steatotic situation. The increase in PUFA that we observe, if translated to the mast cells found *in vivo*, could provide a new source for the PUFA that are dramatically elevated in adipose tissue.

As described above, we find the largest lipid increases in response to chronic insulin to occur in the polyunsaturated fatty acid class, which are the precursor molecules responsible for synthesizing a variety of pro-inflammatory and pro-thrombotic agents in the mast cell. More specifically, we observe significant upregulations in the particular fatty acids involved in the biosynthetic pathway of AA, including large increases in the AA molecule (20:4n6) itself. At least under these experimental conditions, these data indicate that in situations of ectopic lipid deposition caused by chronic exposure to insulin, mast cells may be biased to producing the required lipid-derived precursor molecules necessary and sufficient to drive localized and systemic inflammatory responses. These data also provide a mechanistic basis for the elevated basal and FcεRI-induced leukotriene release that we observed in Chapter 4. This increase in precursors measured lipidomically appear to translate to real gains in the amounts of fully-formed mediators that are released from the cell. Given the role of these mediators in the neovascularization that occurs during wound healing, we can speculate that in the obese

tissue, mast cell derived mediators such as LTC4 may contribute to the angiogenesis that occurs as the adipose deposits expand.

Lipid bodies in mast cells have been less well-studied than their counterparts in adipocytes or the mast cell secretory granule. We performed a lipidomic analysis of isolated lipid bodies in mast cells treated with insulin-FDI for 6 days and that we marked differences between this data set and the whole cell lipidomic analysis. However, the lipid body lipidome was similar to that of the ER/microsomal fraction that we partially analyzed in Chapter 3. We observe the most abundant fatty acids in our lipid body isolation to be palmitic acid (16:0), stearic acid (18:0) and oleic acid (18:1n9), which are the same 3 fatty acids with the highest abundance analyzed from our ER fractions in mast cells treated for 6 days with insulin-FDI. This could reflect the intimate link that has been suggested to exist between the ER and the lipid bodies. However, as described above, contamination of the lipid body fraction with ER may be of concern.

Our data support EM analysis performed by the Dvorak laboratory as well as some studies from other granulocytes, where lipid bodies are thought to be reservoirs of arachidonic acid and its precursors (57, 84, 92). While we have not been able to observe the localization of 5LO and LTC4 synthase in mast cell lipid bodies using confocal colocalization techniques documented by Dvorak, we do see evidence of elevated arachidonic acid compared to other fatty acid species in the lipid body fractions.

The main purpose of initially microaspirating lipid bodies in adipocytes was to provide a proof of concept for the technique, which we would then apply to isolating lipid bodies in steatotic mast cells. In addition to achieving isolation of lipid bodies in the adipocyte using microaspiration, we were also able to isolate lipid bodies from insulin-FDI treated mast cells (Figure 5.9). Anecdotally, we did note that under conditions of microaspiration, the adipocyte LB seems more robust than those in the mast cells. This consistent phenomenon may perhaps underscore our proposal that there are marked compositional differences between LB in the two systems. Perhaps more importantly, the level to which aggressive techniques like the ultracentrifugation approach may differentially compromise the LB integrity is a concern that further justifies our focus on microaspiration.

We were able to isolate and collect lipid bodies through our developed microaspiration technique. Our sample isolation and subsequent lipidomic analysis of microaspirated lipid bodies from 3T3L1 adipocytes provided results that are consistent with current models of adipocyte lipid bodies. These lipid bodies consisted of NTG with a fatty acid profile consistent with that identified in the literature, including higher abundance of particular shorter chain saturated fatty acids. These findings indicate that our microaspiration technique will provide accurate results upon the collection of mast cell lipid bodies and that this technique will yield the most accurate depiction of the lipid body contents associated with insulin-FDI treated mast cells.

These observations are the first of their kind in demonstrating a reliable isolation of lipid bodies by microaspiration in 3T3-L1 adipocytes. The technique also works in principle in RBL2H3, but we estimate that we will need to aspirate ~60,000 LB from approximately 1000 RBL2H3 to perform even a partial lipidomic analysis analogous to that in Figure 5.8. A full lipidomic analysis could require 40 times as much sample. Although time consuming, this technique provides robust results with maximum confidence in sample collection. We believe that this technique has the potential to be utilized in other facets of subcellular biology where observations of subcellular organelles require increased resolution or isolation.

Chapter Six

Discussion and Future Perspectives

The underlying concept that drives the work presented in this thesis is that metabolic perturbations may inadvertantly influence the immune system. There is an extensive literature documenting a close relationship between the metabolic system and the immune system. However, in the face of our current health challenges, there is an obligation to understand the immunological consequences of nutrient abundance and overeating and this body of work addresses one piece of that puzzle. Mast cells have been implicated in metabolic paraflammation, but the effects of metabolic or endocrine inputs on the status of the mast cell have not been studied. We identified that insulin alters mast cell function *in vitro* and we believe that these observations can be used to aid in explaining the participation of the mast cell in various metabolically derived pathologies.

What have we learned about mast cells?

1. Mast cells respond to insulin. Prior to this work, it was accepted that mast cells were refractory to insulin. The work provided in this dissertation provides a new understanding of how mast cells bear the capacity to respond to this metabolic hormone and the functional consequences that attend chronic exposures. The broader implications of this work is that mast cells are responsive to such metabolic inputs as endocrine-derived signals and that evolution has, for some reason, coupled pro-inflammatory capacity to nutrient sensing.

2. Mast cells lipid body formation is mechanistically conserved. We understand that engaging a lipogenic program in a variety of metabolic tissue, including muscle and liver, results in lipid body formation and the ectopic deposition of lipids. Mast cell lipid bodies have previously been very poorly studied organelles and we do not know much about their biogenesis or function. We now know however that lipogenic stimuli have the potential to drive their formation, which is a conserved control mechanism with other metabolically adapted cells. These observations raise a variety of questions to whether insulin has the ability to accomplish this *in vivo*. First of all, is insulin the only stimulus for lipogenesis or are there other insulin-like, or insulin mimicking molecules, which could achieve this same

goal? Second, these data imply mast cell lipid body numbers may respond to variations in insulin levels, perhaps over timecourses as acute as daily feeding cycles. Are gut mast cells suppressed acutely by insulin from releasing inflammatory mediators every time a large influx of antigen-laden food is absorbed? Our data create a need to establish what the threshold is for insulin-induced changes in mast cell lipid body populations in regards to long term chronic exposure or acute cyclic fluctuations.

3. Insulin acts as a switch in mast cells, which adapts their phenotype. We have shown that insulin moves mast cells between a secretory rich and eicosanoid poor to a secretory poor and eicosanoid rich functional status. This is the first observation that an endocrine hormone has the potential to do this in the mast cells. Mast cells have long been recognized for their heterogeneity and their unique secretory characteristics according to the tissue in which they mature and reside (135, 137, 140). There is evidence in the literature that mast cells from different locations are differentially prone to releasing granule contents or leukotrienes in response to stimulation. This work raises the question as to whether the role of insulin or other local metabolic stimuli are fully or partly responsible for this heterogeneity. This data also imply a potential for acute plasticity in mast cell responses if one considers the cyclical secretion of insulin throughout standard feeding cycles.

What have we learned about lipid bodies?

We have made a number of possibly generally applicable observations about lipid bodies. Lipid bodies are not homogeneous within a cell, and between cell types. This implies that lipid bodies could be very complex populations, in terms of different lipid content. This in turn implies that a cell would need a mechanism to generate and then specifically access this complexity, which could add a whole new degree of complication to our understanding of lipid bodies. Thus far, many functions have been ascribed to lipid bodies but the main body of the literature deals with them only as storage depots. Relatively obscure papers on lipid bodies acting as locations for protein synthesis, reaction vessels for housing certain types of necessary lipophilic chemistry should perhaps be given more attention (54, 57, 66, 110, 148).

What did we learn about lipidomes in mast cells?

In this study we described the ability of insulin to regulate the mast cell lipidome. This has not previously been reported and we find that insulin has the ability to shift the mast cell into a more pro-inflammatory program. Our analysis provided a surprising insight into the possibility of the regulation that a metabolic hormone could impose on the lipidomic profile of a proinflammatory cell such as the mast cell. The implications of the alterations in major lipid classes and their attending fatty acid composition may have wide ranging effects on lipid-derived mediator production, in addition to shifts in membrane dynamics, cellular signalling and receptor scaffolding. The degree of resolution provided by this lipidomic analysis is important and identifying further the status of precursor reservoirs in insulin treated mast cells will provide insight into subsequent cellular responses to stimulation.

What did we learn about obesity?

Obesity is the expansion of adipose depots, primarily driven by the accumulation of lipids into stored lipid bodies within hyperplasic adipocytes. In 'healthy' subcutaneous obesity without nutrient overload, lipid is not deposited in ectopic locations. In contrast, pathologic obesity is accompanied by lipid accumulation in a range of tissues. Our work implies that cells of the immune system, especially mast cells, should now be considered as potential locations for ectopic lipid deposition. This deposition may arise from dietary fat import (an idea not tested here), and/or from the previously unrecognised ability of metabolic inputs such as insulin to drive a cell-intrinsic lipogenesis program in the mast cell. Our data imply that an insulin-enriched environment, prevalent during the development of metabolic syndrome, will change the phenotype and pro-inflammatory status of mast cells. In their altered, acquired state, these cells may then contribute causally to the inflammatory component of obesity.

Future perspectives

There are central tests of the ideas emerging from these *in vitro* studies that need to be performed *in vivo*. However, emerging controversy makes these next steps complicated to envision. Since the descriptions of *mastzellen* by Ehrlich in the 1880s, the mast cell has primarily been studied in relation to allergy, anaphylaxis and anti-parasitic responses. Roles in innate immunity, wound healing and various pathologies have emerged from more recent

studies (42, 149). With the advent of the mast cell deficient mouse strains W/W^v and *KitW-sh/W-sh,* a flood of studies have established apparently causal roles for mast cells in the pathogenesis of diverse diseases, from multiple sclerosis and cardiac hypertrophy to cancer, and from migraine to obesity. Recently, a controversial paper by Rodewald has called into question the validity of these models, arguing that they are far from clean cut systems that have led to a significant overestimate of the degree to which mast cells are involved in this vast number of physiological and pathophysiological processes (150). While arguing for revisiting of most of these studies using a new Cpa3-CRE mouse system, Rodewald also suggests that studies such as those implicating mast cells in the development of obesity need additional lines of evidence, specifically mechanistic insights, to support them. Our current study does not address the shortcomings, or otherwise, of various sophisticated *in vivo* systems for the study of mast cells. Rather, we provide one of the critical conceptual links to a potential mechanistic basis for the contribution of mast cells to diet-induced obesity that could be tested as consensus on *in vivo* models emerges in coming years. While *in vivo* experiments will definitely develop this project further, there is also a great deal of biophysical and signaling information at the cellular and subcellular levels that remains to be uncovered.

Bibliography

1. Allison, D.B., K.R. Fontaine, J.E. Manson, J. Stevens, and T.B. VanItallie. 1999. Annual deaths attributable to obesity in the United States. *JAMA* 282:1530-1538.

2. Fontaine, K.R., D.T. Redden, C. Wang, A.O. Westfall, and D.B. Allison. 2003. Years of life lost due to obesity. *JAMA* 289:187-193.

3. Ford, E.S., and A.H. Mokdad. 2008. Epidemiology of obesity in the Western Hemisphere. *J Clin Endocrinol Metab* 93:S1-8.

4. Mokdad, A.H., B.A. Bowman, E.S. Ford, F. Vinicor, J.S. Marks, and J.P. Koplan. 2001. The continuing epidemics of obesity and diabetes in the United States. *JAMA* 286:1195-1200.

5. Must, A., J. Spadano, E.H. Coakley, A.E. Field, G. Colditz, and W.H. Dietz. 1999. The disease burden associated with overweight and obesity. *JAMA* 282:1523-1529.

6. Finkelstein, E.A., J.G. Trogdon, J.W. Cohen, and W. Dietz. 2009. Annual medical spending attributable to obesity: payer-and service-specific estimates. *Health Aff (Millwood)* 28:w822-831.

7. Lev-Ran, A. 2001. Human obesity: an evolutionary approach to understanding our bulging waistline. *Diabetes Metab Res Rev* 17:347-362.

8. Ioannidis, I. 2008. The road from obesity to type 2 diabetes. *Angiology* 59:39S-43S.

9. Muoio, D.M., and C.B. Newgard. 2006. Obesity-Related Derangements in Metabolic Regulation. *Annu Rev Biochem*

10. Sutherland, J.P., B. McKinley, and R.H. Eckel. 2004. The metabolic syndrome and inflammation. *Metab Syndr Relat Disord* 2:82-104.

11. McAuley, P.A., and S.N. Blair. 2011. Obesity paradoxes. *J Sports Sci* 29:773-782.

12. Bevan, P. 2001. Insulin signalling. *J Cell Sci* 114:1429-1430.

13. Galton, D.J., and S. Wallis. 1982. The regulation of adipose cell metabolism. *Proc Nutr Soc* 41:167-173.

14. Bano, G. 2013. Glucose homeostasis, obesity and diabetes. *Best Pract Res Clin Obstet Gynaecol*

15. Ducharme, N.A., and P.E. Bickel. 2008. Lipid droplets in lipogenesis and lipolysis. *Endocrinology* 149:942-949.

16. Beller, M., K. Thiel, P.J. Thul, and H. Jackle. 2010. Lipid droplets: a dynamic organelle moves into focus. *FEBS Lett* 584:2176-2182.

17. Brown, D.A. 2001. Lipid droplets: proteins floating on a pool of fat. *Curr Biol* 11:R446-449.

18. Fujimoto, T., Y. Ohsaki, J. Cheng, M. Suzuki, and Y. Shinohara. 2008. Lipid droplets: a classic organelle with new outfits. *Histochemistry and cell biology* 130:263-279.

19. Guo, Y., K.R. Cordes, R.V. Farese, Jr., and T.C. Walther. 2009. Lipid droplets at a glance. *J Cell Sci* 122:749-752.

20. Listenberger, L.L., and D.A. Brown. 2008. Lipid droplets. *Curr Biol* 18:R237-238.

21. Walther, T.C., and R.V. Farese, Jr. 2012. Lipid droplets and cellular lipid metabolism. *Annual review of biochemistry* 81:687-714.

22. Cusi, K. 2011. Role of obesity and lipotoxicity in the development of nonalcoholic steatohepatitis: pathophysiology and clinical implications. *Gastroenterology* 142:711-725 e716.

23. Despres, J.P., and I. Lemieux. 2006. Abdominal obesity and metabolic syndrome. *Nature* 444:881-887.

24. Unger, R.H., G.O. Clark, P.E. Scherer, and L. Orci. 2010. Lipid homeostasis, lipotoxicity and the metabolic syndrome. *Biochim Biophys Acta* 1801:209-214.

25. Large, V., O. Peroni, D. Letexier, H. Ray, and M. Beylot. 2004. Metabolism of lipids in human white adipocyte. *Diabetes Metab* 30:294-309.

26. Rocha, V.Z., and E.J. Folco. 2011. Inflammatory concepts of obesity. *Int J Inflam* 2011:529061.

27. Yudkin, J.S. 2007. Inflammation, obesity, and the metabolic syndrome. *Horm Metab Res* 39:707-709.

28. Tappy, L., and B. Mittendorfer. 2012. Fructose toxicity: is the science ready for public health actions? *Curr Opin Clin Nutr Metab Care* 15:357-361.

29. Garbarino, J., and S.L. Sturley. 2009. Saturated with fat: new perspectives on lipotoxicity. *Curr Opin Clin Nutr Metab Care* 12:110-116.

30. Nishimura, S., I. Manabe, and R. Nagai. 2009. Adipose tissue inflammation in obesity and metabolic syndrome. *Discov Med* 8:55-60.

31. Tabas, I., and C.K. Glass. 2013. Anti-inflammatory therapy in chronic disease: challenges and opportunities. *Science* 339:166-172.

32. Popa, C., M.G. Netea, P.L. van Riel, J.W. van der Meer, and A.F. Stalenhoef. 2007. The role of TNF-alpha in chronic inflammatory conditions, intermediary metabolism, and cardiovascular risk. *J Lipid Res* 48:751-762.

33. Deng, T., C.J. Lyon, L.J. Minze, J. Lin, J. Zou, J.Z. Liu, Y. Ren, Z. Yin, D.J. Hamilton, P.R. Reardon, V. Sherman, H.Y. Wang, K.J. Phillips, P. Webb, S.T. Wong, R.F. Wang, and W.A. Hsueh. 2013. Class II Major Histocompatibility Complex Plays an Essential Role in Obesity-Induced Adipose Inflammation. *Cell Metab* 17:411-422.

34. De Taeye, B.M., T. Novitskaya, O.P. McGuinness, L. Gleaves, M. Medda, J.W. Covington, and D.E. Vaughan. 2007. Macrophage TNF-alpha contributes to insulin resistance and hepatic steatosis in diet-induced obesity. *Am J Physiol Endocrinol Metab* 293:E713-725.

35. Gordon, S. 2007. Macrophage heterogeneity and tissue lipids. *J Clin Invest* 117:89-93.

36. Nishimura, S., I. Manabe, M. Nagasaki, K. Eto, H. Yamashita, M. Ohsugi, M. Otsu, K. Hara, K. Ueki, S. Sugiura, K. Yoshimura, T. Kadowaki, and R. Nagai. 2009. CD8+

effector T cells contribute to macrophage recruitment and adipose tissue inflammation in obesity. *Nat Med* 15:914-920.

37. Feuerer, M., L. Herrero, D. Cipolletta, A. Naaz, J. Wong, A. Nayer, J. Lee, A.B. Goldfine, C. Benoist, S. Shoelson, and D. Mathis. 2009. Lean, but not obese, fat is enriched for a unique population of regulatory T cells that affect metabolic parameters. *Nat Med* 15:930-939.

38. Kintscher, U., M. Hartge, K. Hess, A. Foryst-Ludwig, M. Clemenz, M. Wabitsch, P. Fischer-Posovszky, T.F. Barth, D. Dragun, T. Skurk, H. Hauner, M. Bluher, T. Unger, A.M. Wolf, U. Knippschild, V. Hombach, and N. Marx. 2008. T-lymphocyte infiltration in visceral adipose tissue: a primary event in adipose tissue inflammation and the development of obesity-mediated insulin resistance. *Arterioscler Thromb Vasc Biol* 28:1304-1310.

39. Rocha, V.Z., E.J. Folco, G. Sukhova, K. Shimizu, I. Gotsman, A.H. Vernon, and P. Libby. 2008. Interferon-gamma, a Th1 cytokine, regulates fat inflammation: a role for adaptive immunity in obesity. *Circ Res* 103:467-476.

40. Ohmura, K., N. Ishimori, Y. Ohmura, S. Tokuhara, A. Nozawa, S. Horii, Y. Andoh, S. Fujii, K. Iwabuchi, K. Onoe, and H. Tsutsui. 2010. Natural killer T cells are involved in adipose tissues inflammation and glucose intolerance in diet-induced obese mice. *Arterioscler Thromb Vasc Biol* 30:193-199.

41. Abraham, S.N., and A.L. St John. 2010. Mast cell-orchestrated immunity to pathogens. *Nat Rev Immunol* 10:440-452.

42. Galli, S.J., and M. Tsai. 2010. Mast cells in allergy and infection: versatile effector and regulatory cells in innate and adaptive immunity. *Eur J Immunol* 40:1843-1851.

43. Noli, C., and A. Miolo. 2001. The mast cell in wound healing. *Vet Dermatol* 12:303-313.

44. Okayama, Y., and T. Kawakami. 2006. Development, migration, and survival of mast cells. *Immunol Res* 34:97-115.

45. Liu, J., A. Divoux, J. Sun, J. Zhang, K. Clement, J.N. Glickman, G.K. Sukhova, P.J. Wolters, J. Du, C.Z. Gorgun, A. Doria, P. Libby, R.S. Blumberg, B.B. Kahn, G.S.

Hotamisligil, and G.P. Shi. 2009. Genetic deficiency and pharmacological stabilization of mast cells reduce diet-induced obesity and diabetes in mice. *Nat Med* 15:940-945.

46. Sismanopoulos, N., D.A. Delivanis, K.D. Alysandratos, A. Angelidou, A. Therianou, D. Kalogeromitros, and T.C. Theoharides. 2012. Mast cells in allergic and inflammatory diseases. *Curr Pharm Des* 18:2261-2277.

47. Sismanopoulos, N., D.A. Delivanis, D. Mavrommati, E. Hatziagelaki, P. Conti, and T.C. Theoharides. 2013. Do mast cells link obesity and asthma? *Allergy* 68:8-15.

48. Theoharides, T.C., N. Sismanopoulos, D.A. Delivanis, B. Zhang, E.E. Hatziagelaki, and D. Kalogeromitros. 2011. Mast cells squeeze the heart and stretch the gird: their role in atherosclerosis and obesity. *Trends Pharmacol Sci* 32:534-542.

49. Carvalho, V.F., E.O. Barreto, R.S. Cordeiro, V. Lagente, M.A. Martins, and P.M. e Silva. 2005. Mast cell changes in experimental diabetes: focus on attenuation of allergic events. *Mem Inst Oswaldo Cruz* 100 Suppl 1:121-125.

50. Casaco, A., D. Carvajal, and Z. Tolon. 1991. Diabetes-induced rat hyposensitivity to compound 48/80. *Can J Physiol Pharmacol* 69:886-888.

51. Cavalher-Machado, S.C., R.K. Cuman, J.L. Sartoretto, J.O. Martins, W.T. de Lima, M.A. Martins, P.M. Silva, and P. Sannomiya. 2008. The allergic inflammatory reaction in neonatal streptozotocininduced diabetic rats: evidence of insulin resistance and microvascular dysfunction. *Inflamm Res* 57:535-541.

52. Vianna, E.O., and J. Garcia-Leme. 1995. Allergen-induced airway inflammation in rats. Role of insulin. *Am J Respir Crit Care Med* 151:809-814.

53. Diaz, B.L., M.F. Serra, A.C. Alves, A.L. Pires, F.M. Correa, R.S. Cordeiro, M.A. Martins, and P.M. e Silva. 1996. Alloxan diabetes reduces pleural mast cell numbers and the subsequent eosinophil influx induced by allergen in sensitized rats. *Int Arch Allergy Immunol* 111:36-43.

54. Silva, A.R., P. Pacheco, A. Vieira-de-Abreu, C.M. Maya-Monteiro, B. D'Alegria, K.G. Magalhaes, E.F. de Assis, C. Bandeira-Melo, H.C. Castro-Faria-Neto, and P.T. Bozza. 2009. Lipid bodies in oxidized LDL-induced foam cells are leukotriene-synthesizing organelles: a MCP-1/CCL2 regulated phenomenon. *Biochim Biophys Acta* 1791:1066-1075.

55. Barba, I., L. Chavarria, M. Ruiz-Meana, M. Mirabet, E. Agullo, and D. Garcia-Dorado. 2009. Effect of intracellular lipid droplets on cytosolic Ca2+ and cell death during ischaemia-reperfusion injury in cardiomyocytes. *J Physiol* 587:1331-1341.

56. Park, J.E., H.T. Kim, S. Lee, Y.S. Lee, U.K. Choi, J.H. Kang, S.Y. Choi, T.C. Kang, M.S. Choi, and O.S. Kwon. 2011. Differential expression of intermediate filaments in the process of developing hepatic steatosis. *Proteomics* 11:2777-2789.

57. Bozza, P.T., I. Bakker-Abreu, R.A. Navarro-Xavier, and C. Bandeira-Melo. 2011. Lipid body function in eicosanoid synthesis: an update. *Prostaglandins Leukot Essent Fatty Acids* 85:205-213.

58. Mak, H.Y. 2012. Lipid droplets as fat storage organelles in Caenorhabditis elegans: Thematic Review Series: Lipid Droplet Synthesis and Metabolism: from Yeast to Man. *Journal of lipid research* 53:28-33.

59. Walther, T.C., and R.V. Farese, Jr. 2009. The life of lipid droplets. *Biochim Biophys Acta* 1791:459-466.

60. Robenek, H., I. Buers, O. Hofnagel, M.J. Robenek, D. Troyer, and N.J. Severs. 2009. Compartmentalization of proteins in lipid droplet biogenesis. *Biochim Biophys Acta* 1791:408-418.

61. Robenek, H., M.J. Robenek, and D. Troyer. 2005. PAT family proteins pervade lipid droplet cores. *J Lipid Res* 46:1331-1338.

62. Wolins, N.E., D.L. Brasaemle, and P.E. Bickel. 2006. A proposed model of fat packaging by exchangeable lipid droplet proteins. *FEBS Lett* 580:5484-5491.

63. Wolins, N.E., B.K. Quaynor, J.R. Skinner, M.J. Schoenfish, A. Tzekov, and P.E. Bickel. 2005. S3-12, Adipophilin, and TIP47 package lipid in adipocytes. *The Journal of biological chemistry* 280:19146-19155.

64. Brasaemle, D.L., G. Dolios, L. Shapiro, and R. Wang. 2004. Proteomic analysis of proteins associated with lipid droplets of basal and lipolytically stimulated 3T3-L1 adipocytes. *J Biol Chem* 279:46835-46842.

65. Brasaemle, D.L., and N.E. Wolins. 2012. Packaging of fat: an evolving model of lipid droplet assembly and expansion. *The Journal of biological chemistry* 287:2273-2279.

66. Cermelli, S., Y. Guo, S.P. Gross, and M.A. Welte. 2006. The lipid-droplet proteome reveals that droplets are a protein-storage depot. *Curr Biol* 16:1783-1795.

67. Guo, Y., T.C. Walther, M. Rao, N. Stuurman, G. Goshima, K. Terayama, J.S. Wong, R.D. Vale, P. Walter, and R.V. Farese. 2008. Functional genomic screen reveals genes involved in lipid-droplet formation and utilization. *Nature* 453:657-661.

68. Hotamisligil, G.S., and E. Erbay. 2008. Nutrient sensing and inflammation in metabolic diseases. *Nat Rev Immunol* 8:923-934.

69. Lai, E., T. Teodoro, and A. Volchuk. 2007. Endoplasmic reticulum stress: signaling the unfolded protein response. *Physiology (Bethesda)* 22:193-201.

70. Hotamisligil, G.S. 2010. Endoplasmic reticulum stress and atherosclerosis. *Nat Med* 16:396-399.

71. Fu, S., L. Yang, P. Li, O. Hofmann, L. Dicker, W. Hide, X. Lin, S.M. Watkins, A.R. Ivanov, and G.S. Hotamisligil. 2011. Aberrant lipid metabolism disrupts calcium homeostasis causing liver endoplasmic reticulum stress in obesity. *Nature* 473:528-531.

72. Hodges, B.D., and C.C. Wu. 2010. Proteomic insights into an expanded cellular role for cytoplasmic lipid droplets. *J Lipid Res* 51:262-273.

73. Wolins, N.E., J.R. Skinner, M.J. Schoenfish, A. Tzekov, K.G. Bensch, and P.E. Bickel. 2003. Adipocyte protein S3-12 coats nascent lipid droplets. *The Journal of biological chemistry* 278:37713-37721.

74. Yamaguchi, T., N. Omatsu, E. Morimoto, H. Nakashima, K. Ueno, T. Tanaka, K. Satouchi, F. Hirose, and T. Osumi. 2007. CGI-58 facilitates lipolysis on lipid droplets but is not involved in the vesiculation of lipid droplets caused by hormonal stimulation. *J Lipid Res* 48:1078-1089.

75. Church, M.K., Y. Okayama, and S. el-Lati. 1991. Mediator secretion from human skin mast cells provoked by immunological and non-immunological stimulation. *Skin Pharmacol* 4:15-24.

76. Cavalher-Machado, S.C., W.T. de Lima, A.S. Damazo, V. de Frias Carvalho, M.A. Martins, P.M. e Silva, and P. Sannomiya. 2004. Down-regulation of mast cell activation and airway reactivity in diabetic rats: role of insulin. *Eur Respir J* 24:552-558.

77. de Oliveira Barreto, E., V. de Frias Carvalho, B.L. Diaz, A. Balduino, R.S. Cordeiro, M.A. Martins, and P.M. Rodrigues e Silva. 2003. Adoptive transfer of mast cells abolishes the inflammatory refractoriness to allergen in diabetic rats. *Int Arch Allergy Immunol* 131:212-220.

78. Benyon, R.C. 1989. The human skin mast cell. *Clin Exp Allergy* 19:375-387.

79. Church, M.K., S. el-Lati, and Y. Okayama. 1991. Biological properties of human skin mast cells. *Clin Exp Allergy* 21:1-9.

80. Galli, S.J. 2000. Mast cells and basophils. *Curr Opin Hematol* 7:32-39.

81. Pejler, G., E. Ronnberg, I. Waern, and S. Wernersson. 2010. Mast cell proteases: multifaceted regulators of inflammatory disease. *Blood* 115:4981-4990.

82. Sharma, B.B., J.R. Apgar, and F.T. Liu. 2002. Mast cells. Receptors, secretagogues, and signaling. *Clin Rev Allergy Immunol* 22:119-148.

83. Dichlberger, A., S. Schlager, J. Lappalainen, R. Kakela, K. Hattula, S.J. Butcher, W.J. Schneider, and P.T. Kovanen. 2012. Lipid body formation during maturation of human mast cells. *J Lipid Res* 52:2198-2208.

84. Dvorak, A.M., H.F. Dvorak, S.P. Peters, E.S. Shulman, D.W. MacGlashan, Jr., K. Pyne, V.S. Harvey, S.J. Galli, and L.M. Lichtenstein. 1983. Lipid bodies: cytoplasmic organelles important to arachidonate metabolism in macrophages and mast cells. *J Immunol* 131:2965-2976.

85. Dvorak, A.M., I. Hammel, E.S. Schulman, S.P. Peters, D.W. MacGlashan, Jr., R.P. Schleimer, H.H. Newball, K. Pyne, H.F. Dvorak, L.M. Lichtenstein, and et al. 1984. Differences in the behavior of cytoplasmic granules and lipid bodies during human lung mast cell degranulation. *J Cell Biol* 99:1678-1687.

86. Greineisen, W.E., L.M. Shimoda, K. Maaetoft-Udsen, and H. Turner. 2012. Insulin-containing lipogenic stimuli suppress mast cell degranulation potential and up-regulate lipid

body biogenesis and eicosanoid secretion in a PPARgamma-independent manner. *J Leukoc Biol* 92:653-665.

87. Hammel, I., A.M. Dvorak, S.P. Peters, E.S. Schulman, H.F. Dvorak, L.M. Lichtenstein, and S.J. Galli. 1985. Differences in the volume distributions of human lung mast cell granules and lipid bodies: evidence that the size of these organelles is regulated by distinct mechanisms. *J Cell Biol* 100:1488-1492.

88. Bozza, P.T., K.G. Magalhaes, and P.F. Weller. 2009. Leukocyte lipid bodies - Biogenesis and functions in inflammation. *Biochimica et biophysica acta* 1791:540-551.

89. Mattos, K.A., H. D'Avila, L.S. Rodrigues, V.G. Oliveira, E.N. Sarno, G.C. Atella, G.M. Pereira, P.T. Bozza, and M.C. Pessolani. 2010. Lipid droplet formation in leprosy: Toll-like receptor-regulated organelles involved in eicosanoid formation and Mycobacterium leprae pathogenesis. *J Leukoc Biol* 87:371-384.

90. Weller, P.F., S.J. Ackerman, A. Nicholson-Weller, and A.M. Dvorak. 1989. Cytoplasmic lipid bodies of human neutrophilic leukocytes. *Am J Pathol* 135:947-959.

91. Bozza, P.T., R.C. Melo, and C. Bandeira-Melo. 2007. Leukocyte lipid bodies regulation and function: contribution to allergy and host defense. *Pharmacol Ther* 113:30-49.

92. Dvorak, A.M., E. Morgan, R.P. Schleimer, S.W. Ryeom, L.M. Lichtenstein, and P.F. Weller. 1992. Ultrastructural immunogold localization of prostaglandin endoperoxide synthase (cyclooxygenase) to non-membrane-bound cytoplasmic lipid bodies in human lung mast cells, alveolar macrophages, type II pneumocytes, and neutrophils. *J Histochem Cytochem* 40:759-769.

93. Johnson, M.M., B. Vaughn, M. Triggiani, D.D. Swan, A.N. Fonteh, and F.H. Chilton. 1999. Role of arachidonyl triglycerides within lipid bodies in eicosanoid formation by human polymorphonuclear cells. *Am J Respir Cell Mol Biol* 21:253-258.

94. Bozza, P.T., W. Yu, J.F. Penrose, E.S. Morgan, A.M. Dvorak, and P.F. Weller. 1997. Eosinophil lipid bodies: specific, inducible intracellular sites for enhanced eicosanoid formation. *J Exp Med* 186:909-920.

95. Dvorak, A.M. 1991. Basophil and mast cell degranulation and recovery. Plenum Press, New York. viii, 415 p. pp.

96. Passante, E., and N. Frankish. 2009. The RBL-2H3 cell line: its provenance and suitability as a model for the mast cell. *Inflamm Res* 58:737-745.

97. Berlin, G., and L. Enerback. 1983. Fluorescent berberine binding as a marker of secretory activity in mast cells. *Int Arch Allergy Appl Immunol* 71:332-339.

98. Enerback, L. 1974. Berberine sulphate binding to mast cell polyanions: a cytofluorometric method for the quantitation of heparin. *Histochemistry* 42:301-313.

99. Zou, C., and Z. Shen. 2007. One-step intracellular triglycerides extraction and quantitative measurement in vitro. *J Pharmacol Toxicol Methods* 56:63-66.

100. Pfaffl, M.W. 2001. A new mathematical model for relative quantification in real-time RT-PCR. *Nucleic Acids Res* 29:e45.

101. Kopecky, J., P. Flachs, K. Bardova, P. Brauner, T. Prazak, and J. Sponarova. 2002. Modulation of lipid metabolism by energy status of adipocytes: implications for insulin sensitivity. *Ann N Y Acad Sci* 967:88-101.

102. Eckel, R.H., W.Y. Fujimoto, and J.D. Brunzell. 1978. Insulin regulation of lipoprotein lipase in cultured 3T3-L1 cells. *Biochem Biophys Res Commun* 84:1069-1075.

103. Green, H., and O. Kehinde. 1975. An established preadipose cell line and its differentiation in culture. II. Factors affecting the adipose conversion. *Cell* 5:19-27.

104. Green, H., and O. Kehinde. 1979. Formation of normally differentiated subcutaneous fat pads by an established preadipose cell line. *J Cell Physiol* 101:169-171.

105. Russell, T.R., and R. Ho. 1976. Conversion of 3T3 fibroblasts into adipose cells: triggering of differentiation by prostaglandin F2alpha and 1-methyl-3-isobutyl xanthine. *Proc Natl Acad Sci U S A* 73:4516-4520.

106. Lessmann, E., G. Grochowy, L. Weingarten, T. Giesemann, K. Aktories, M. Leitges, G. Krystal, and M. Huber. 2006. Insulin and insulin-like growth factor-1 promote mast cell survival via activation of the phosphatidylinositol-3-kinase pathway. *Exp Hematol* 34:1532-1541.

107. Kettner, A., M. Di Matteo, and A. Santoni. 2010. Insulin potentiates FcepsilonRI-mediated signaling in mouse bone marrow-derived mast cells. *Mol Immunol* 47:1039-1046.

108. Melo, R.C., H. D'Avila, D.L. Fabrino, P.E. Almeida, and P.T. Bozza. 2003. Macrophage lipid body induction by Chagas disease in vivo: putative intracellular domains for eicosanoid formation during infection. *Tissue Cell* 35:59-67.

109. Wan, H.C., R.C. Melo, Z. Jin, A.M. Dvorak, and P.F. Weller. 2007. Roles and origins of leukocyte lipid bodies: proteomic and ultrastructural studies. *Faseb J* 21:167-178.

110. Dvorak, A.M. 2005. Mast cell secretory granules and lipid bodies contain the necessary machinery important for the in situ synthesis of proteins. *Chem Immunol Allergy* 85:252-315.

111. Dvorak, A.M., H.F. Dvorak, and S.J. Galli. 1983. Ultrastructural criteria for identification of mast cells and basophils in humans, guinea pigs, and mice. *Am Rev Respir Dis* 128:S49-52.

112. Schmidt, M.V., B. Brune, and A. von Knethen. 2011. The nuclear hormone receptor PPARgamma as a therapeutic target in major diseases. *ScientificWorldJournal* 10:2181-2197.

113. Sugii, S., P. Olson, D.D. Sears, M. Saberi, A.R. Atkins, G.D. Barish, S.H. Hong, G.L. Castro, Y.Q. Yin, M.C. Nelson, G. Hsiao, D.R. Greaves, M. Downes, R.T. Yu, J.M. Olefsky, and R.M. Evans. 2009. PPARgamma activation in adipocytes is sufficient for systemic insulin sensitization. *Proc Natl Acad Sci U S A* 106:22504-22509.

114. Tontonoz, P., and B.M. Spiegelman. 2008. Fat and beyond: the diverse biology of PPARgamma. *Annu Rev Biochem* 77:289-312.

115. Bickel, P.E., J.T. Tansey, and M.A. Welte. 2009. PAT proteins, an ancient family of lipid droplet proteins that regulate cellular lipid stores. *Biochimica et biophysica acta* 1791:419-440.

116. Greenspan, P., and S.D. Fowler. 1985. Spectrofluorometric studies of the lipid probe, nile red. *J Lipid Res* 26:781-789.

117. Greenspan, P., E.P. Mayer, and S.D. Fowler. 1985. Nile red: a selective fluorescent stain for intracellular lipid droplets. *J Cell Biol* 100:965-973.

118. Dvorak, A.M., J.A. Warner, E. Morgan, S. Kissell-Rainville, L.M. Lichtenstein, and D.W. MacGlashan, Jr. 1992. An ultrastructural analysis of tumor-promoting phorbol diester-induced degranulation of human basophils. *Am J Pathol* 141:1309-1322.

119. Kohno, K. 2010. Stress-sensing mechanisms in the unfolded protein response: similarities and differences between yeast and mammals. *J Biochem* 147:27-33.

120. Liang, C.P., S. Han, G. Li, I. Tabas, and A.R. Tall. 2012. Impaired MEK signaling and SERCA expression promote ER stress and apoptosis in insulin-resistant macrophages and are reversed by exenatide treatment. *Diabetes* 61:2609-2620.

121. Harding, H.P., H. Zeng, Y. Zhang, R. Jungries, P. Chung, H. Plesken, D.D. Sabatini, and D. Ron. 2001. Diabetes mellitus and exocrine pancreatic dysfunction in perk-/- mice reveals a role for translational control in secretory cell survival. *Mol Cell* 7:1153-1163.

122. Di Capite, J., and A.B. Parekh. 2009. CRAC channels and Ca2+ signaling in mast cells. *Immunol Rev* 231:45-58.

123. Di Capite, J.L., G.J. Bates, and A.B. Parekh. 2011. Mast cell CRAC channel as a novel therapeutic target in allergy. *Curr Opin Allergy Clin Immunol* 11:33-38.

124. Ma, H.T., and M.A. Beaven. 2011. Regulators of Ca(2+) signaling in mast cells: potential targets for treatment of mast cell-related diseases? *Adv Exp Med Biol* 716:62-90.

125. Siraganian, R.P. 2003. Mast cell signal transduction from the high-affinity IgE receptor. *Curr Opin Immunol* 15:639-646.

126. Perretti, M., S. Nuti, and L. Parente. 1990. Investigation of rat mast cell degranulation using flow cytometry. *J Pharmacol Methods* 23:187-194.

127. Williams, R.M., J.B. Shear, W.R. Zipfel, S. Maiti, and W.W. Webb. 1999. Mucosal mast cell secretion processes imaged using three-photon microscopy of 5-hydroxytryptamine autofluorescence. *Biophys J* 76:1835-1846.

128. Triggiani, M., A. Oriente, G. de Crescenzo, G. Rossi, and G. Marone. 1995. Biochemical functions of a pool of arachidonic acid associated with triglycerides in human inflammatory cells. *Int Arch Allergy Immunol* 107:261-263.

129. Papanicolaou, D.A., R.L. Wilder, S.C. Manolagas, and G.P. Chrousos. 1998. The pathophysiologic roles of interleukin-6 in human disease. *Ann Intern Med* 128:127-137.

130. Hogan, P.G., L. Chen, J. Nardone, and A. Rao. 2003. Transcriptional regulation by calcium, calcineurin, and NFAT. *Genes Dev* 17:2205-2232.

131. Klein, M., S. Klein-Hessling, A. Palmetshofer, E. Serfling, C. Tertilt, T. Bopp, V. Heib, M. Becker, C. Taube, H. Schild, E. Schmitt, and M. Stassen. 2006. Specific and redundant roles for NFAT transcription factors in the expression of mast cell-derived cytokines. *J Immunol* 177:6667-6674.

132. Miyakawa, T., A. Maeda, T. Yamazawa, K. Hirose, T. Kurosaki, and M. Iino. 1999. Encoding of Ca2+ signals by differential expression of IP3 receptor subtypes. *Embo J* 18:1303-1308.

133. Yoneshima, H., A. Miyawaki, T. Michikawa, T. Furuichi, and K. Mikoshiba. 1997. Ca2+ differentially regulates the ligand-affinity states of type 1 and type 3 inositol 1,4,5-trisphosphate receptors. *Biochem J* 322 (Pt 2):591-596.

134. Steinberg, G.R., and B.E. Kemp. 2009. AMPK in Health and Disease. *Physiol Rev* 89:1025-1078.

135. Barrett, K.E., and D.D. Metcalfe. 1987. Heterogeneity of mast cells in the tissues of the respiratory tract and other organ systems. *Am Rev Respir Dis* 135:1190-1195.

136. Bradding, P. 2009. Human lung mast cell heterogeneity. *Thorax* 64:278-280.

137. Galli, S.J. 1990. New insights into "the riddle of the mast cells": microenvironmental regulation of mast cell development and phenotypic heterogeneity. *Lab Invest* 62:5-33.

138. Gesta, S., Y.H. Tseng, and C.R. Kahn. 2007. Developmental origin of fat: tracking obesity to its source. *Cell* 131:242-256.

139. Moon, T.C., C.D. St Laurent, K.E. Morris, C. Marcet, T. Yoshimura, Y. Sekar, and A.D. Befus. 2010. Advances in mast cell biology: new understanding of heterogeneity and function. *Mucosal Immunol* 3:111-128.

140. Triggiani, M., V. Casolaro, A. Genovese, G. Spadaro, and G. Marone. 1993. Heterogeneity of human Fc epsilon RI-bearing cells. *Ann Allergy* 71:133-138.

141. Dennis, E.A., R.A. Deems, R. Harkewicz, O. Quehenberger, H.A. Brown, S.B. Milne, D.S. Myers, C.K. Glass, G. Hardiman, D. Reichart, A.H. Merrill, Jr., M.C. Sullards, E. Wang, R.C. Murphy, C.R. Raetz, T.A. Garrett, Z. Guan, A.C. Ryan, D.W. Russell, J.G. McDonald, B.M. Thompson, W.A. Shaw, M. Sud, Y. Zhao, S. Gupta, M.R. Maurya, E. Fahy, and S. Subramaniam. 2010. A mouse macrophage lipidome. *J Biol Chem* 285:39976-39985.

142. Quehenberger, O., A. Armando, D. Dumlao, D.L. Stephens, and E.A. Dennis. 2008. Lipidomics analysis of essential fatty acids in macrophages. *Prostaglandins Leukot Essent Fatty Acids* 79:123-129.

143. Shevchenko, A., and K. Simons. 2010. Lipidomics: coming to grips with lipid diversity. *Nat Rev Mol Cell Biol* 11:593-598.

144. Subramaniam, S., E. Fahy, S. Gupta, M. Sud, R.W. Byrnes, D. Cotter, A.R. Dinasarapu, and M.R. Maurya. 2011. Bioinformatics and systems biology of the lipidome. *Chem Rev* 111:6452-6490.

145. Yetukuri, L., M. Katajamaa, G. Medina-Gomez, T. Seppanen-Laakso, A. Vidal-Puig, and M. Oresic. 2007. Bioinformatics strategies for lipidomics analysis: characterization of obesity related hepatic steatosis. *BMC Syst Biol* 1:12.

146. Sheldon, H., C.H. Hollenberg, and A.I. Winegrad. 1962. Observations on the morphology of adipose tissue. I. The fine structure of cells from fasted and diabetic rats. *Diabetes* 11:378-387.

147. Pietilainen, K.H., T. Rog, T. Seppanen-Laakso, S. Virtue, P. Gopalacharyulu, J. Tang, S. Rodriguez-Cuenca, A. Maciejewski, J. Naukkarinen, A.L. Ruskeepaa, P.S. Niemela, L. Yetukuri, C.Y. Tan, V. Velagapudi, S. Castillo, H. Nygren, T. Hyotylainen, A. Rissanen, J. Kaprio, H. Yki-Jarvinen, I. Vattulainen, A. Vidal-Puig, and M. Oresic. 2011. Association of lipidome remodeling in the adipocyte membrane with acquired obesity in humans. *PLoS Biol* 9:e1000623.

148. Mattos, K.A., V.G. Oliveira, H. D'Avila, L.S. Rodrigues, R.O. Pinheiro, E.N. Sarno, M.C. Pessolani, and P.T. Bozza. 2011. TLR6-driven lipid droplets in Mycobacterium leprae-infected Schwann cells: immunoinflammatory platforms associated with bacterial persistence. *J Immunol* 187:2548-2558.

149. Galli, S.J., J. Wedemeyer, and M. Tsai. 2002. Analyzing the roles of mast cells and basophils in host defense and other biological responses. *Int J Hematol* 75:363-369.

150. Rodewald, H.R., and T.B. Feyerabend. 2012. Widespread immunological functions of mast cells: fact or fiction? *Immunity* 37:13-24.